FACULTY OF SCIENCE
UNIVERSITY OF COPENHAGEN

Master's thesis in Physics

Phosphate in Ice Cores

Finding a method for continuous detection of phosphate in ice cores

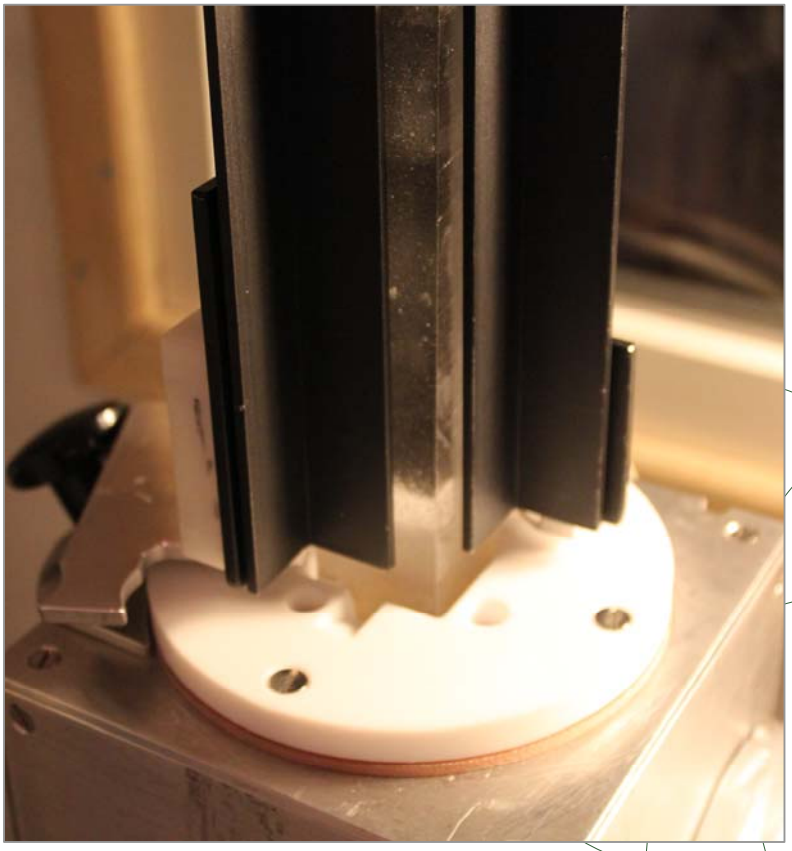

Helle Astrid Kjær
Centre for Ice and Climate
Niels Bohr Institute
University of Copenhagen

Supervisor:
Anders Svensson

December 2010

Master's Thesis

Title:	Phosphate in Ice Cores-Finding a method for continuous detection of phosphate in ice cores
ECTS-points:	60
Supervisor:	Anders Svensson
Name of department:	Centre for Ice and Climate Niels Bohr Institute University of Copenhagen
Sinature:	
	_____
Author:	Helle Astrid Kjær
Submitted:	1st of December, 2010

Abstract

In the present study, the phosphate cycle was investigated, general information regarding the use of ice cores as a climate archive is presented and a method for detecting phosphate in ice cores using continuous flow analysis (CFA) was found, optimized and used for detection of phosphate in two ice cores.

Phosphorus is an important and sometimes limiting nutrient for primary production in the oceans. Because of deforestation and the use of phosphate as a fertilizer changes in the phosphorus cycle have occurred over the last centuries. On longer time scales, sea level changes are thought as well to have caused changes in the phosphorus cycle. Analysing phosphate concentrations in ice cores may help gain important knowledge about those processes.

A continuous and highly sensitive absorption method was applied for the detection of phosphate in ice cores. It has previously been successfully applied for determining phosphate concentrations of sea water [Zhang and Chi, 2002]. The method was optimized for the low concentrations of phosphate expected in the ice cores. Parameters such as temperature and mixing length as well as reagent and buffer chemistry and others were investigated.

A line of melt water from the CFA melt head (1.68 mL per minute) was mixed with a molybdate blue reagent and an ascorbic acid buffer. A reaction took place in at least 300 cm of heated mixing coils before the absorption measurement at a wavelength of 710 nanometer was done in a 2 meter long liquid waveguide cell (LWCC) with an inner volume of 0.5 mL. The method has a detection limit of around 0.1 ppb and the resolution was approximate 2 cm, with a melt speed of 1.5 cm per minute, giving sub annual resolution in firn ice cores. A filter was inserted for removing dust, which otherwise gave optical interferences. Several filter types were investigated and a filter consisting of a glass capillary filled with glass wool provided the best results.

Phopshate was detected and investigated in two different ice cores from Greenland; the NEEM S1 shallow ice core and the NEEM ice core. In the NEEM S1 shallow ice core detection of phosphate covers part of the last 120 yr, while detection in the NEEM ice core covered the period 22.4 to 36.8 kyr B.P. Results showed a mean level in the NEEM S1 shallow ice core of 0.32 ppb phosphate and no anthropogenic change. The NEEM ice core had mean concentration in the glacial stadials between 6 ppb and 20 ppb, while the glacial interstadials had levels of only 2 ppb. A high correlation with dust was found in the NEEM S1 shallow ice core suggesting dust as either source or transport mechanism for phosphate. Phosphate in the glacial part also correlates with dust, but the ratio between phosphate and potassium shows evidence of a sea salt signal.

Acknowledgement

I would like to acknowledge my supervisor Anders Svensson, who always has an open door and has a way of leading me towards great ideas, before I even know I need them; Paul Vallelonga for valuable ideas regarding the more experimental part of the project as well as during detection of the NEEM S1 shallow core; Ernesto Kettner, who was a great help with the experimental set up especially in the beginning of project; Simone Sauer, who joined me for detection of the NEEM S1 shallow ice core; Mathias Bigler for suggesting that phosphate should be detected in ice and for leaving the idea here in Copenhagen, for articles useful in the initial study and for great ideas towards the end; Agnete Aslaug Kjær, Anna Naemi Nilsson and Kristian Kjær for proof reading; Hans Riber, who was a source for basic biological phosphate knowledge; Bo Svensmark for giving an introduction to the molybdenum blue method; Center for Ice and Climate should be thanked for the great opportunities I have been offered while working as a master student-especially for trips to Iceland and Greenland and for the opportunity of presenting this project at EGU-2010 in Vienna.

Finally I would like to thank the rest of the people at Center for Ice and Climate for a great working environment full of laughs, happy faces and extreme amounts of cake, as well as all you international colleagues, who made June 2010 at NEEM unforgettable.

Helle Astrid Kjær
Copenhagen, November 2010

1 Motivation and outline

The motivation for the subject of this thesis was the fact that there is no proxy for biological ocean activity measured in ice cores, which is not influenced by other sources. Phosphate, which has not been detected in ice cores previously to this study, could be a proxy of biological ocean activity, since the primary activity in the oceans is believed limited by phosphorus. Thus a method capable of detecting phosphate in ice cores was the target of this study. In order to do so, a large amount of literature had to be studied, before the experimental work could be initiated. Thus the thesis is divided in two major parts: **Section 2 to 6** provide the necessary background information, while the second part, **section 7 to 10** deals with the experiments I have conducted and analysed.

In **section 2** the importance of phosphate to the biosphere is explained. This is done to emphasize why it is important that phosphate variations in the ice cores are detected. Information on the phosphate cycle level as well as on transport path ways including changes over time follows in **section 3**. This was necessary to get an idea of the limit of detection required to detect phosphate in ice, and secondly to have an idea of whether the detected levels and variations found in the ice cores used in this study are reasonable. **Section 4** explains why ice cores can be used as a climate archive and includes information derived from ice cores. **Section 5** provides information on continuous flow analysis used for detection of ions in ice cores, to explain the idea behind CFA detection techniques. The section also provides information on the two CFA systems used for this project. To find the best method for continuous detection in ice cores a literature study on available phosphate detection methods was undertaken as described in **section 6**, with emphasis on the absorption method chosen, a method which was originally proposed for detection in sea water by *Zhang and Chi* [2002].

Section 7 investigate the optimization of various parameters for detection of phosphate in ice cores. **Section 8** presents and discusses the phosphate data obtained using optimum conditions in the NEEM S1 shallow ice core. The phosphate was detected in parts of the last 120 yr. **Section 9** presents phosphate measurements of the NEEM ice core conducted in field 2010. Finally **section 10** suggests further optimization of the method as well as ideas for ice cores in which phosphate could be further investigated. Each section ends with a summary of the found results. A conclusion on the entire project can be found in **section 11**.

Contents

2 Biological importance of phosphorus

In this section an introduction of the importance of phosphorus to the biosphere is given. This is done through a literature study.

Phosphorus (P) is an important part of the photosynthesis. It is part of all organisms. It is present in our bones and teeth as well as in our DNA. More precisely Earth's biological system is and has been dependent on phosphorus since the beginning of life [*Filippelli*, 2008].

The availability of phosphorus for plants is highly dependent on chemical, physical, and biological processes. The first two accounts absorption, desorption, precipitation and dilution and the biological processes are for example immobilisation and mineralisation [*Tiessen*, 1995].

Plants contain phosphorus (P) levels from 0.1-100 [mg/L], but seeds have P concentrations as high as 4000 [mg/L], while in mammals the concentration is 5 times larger. These high levels and the high dependence on P in biological systems has made the ecosystems recycle P very efficiently [*Tiessen*, 1995].

This also means that P is one of the limiting elements in ecosystems, though how limiting is intensively debated reaching from the opinion that P is a controlling factor to P being important but not comparable to other macro nutrients such as nitrate [*Tamburini and Föllmi*, 2009].

The size of the biosphere can effect the uptake of carbon, which has a huge influence on climate, because for example CO_2 works as a green house gas.

The phosphorus in the biosphere eventually returns to the global phosphate (PO_4^{3-}) cycle through waste and decay.

2.1 Influence of phosphorus in different biological systems

The recycling of phosphorus (P) in the tropics is important due to the large biosphere, combined with a lower inorganic P availability. The high turnover rate in the tropics can be exemplified by the fact that it is possible to harvest 4 times a year at some places in the tropical [*Tiessen*, 1995].

In the ocean dissolved P can be the limiting nutrient for primary biological activity. The concentration of P is 0.01 [mg/L] in ocean waters. Although some marine organisms also need nitrogen, phosphorus seems to be the only nutrient really limiting the system, thus making the removal of carbon in the form of organic matter from the surface layers to first order, totally P controlled. This is especially so for the easy accessible form of orthophosphate [*Bolin et al.*, 1981; *Paytan and McLaughlin*, 2007; *Tiessen*, 1995]. However recent evidence has emerged that some biological species can use the monophosphate esters (with C-O-P bonds) as well as carbon phosphorus (C-P bonds)[*Sañudo-Wilhelmly*, 2006]. The general ocean photosynthesis can be written as [*Paytan and McLaughlin*, 2007]:

$$106\,CO_2 + 16\,HNO_3 + H_3PO_4 + 122\,H_2O \xrightarrow{\text{light, trace elements and vitamins}} C_{106}H_{263}O_{110}N_{16}P + 138\,O_2$$

Looking at the general ocean photosynthesis it becomes evident that both carbon and phosphorus are needed and the ratio between carbon, nitrogen and phosphorus is [106:16:1]. This means that the carbon uptake from the atmosphere and in the euphotic

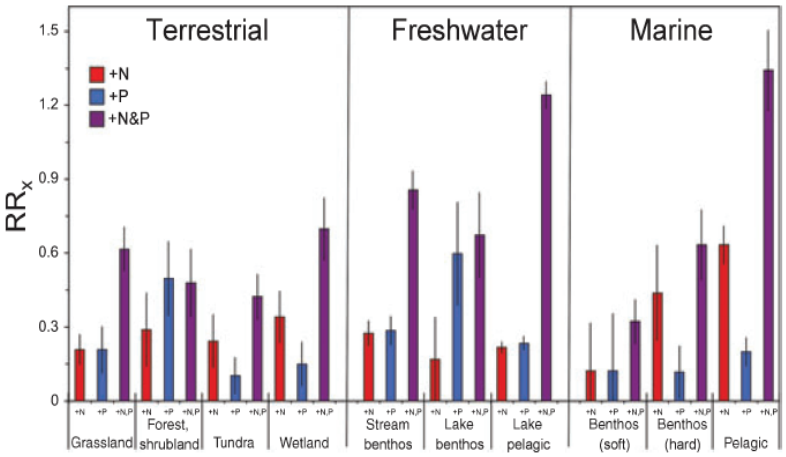

Figure 1: Natural-log transformed response ratios (RRx) in which autotroph biomass or production in the enriched treatment is divided by its value in the control treatment and then ln-transformed to single enrichment of N (red) or P (blue) or to combined N + P (purple) enrichment in various subhabitats in terrestrial, freshwater and marine ecosystems. Error bars indicate plus or minus one standard error *Elser et al.* [2007].

zone[1] by the marine life in the oceans, called the "biological pump", can be limited by P, while conversely in theory the carbon available can limit the uptake of P. The uptake of carbon influences the climate, and since P is likely to have been limited in geological time, it may have had an effect on production of phytoplankton. Thus more P available to the biosphere can enhance the CO_2 draw down from the atmosphere [*Paytan and McLaughlin*, 2007; *Falkowski et al.*, 1998; *Delaney*, 2000].

Though phosphorus is needed to drive the ocean photosynthesis, too much available phosphate can cause eutrophication, a process in which the primary production[2] exceeds the rate needed to drive the food chain and the algal bloom reduces the oxygen, which causes death of other organisms, shutting down the ecosystem [*Paytan and McLaughlin*, 2007]. Eutrophication requires a P concentration >0.025 [mg/L] to > 1 [mg/L] in freshwaters. In coastal systems entry of high concentration of P relative to N and Si make the primary biologic community change from silicon containing diatoms[3], which are essential for the higher food web system, to blue-green and brown algae [*Bolin et al.*, 1981].

Dead zones of strong eutrophicated waters have recently been seen in continental areas, *e.g.*, the Baltic Sea, Kattegat, the Black Sea, the Gulf of Mexico, and the East China Sea, causing problems for the fishing industry [*Diaz and Rosenberg*, 2008; *Oelkers and Valsami-Jones*, 2008].

Though as previously mentioned P is believed to be the key limiter in oceans recent evidence has come up, indicating that in some oceans limitation is by other nutrients. *Ryther and Dunstan* [Mar. 12, 1971] found looking at the effect of adding P and N to coastal waters of East Coast of the United States that Nitrogen was the key limiter for algae growth and eutrophication.

The tropical Atlantic was found by *Mills et al.* [2004] to be N limited, but they also found that N-fixation was co-limited by phosphorus and iron.

In freshwater P is very often the limiting nutrient. It has been suggested that this is partly due to the P getting stuck on particles and falling to the bottom, where the P is not available to the biosphere in the water [*Caraco et al.*, 1990].

[1]The euphotic zone is the layer of water where the photosynthesis can take place. That is from the water atmosphere interface and till where the light intensity reaches 1%.

[2]The primary production is the first step of living organisms in the food chain- in the water biosphere algae

[3]a certain type of algae

Schindler [1977] investigated the effect of different nutrients in three different freshwater lakes and found that P was the limiting nutrient in all three, though during short periods of time if sufficient amounts of P was added, they could be N or C limited for some weeks, only to return to P limitation again over time.

Carrillo et al. [2008] investigated the effects of P and ultraviolet radiation in a mountain lake and found that adding P can enhance primary production by up to a factor of two, and that high amounts of P might have a limiting effect on the damage of ultraviolet radiance.

However recent studies by *Elser et al.* [2007] with a more statistical approach comparing several hundreds experiments found that there was no significant difference in the limitation in the different biological systems, and that systems were partly P and N limited, and that a combination of both were most effective in enhancing activity in the biosphere, though adding either N or P also had significant effect in all systems (see figure 1). The same study showed that there was only a weak negative correlation between fertilizer response and latitude in the terrestrial system.

Phosphorus is important for the entire biosphere. It is an important nutrient for most primary production, especially in waters. Whether it is the limiting nutrient is still debated. P is important because it might control the primary production in the oceans which influences on the amount of carbon drawn into the ocean by the so called biological pump. Thus the amount of P available can control the amount of carbon uptake by the oceans, influencing climate on a larger scale. In the next section the phosphorus cycle is presented to provide information on the sources of phosphorus.

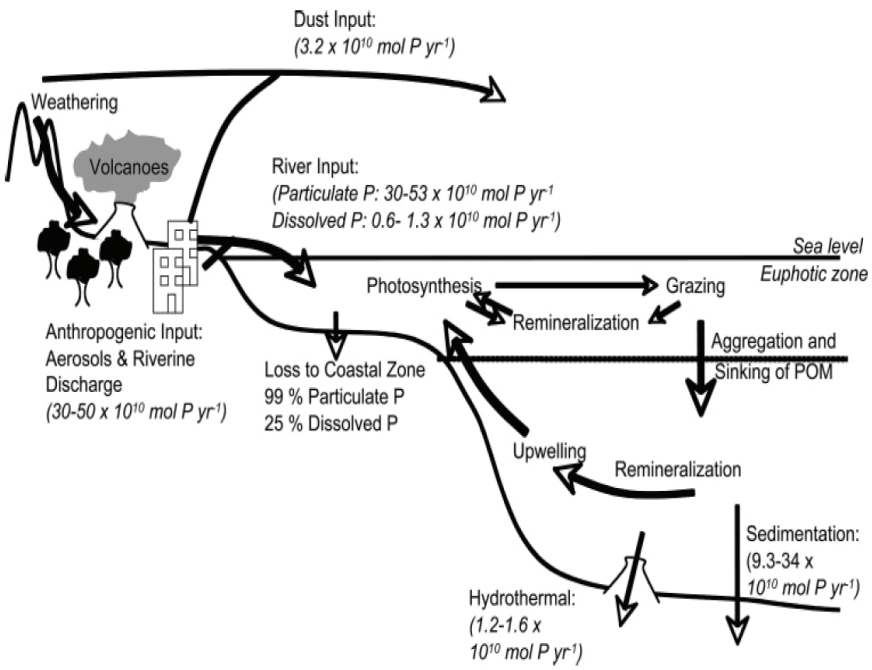

Figure 2: The figure shows the oceanic phosphorus cycle. Weathering is the main input of phosphorus to the oceans and the main sink is sedimentation. Human activities such as fertilization of grounds has increased in reason times. From *Paytan and McLaughlin* [2007].

3 The global phosphorus cycle

In the last section we learned that phosphorus is an important nutrient for the biosphere. This section discusses the global phosphorus cycle to provide background information on the sources and sinks of phosphorus: This includes the ocean phosphorus cycle, which gives detailed information on the amount of phosphorus found in the oceans as well as the availability to the biosphere and concentrations of phosphorus and phosphate found in atmosphere and sources for atmospheric aerosols. It also contains more detailed observations on the phosphorus concentration in glaciers found going through previous results, which is useful to find the limit of detection necessary in a method for detecting phosphate in ice cores. The section also includes information on the changes in the phosphorus cycle over time. Be aware that sometimes phosphorus is discussed and sometimes phosphate is.

Even though, as discussed in section 2, life can not exist without phosphorus (P), the amount of P in the earth system is limited. It is the 11th most abundant element on earth and is the limiter for primary production in some marine and estuarine environments [*Paytan and McLaughlin*, 2007].

Phosphorus does not have a stable gaseous phase and the atmospheric cycle of P is thus fundamentally different from the cycle of nitrogen and carbon, its aerial transportation being restricted to transport by aerosols [*Mahowald et al.*, 2008]. The transport by aerosols is not very large, and in the global phosphorus system most phosphorus is water transported [*Schlesinger*, 1991; *Filippelli*, 2008].

Figure 2 shows the oceanic phosphorus cycle as well as some quantification of the transport.

3.1 Phosphorus on land and transport to the oceans

The concentration of phosphorus (P) in the crust is only 1200 [mg/kg]. In soils the concentration of P is down to 200-800 [mg/kg]. With age the P is washed out of the soil. The phosphorus is mainly bonded to Ca^{2+} and Mg^{+}, and 0.5 [μg/L] is water soluble [*Tiessen*, 1995].

Weathering of calcium phosphate minerals is the most dominant source of P. The phosphorous content of rocks is very small, and most commonly only a small fraction is available to the biosphere [*Schlesinger*, 1991]. Weathering releases P in several ways: 1) Biochemical respiration releases CO_2 which increases the acidity. This releases the crystallized P. 2) Plant roots can release organic acids, which again makes the rocks dissolve and frees the phosphorus [*Filippelli*, 2008].

Even though P is freed from the crystalline structure of the rock it is not readily available for the biosphere. Weathering can also co-precipitate Fe and Mn, that have large binding potential for PO_4^{3-} because their positive charge works as a long term storage pool [*Filippelli*, 2008].

The most significant transfer of PO_4^{3-} from land is through weathering and riverine fluxes. Approximate 33 million tonnes of P is transported to the ocean a year. Half is transported by river and half is coastal run off [*Tiessen*, 1995].

When transported to the oceans by rivers the phosphorus occurs in particulate and in dissolved form. The particulate does not take part of the biochemical cycle, however clay particles can absorb PO_4^{3-} from freshwater, and can release some of the phosphorus as salinity increases. Only about 10-30 % of the P transported by rivers ends up being available to the marine biosphere. This is partly due to estuarine water processes. *Nixon et al.* [1996] found that at the margin of the North Atlantic Ocean estuarine water processes removed 10-55 % of the total P that would have passed into the coastal oceans. Approximately a quarter of the phosphorus available to the biosphere as well as almost all the non reactive phosphorus is deposited in the shelf area and thus does not affect the open ocean [*Schlesinger*, 1991; *Paytan and McLaughlin*, 2007; *Filippelli*, 2008].

3.2 The oceanic phosphorus cycle

Contrary to the phosphorus on land, that in the oceans is much more easily accessible to living organisms due to constant mixing and a scarcity of absorbant surfaces. Thus, in the oceans, the sensitivity of the biological systems to phosphorus concentration is higher. Phosphate coming from land to water can have an eutrophying effect especially on the surface waters in the high oceans that are currently P limited [*Tiessen*, 1995]. The P concentration in surface waters vary between 0.05 and 3.5 [μM][4] (1.6 and 108 [ppb]) according to *Concright et al.* [2000], while previously *Levitus et al.* [1993] found mean yearly values between 0.1 and 2 [μM] (4 and 62 [ppb]). A map produced by *Concright et al.* [2000] of mean surface water phosphorus concentration can be found in figure 3.

The surface water P content is most abundant in the Antarctic, also the high pacific Subpolar gyre and the Peru upwelling region show high values. In the Subarctic Pacific yearly mean values of P in surface waters are between 0.4 [μM] (12 [ppb]) and increases to 1.4 [μM] (44 [ppb]) at higher latitude. The western side also shows higher values than the eastern. The north Atlantic has the highest values in the Labrador and North Sea, and varies between 0.4 and 1.4 [μM] P (12 and 44 ppb). In the South Atlantic the amount

[4] M is mol/L and can be calculated to ng/g (pbb) using the molar weight of P (31 g/mol) or PO_4^{3-} (95 g/mol).

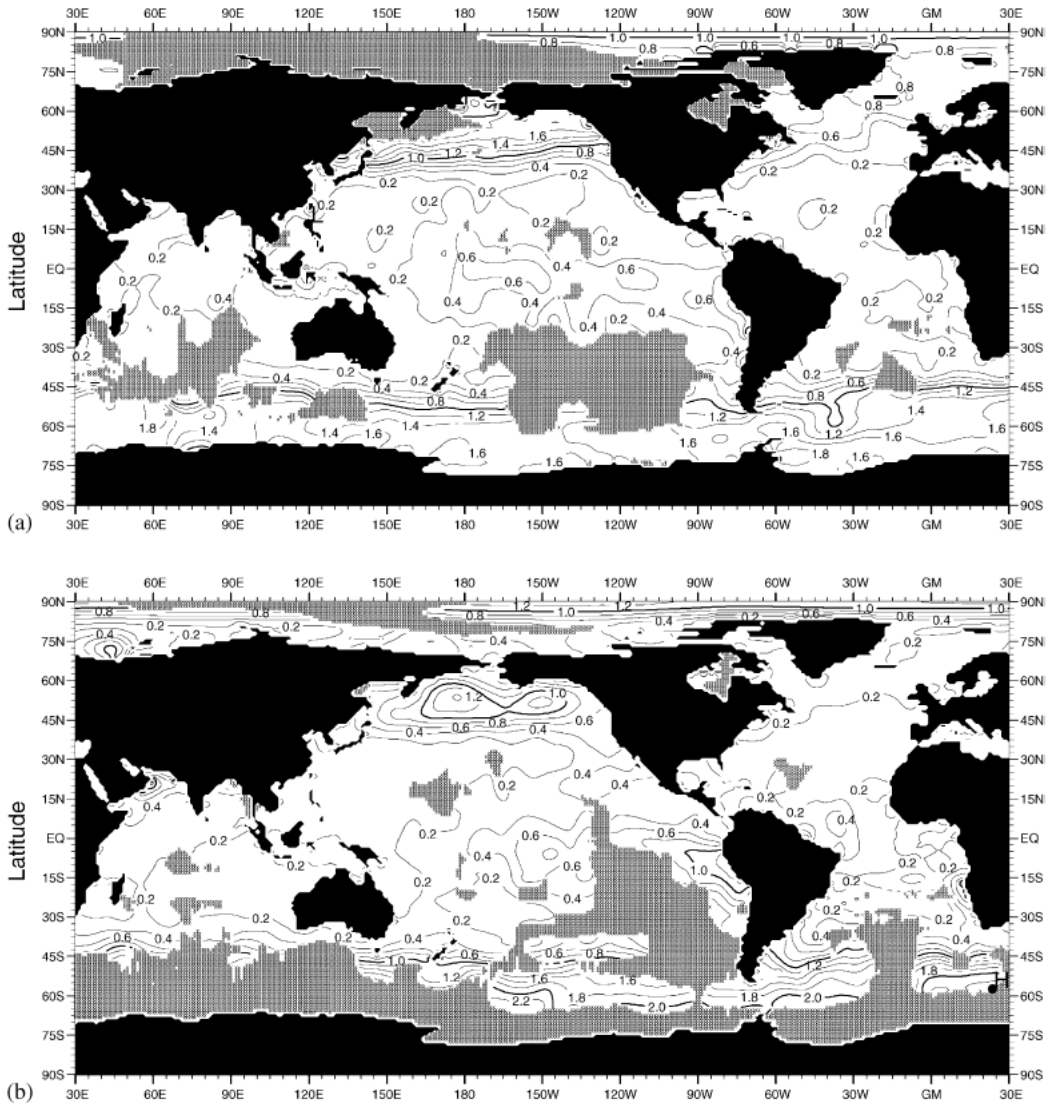

Figure 3: The surface seasonal mean PO_4^{3-} [μM] observations in the oceans. Using observation data from mostly 1950-1980. Figure a) shows Jan-march and b) jul-sep. Grey marks areas with a scarcity of data. The figure is from *Concright et al.* [2000].

exceed 2.0 [μM] (62 [ppb]). Finally concentrations are high in all coastal areas except for Australian and East Asian surface waters [*Levitus et al.*, 1993].

It is apparent from figure 3 that the phosphate concentration is depressed in the summer season. Large differences exist between summer and winter values, *e.g.*, the winter concentration in the north Atlantic and north pacific are double the summer concentration. The same effects can be seen in the temperate regions, while the tropic regions have almost no seasonal variations. In the North Atlantic there is a depletion all year round due to the loss of nutrients to deep water and the opposite effect causes a higher amount of PO_4^{3-} in the North Pacific. Higher phosphate concentration can also be observed near river mouths [*Concright et al.*, 2000].

In surface waters of the ocean the residence time is only a few days and concentrations are low. Only 10 % of the P goes to the deeper oceans, where most of it is mineralized, while 90 % is taken up by the marine biosphere in the surface waters [*Schlesinger*, 1991].

Phosphate burial occurs mainly by dead organic material sinking to the bed of the oceans. Organic phosphate can be released under oxidation in the water column and some research suggest recycling of P in some ocean environments, since the uptake by biological activity is larger than the input from atmosphere and ocean deep water sources [*Paytan and McLaughlin*, 2007; *Filippelli*, 2008].

In the Subantarctic the growing season of primary production account for 66-75 % of the annual export flux. The annual export flux of phosphorus was found by modelling to be 68-83 [mmol/m^2] (2.1 [g/m^2]) in the Polar frontal zone and 52-61 [mmol/m^2] (1.6 to 1.9 [g/m^2]) in the SubAntarctic zone. The difference is explained by vertical mixing (37%) as well as horizontal mixing (63%) from Ekman transport occurring in the Polar frontal zone, whereas the Subantarctic were highly dominated by vertical mixing [*Wang et al.*, dec. 15, 2001].

Comparison between fresh and ocean or brackish water suggests that P is more easy recycled in salt water [*Caraco et al.*, 1990]. In the end however it is stored in the deep ocean as sediments. On larger time scale these become uplifted and the cycle restarts with weathering of cliffs [*Schlesinger*, 1991].

Another, but minor, sink is uptake through seawater associated with thermal crust activity on the floor of the ocean. It is estimated that hydrothermal processes remove similar to 10% of the sedimentary burial flux [*Paytan and McLaughlin*, 2007].

The mean residence time for PO_4^{3-} in the ocean is estimated between 20 and 100 kyr. But smaller time cycles are evident. The turnover time of the surface PO_4^{3-} is 3 years or less, while the deep water turnover time is 1500 years [*Schlesinger*, 1991; *Paytan and McLaughlin*, 2007].

The concentration of phosphate in deep water is age dependent. The older the water the more PO_4^{3-}. *E.g.*, the Atlantic young deep water has a 40 % lower concentration of phosphate than the Pacific oceans older deep waters [*Filippelli*, 2008].

3.3 Atmospheric phosphorus sources

Atmospheric phosphorus is in the form of mineral dust and aerosols. About 4.6 [Tg/yr] Phosphorus is deposited of this 70 % falls on land [*Schlesinger*, 1991]. It is critical to oligotrophic[5] terrestrial and freshwater systems. The transportation by the atmosphere is however mostly important in remote ocean areas. The deposition comes from aerosols, volcanic ash, mineral dust and sea salt. Approximately 83 % is from crustal sources. The concentration of phosphorus in measurements range from 0.2 to 1450 [ng/m^3], but using

[5]Oligotrophic means a system with very few nutrients available

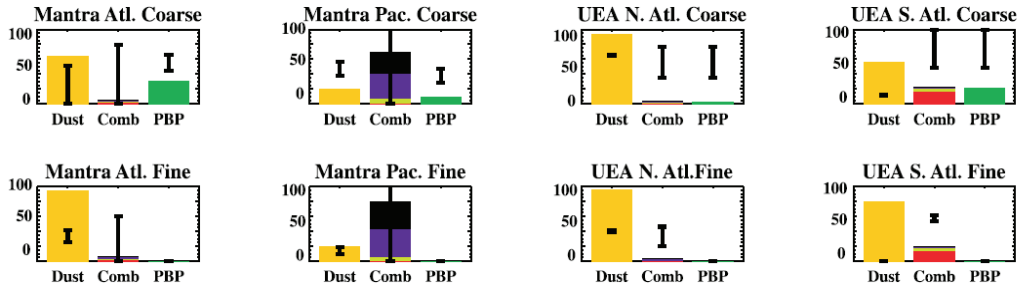

Figure 4: Modelled values for the source apportionment (percentages) of PO_4^{-3}. Fine is aerosols below 2.5 μm and coarse is up to 10 μm. The stations mentioned are in the Atlantic and in the Pacific. The first column is for mineral aerosol (dust, yellow), the second column is for combustion aerosols (Comb), and the third column is for primary biogenic particles (PBP, green). The filled bars are the model estimates. For combustion aerosols, the model estimate is the sum of four different components: biomass burning (BB, red); fossil fuels (FF, purple); biofuels (BF, light green); and volcanoes (VOL, black). The vertical lines on each of the filled bars represent the minimum and maximum estimates derived from the observations. The figure is from *Mahowald et al.* [2008].

only the newer measurements, results ranges 0.12 to 378 [ng/m^3] [*Graham and Duce*, 1982; *Baker et al.*, 2006; *Mahowald et al.*, 2008]. Not only the P transported by aerosols is interesting also the source area, the deposition type, the solubility in water and variation of it to different pH and salt concentration influences the limitation of P to the deposition site [*Mills et al.*, 2004].

The mineral dust is approximately 5% of the pre-industrial source to the ocean, the further from shore the larger the importance. Globally mineral dust consists of 720 [ppm] ([mg/kg]) P with variation of up to 30% [*Mahowald et al.*, 2008].

Combustion sources has a phosphate content of between 0.17 and 1.3 % for fine aerosols and 0.2 and 1.95 % for coarse aerosols [*Mahowald et al.*, 2008].

Sea salt aerosols have a wide range of phosphorus content. It can be assumed that sea salt has the same range as surface waters and thus vary between 0.05 and 3.5 [μM] (1.6 to 108 [ppb]). Sea salt accounts for approximately 7 % of the total air transport.

Biogenic aerosols are spores or plant bits emitted directly to the atmosphere. They are very poorly understood since there is not any specific way of measuring them.

The amount of P in volcanic aerosols has been measured in an ash plume from mount Edna as well as in one from Hawaii and is suggested to be important for remote areas. *Mahowald et al.* [2008] suggest that volcanoes are most often not important for primary ocean activity and conclude that the contribution is less than 10 % of the annual atmospheric phosphorus budget. However during short time periods it might have an effect since volcanic ash has a high concentration of P, up to 1%; but the effect is localised. Concentrations can be as high as 36 [μM] (1.1 [ppm]) corresponding to 50 times background concentration *Paytan and McLaughlin* [2007]; *Mahowald et al.* [2008].

Sources of phosphorus aerosols and phosphate aerosols as seen in *Mahowald et al.* [2008] can be seen in figure 4.

In ocean regions only the soluble fraction is bioavailable. The soluble fraction is estimated to be between 7 % and 100 %. *Baker et al.* [2006] measured transects of the Atlantic ocean and found that mean soluble fraction of phosphorus was 32 % with a soluble fraction of the Saharan dust being 10%, however variations were spanning 0.01-87 %. *Herut et al.* [1999] found a soluble fraction of phosphorus spanning from 6-85% in the Mediterranean, they found the mean soluble fraction of Saharan dust to be 25 % and the soluble fraction of phosphorus in European aerosols to be 45 %.

Graham and Duce [1982] found that the atmospheric input over the North Atlantic ocean varied between 0.6 [ng/m^3] and 47 [ng/m^3], with an average of 7 [ng/m^3]. Assuming

a soluble fraction of 37 % during contact with sea water for 12 hours, they found that 2-4 [g/yr] P was added to the north Atlantic surface waters, corresponding to 10 % of the dissolved phosphorus coming from the riverine input.

During a cruise in the Atlantic ocean *Baker et al.* [2006] found that P values in aerosols varied from 0.12 [ng/m^3] to 5.57 [ng/m^3]. However they suggest that their method might overestimate P values by a factor of two. *Baker et al.* [2006] also find that Sahara is the most likely source and that some P close to land might come from tropical forests. Further they conclude that in general aerosols in the Atlantic is depleted on P compared to other nutrients.

Bergametti et al. [1992] found measuring aerosols over the Mediterranean that air transported phosphorus needed to support 3000-5300 [μg/m^2] per day (1-2 [g/m^2] per yr) to support the primary production, while 680-1500 [μg/m^2] per day (0.25-0.55 [g/m^2] per yr) is needed to start new production. They found that the phosphorus from the atmosphere only supported 2 to 20 % of the used P for new production.

From measurements of aerosols from three sites in the Mediterranean *Herut et al.* [1999] found fluxes of seawater soluble inorganic P in the coastal and SE Mediterranean to be 0.009 [g/m^2] per yr and 0.008 [g/m^2] per yr from wet deposition and estimated the dry deposition to amount for 0.01 [g/m^2] per yr.

Looking at Saharan dust deposited in the west Mediterranean *Ridame and Guieu* [2002] found the soluble fraction of Phosphorus varying from 1-21 %. They also found that if large amounts of dust were carried with little rain the soluble fraction of phosphorus was low. Further *Ridame and Guieu* [2002] found that the duration of contact between particles and rainwater could influence the soluble fraction detected in the seawater.

Chen et al. [2006] looked at aerosols collected close to the East China Sea. They found mean concentrations of 0.157 [mg/m^3] P, which is significantly higher than the results presented above. This is most likely due to the fact that the monsoon does play a big role in transporting particulate matter from inland China to the area.

Many locations seem to have a strong seasonal cycle, with maximum in summer and fall at mid latitudes. The seasonal cycle seems less pronounced in the tropics. *Mahowald et al.* [2008] finds that the seasonal cycle near dust cycles show a dust seasonality, while they *e.g.*, near the Amazona has a strong biomass burning signal. They find no evidence of a seasonal biosphere cycle.

Mahowald et al. [2008] have made a global chemical transport model to simulate the total phosphorus content in the atmosphere, using horizontal resolution of 1.8*1.8 degrees and 28 vertical layers. They make simulations for the year 2000. The model divides the sources of total phosphorus into mineral aerosol sources, combustion sources, primary biogenic sources, sea salt aerosols and volcanic sources.

Phosphate arriving with the mineral dust is assumed to have a soluble fraction of 10%, volcanic aerosols 100 % soluble and the rest is assumed to have a soluble fraction of approximate 50 %. It is however pointed out that the knowledge on the fraction of soluble phosphate is highly uncertain. Using this model they find that the amount of total phosphorus show high concentrations over land and in the north Africa dust region. *Mahowald et al.* [2008] have created a map (see figure 5), showing the aerosol distribution of phosphorus and phosphate, as it is today (year 2000) and as it would have been without human influences.

The global amount of P transported by the atmosphere to the oceans is 1.39 Tg/yr, of which 4.8 % in mean is anthropogenic, though it should be mentioned that anthropogenic sources can account for as much as 50 %, the source of phosphate or soluble phosphorus is 0.24 Tg P/yr, 14 % is of anthropogenic origin, all according to the model by Mahowald et

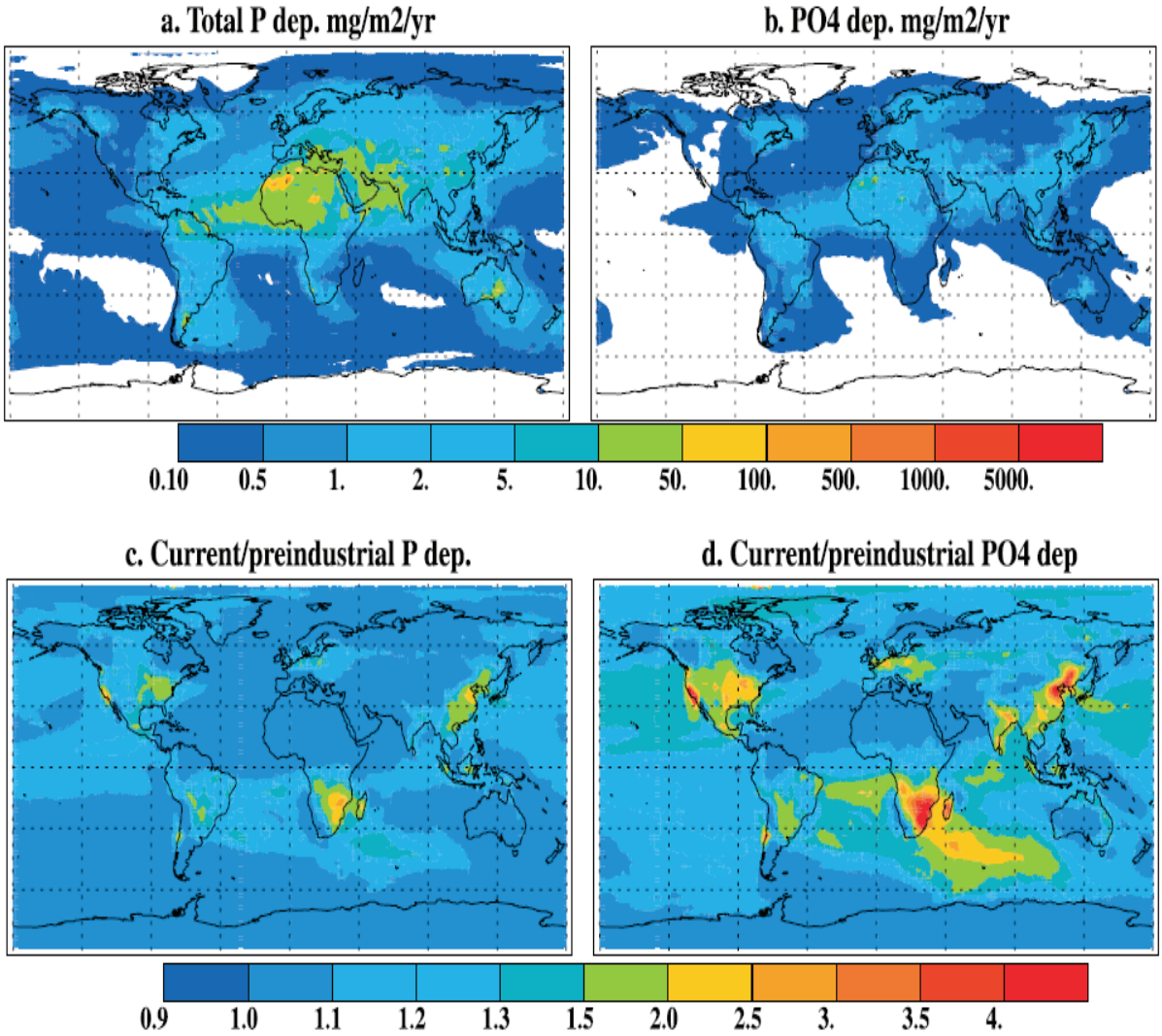

Figure 5: Model estimated fluxes of a) Total phosphorus, b) PO_4^{-3}, c) and d) show ratio of current to pre industrial for c) total phosphorus and d) PO_4^{-3}. From *Mahowald et al.* [2008].

	total P [Tg yr^{-1} P]	PO_4^{3-} [Tg yr^{-1} P]
Dust	1.150	0.115
Primary biogenic particles	0.164	0.082
Biomass burning	0.025	0.012
Fossil fuels	0.024	0.0.012
Biofuels	0.021	0.010
Volcanoes	0.006	0.003
Sea salt	0.0049	0.0049
Total	1.39	0.24
Percent Anthropogenic	4.8	14.3

Table 1: Global sources of atmospheric phosphorus less than 10 μm as found in a model by *Mahowald et al.* [2008]

al (2008), see table 1. But it should again be emphasized that there are large uncertainties in the PO_4^{3-} budget due to lack of observations.

3.4 The Arctic and glacier phosphorus concentrations

Due to its remote location not much is known about the concentration of phosphorus in the Arctic in general.

Using the before mentioned model (see section 3.3), *Mahowald et al.* [2008] found that the amount of phosphorus deposited in the Arctic basin from the atmosphere is 6.9 [Gg/yr], of this 32.3 % is soluble giving 2.2 [Gg/yr] PO_4^{3-}; of the soluble phosphorus 9.3 % is suggested to have anthropogenic origin.

Looking at the ice sheets only *Edwards et al.* [2007] has presented results on the phosphorus concentration of the Greenland ice sheet. The results showed phosphorus concentration from Greenland ice cores measured by ICP-MS[6] with a detection level of 20 [ppt] having a mean of 0.25 [ppb] during the last century. These authors also found that the concentration in ice cores in the period from 1990-2005 had increased dramatically; they suggested forest fires caused the increase [*Edwards et al.*, 2007; *Edwards*, 2009].

In a personal correspondence with Goto-Azuma in 2010, who is measuring ice cores by IC[7]. The level, we were told, most likely in recent times was below 1 ppb.

I am not aware of any further measurements of PO_4^{3-} or P made directly on glaciers. However some measurements have been done on the melt water from glaciers. Using the molybdenum method *Tockner et al.* [2002] made measurements on melt water from a glacier in Switzerland and found that the concentrations of total dissolved phosphorus was 8 [μg/L] ([ppb]) when coming from snow and that glacier melt water had a concentration of 5 [μg/L]. The concentration of total phosphorus was found to be 12 [μg/L] for snow and for glacial run off 97 [μg/L], implying that the soluble fraction of phosphorus is very low in glaciers and that there might have been a change over time in P deposited on the glacier or that something happens to the concentrations during the firnification process in the glaciers.

Chillrud et al. [1994] looked at particulate matter in streams from three glaciers in Argentina and found that the total phosphorus concentrations were high in all three but that the solubility of phosphorus differs from 1-5 % (0.01-0.23 [μM] (0.3 to 22 [ppb])),

[6]ICP-MS is inductively coupled plasma mass spectrometry, which is capable of tracing metals and some non-metals down to the limit of ppt, by ionization of the metals and using the mass spectrometer to separate and detecting them.

[7]IC is ion chromatography

in one of the glaciers to a solubility of 20-32 % (0.12 to 4.69 [μM] (4 to 145 [ppb])) in the smaller side glaciers. They suggest that the difference is due to the iron hydroxides adsorbs the soluble phosphorus.

Hodson et al. [2004] made a more extensive study looking at the particulate matter in the melt water from 6 glaciers positioned in France, Pakistan, Svalbard and Sweden and found that all had low values of soluble phosphorus (0.9 to 23 [μg/g] phosphorus ([ppm])) and relative high values of total phosphorus corresponding to the mean concentration of rock (230-670 [μg/g]). The ratio of soluble over total phosphorus varied between 0.2 and 3.4 %.

Hood and Scott [2008] looked at watersheds in Alaska and found that the soluble reactive phosphorus as well as total phosphorus went up when connected to glacial run off. However they suggest that the reason why the soluble fraction is high could be due to limited sunlight in the water due to the turbidity and the high loads of particulate matter in glacial rivers, which would inhibit the bioactivity. They also suggest that higher glacial weathering could explain the difference.

3.5 Changes in the phosphorus cycle in time

It is interesting to note what variations there have been over time and even more interesting to know what caused them. This section presents such results and increases our knowledge on the changes that could be expected in the ice core records.

Over time P is continuously washed out, which effects both the terrestrial biochemistry and the oceanic cycle [*Mahowald et al.*, 2008]. The amount of phosphorus available in the surface waters might have effected the concentration of phytoplankton and thus the carbon uptake. In recent time alterations of the cycle due to human activities such as use of fertilizers has caused eutrophication where none was previously observed in some oligotrophic waters.

3.5.1 Glacial time scale - ocean water

Evidence of a glacial cycle has been investigated. During the ice ages sea level has been up to 125 meters lower than today, diminishing the shelf area up to 60%. The shelf-nutrient hypothesis suggests that the loss of continental margin can make the previous continental margin sink into a deep ocean sink. This could significantly change the phosphorus budget in the oceans.

It is plausible that the oceanic phosphorous cycle can respond in the time scales of glacial cycles, since the residence time is about 20 kyr. Further there are indications that the continental margin sink is the same size as the deep ocean sink and if the continental margin was exposed to weathering, PO_4^{3-} previously deposited in this area it would again go into the phosphorus cycle. Not only weathering of the exposed continental margin would be the source of increased P led to the oceans; there is evidence of increased weathering of the continents during glacial periods too [*Filippelli*, 2008; *Tamburini and Föllmi*, 2009].

Filippelli [2008] found a peak in primary productivity after the onset of a glacial period by looking at marine sediment cores. The marine records also indicated a high excess of P occurring 40-60 k yr after an onset of a glacial period. Using a simple mass balance model *Filippelli* [2008] finds that the lag is predictable using the residence time of 20-25 kyr (see figure 6).

Tamburini and Föllmi [2009] looked at several marine cores and found that concentrations of reactive P was lower during glacial times and that the accumulation rates show higher variability. They find that the lack of burial on the shelf was not compensated by

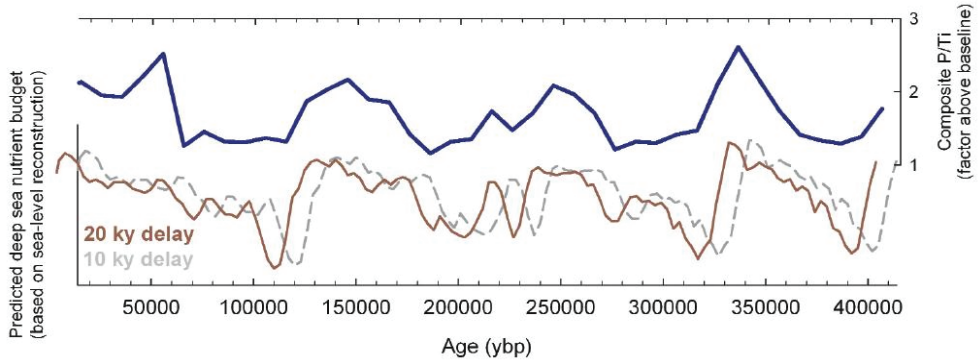

Figure 6: Changes in the mass balance of phosphorus on glacial timescales interpreted from the marine record of phosphorus burial (P/Ti) composed by individual cores from the equatorial pacific and southern ocean compared to a sea-level-based model (using the marine oxygen isotope record of ice volume) of phosphorus mass balance changes due to the redistribution of phosphorus from exposed continental margins during glacial sea level lowstands. From *Filippelli* [2008].

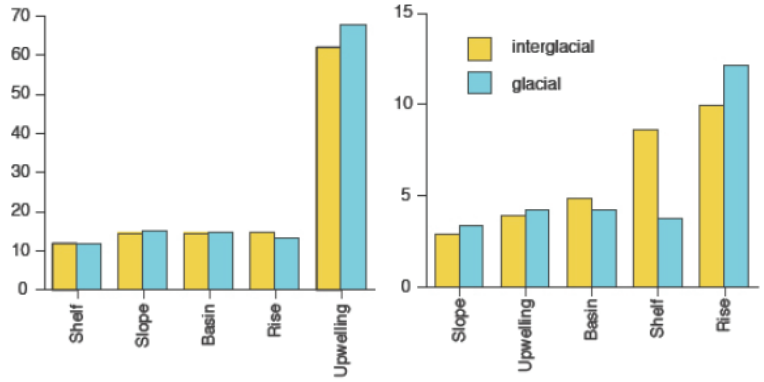

Figure 7: Avarage concentrations of reactive P concentrations in μ M/g sediment (left) and mass accumulation rates in [μmol/cm^2/kyr] (right) for interglacial (dark bars) and glacial (light bars) periods for different settings. The figure is from *Tamburini and Föllmi* [2009].

burial other places and using a simple model they show that the P in the water during glacial stages could have been 17-40 % higher than today's concentration (see figure 7). They also show that during onset of glacial periods the shallower sites have an increase in the reactive phosphorus. All this supports the shelf-nutrient hypothesis.

Increased phosphorus flow to the remote ocean surface waters from aerosols transported by wind at increased speed could also effect the phytoplankton productivity. But intense discussion is still ongoing on the question on how P limited the ocean surface productivity is.

Many find that there has been higher levels of nutrients in the surface waters during the glacial period. The interpretation however is not straight forward. Most explain the higher concentrations of nutrients support more primary biological activity in the surface oceans [*Delaney*, 2000; *Filippelli*, 2008; *Tamburini and Föllmi*, 2009].

Elderfield and Rickaby [2000] found that there was no significant change between glacial and interglacials in the amount of P present in the surface waters in the Subantarctic, but an increase of +0.6 [mmol/kg] (19 [ppm]) in the glacial Antarctic, probably explainable by a sea surface temperature change of 4±5 [°C]. They compared to other proxies and came up with a theory that sea ice coverage inhibiting primary activity in the Arctic led to less use of the P, since shutting out light important to the photosynthesis would inhibit primary biological activity [*Elderfield and Rickaby*, 2000].

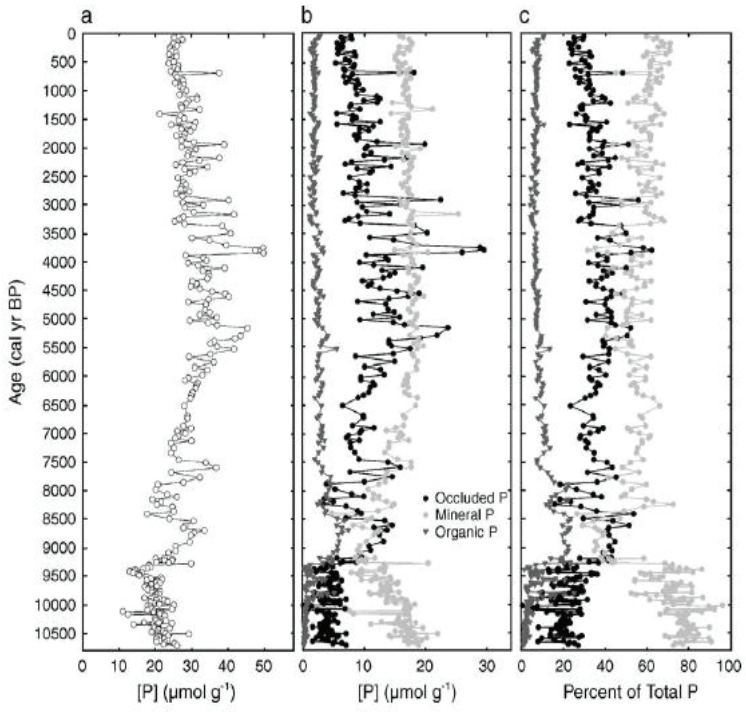

Figure 8: Changes in phosphorus on glacial timescales interpreted from a sediment core from Lower Joffre lake, Southern coast, British Columbia, Canada. Total P concentration ([μmol/g]) (sum of the three fractions); (b) P concentration for each P-bearing fraction; (c) and percent of total P for each fraction. The figure is from *Filippelli et al.* [2006].

3.5.2 Holocene time scale - fresh water

Filippelli et al. [2006] looked at the mineral P, occluded[8] P and organic P fractions in lake sediment cores from the coast mountains of British Columbia covering the Holocene[9](see figure 8). They find several changes in the P budget over time. In 8000-8500 BP they find an increase in the mineral P that could signal advances of the nearby glaciers, and thus increase in the mineral P from increased weathering, this also corresponds to the cold event in the North Atlantic at 8200 BP. Another peak in mineral P is observed 7500 yr BP. In 3500 BP mineral P increases abruptly and the same is the case in 2800-2300, 1400 and 250 BP, corresponding to terrestrial records of that period. Beneath the spikes a trend of increase in the mineral P indicating a trend towards cooler conditions is observed.

3.5.3 Anthropogenic sources

The anthropogenic sources have altered the global phosphate cycling. Due to human act PO_4^{3-} levels of more than twice the natural level is today found in rivers [*Filippelli*, 2008; *Paytan and McLaughlin*, 2007]. Human occupation also influences the concentration in, *e.g.*, watersheds giving loss rates of 0.3 [kg/km^2] ([ppb/m^2]) P at a population density of 0.1 [persons/km^2], rising to 30 [kg/km^2] at densities of 300 [persons/km^2] [*Tiessen*, 1995].

The flux of phosphorus in rivers have mainly increased due to the use of fertilizers in human agriculture. The fertilizers are mined from sedimentary rocks and thus enhances the global phosphorus cycle [*Schlesinger*, 1991; *Tiessen*, 1995]. The amounts of PO_4^{3-} mined and used can be found in figure 9. A growing trend of phosphate rock use was observed until the 1980's after which it has been slowly declining partly due to concern about eutrophication in water [*Diaz and Rosenberg*, 2008; *Oelkers and Valsami-Jones*, 2008].

[8]Occluded P is the P bound to soil oxides such as for example to those of iron

[9]The Holocene is the present inter glacial period for information see section 4.4.1

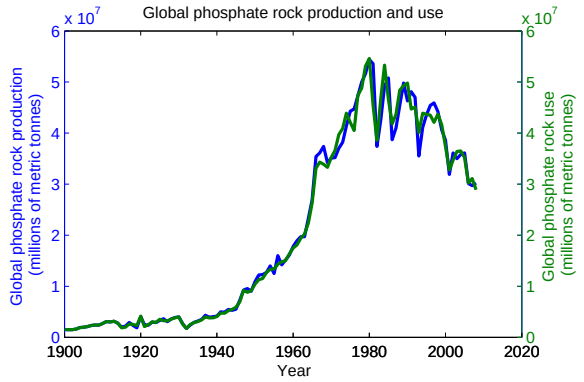

Figure 9: Global production and use of phosphate rock increased rapidly from 1940 to 1980 and shows a more decreasing trend in the last 30 years. The data is from *Survey* [2010].

The trade of phosphorus is making a deficient between the poor and the wealthy countries. The wealthy countries risk that their higher use and outlet of P will cause eutrophication in the surface waters, because the P let out is very bioavailable. The eutrophication effect will however not account for more than 10-15 years of CO_2 emissions, since the amount of PO_4^{3-} available for mining is limited [*Filippelli*, 2008; *Tiessen*, 1995]. The trade deficient can alter the global distribution of phosphorus.

In Sweden gain in watershed showed a 3 times as high input than output of P. The increased input was divided on sources: 62% came from inorganic fertilizer, 30 % from manure, 5% from sewage, 2% from atmospheric deposition and 0.3% from the natural weathering of rocks [*Tiessen*, 1995].

Fertilizers are preferentially nitrogen and there is the possibility that over time increased outlet of nitrogen compared to other fertilizers will change some ecosystems currently nitrogen limited to phosphate or iron limitation.

The phosphate flux has also been increased by burning of forests. In ash form PO_4^{3-} is dissolved and transported by rivers on time scales of years. Further the lack of roots destabilizes the PO_4^{3-} rich soil below, which causes wash out of the phosphate and other nutrients. The P loss from deforestation is estimated to be 2.29 [Tg/yr] from rain forest and 0.13 [Tg/yr] from seasonal forrests [*Filippelli*, 2008; *Paytan and McLaughlin*, 2007; *Bolin et al.*, 1981].

Minor impacts are human waste, waste from processing of foodstuff, and industrial use of detergents, which in the period 1940-1970 was a major source of P to the environment. Detergents used to have P content of up to 7 % but are today low on P [*Filippelli*, 2008; *Tiessen*, 1995].

When looking at air transported man made P pollution it is important to note that the aerosol size is often smaller when the aerosolos is from combustion than from natural soil. This causes the pollution to have a more widespread effect, since it is transported over large distances and with a high diffusion meanwhile [*Mahowald et al.*, 2008].

All in all man has a huge effect on the phosphorus cycle. The amount of total phosphorus in the atmosphere is effected by combustion and biomass burning and both rivers and ocean waters show heavily increased P content in populated areas.

The phosphorus (P) cycle is dominated by water transport. The concentration of phosphorus in the crust is 1200 mg/kg. P is transported to the oceans mainly by rivers. In the oceans the concentration of P is between 1.6 and 108.4 ppb. P is most abundant in the Arctic and Antarctic waters as well as in upwelling regions. In the oceans P is depressed in the summer. Phosphorus is buried by transport to the bottom of the seas by dead algae.

The atmospheric phosphorus is only a fraction of the global cycle: It is in total 4.6 Tg/yr of which 70% falls on land. Phosphorus does not have a gaseous phase and the transport in the atmosphere is thus solely as particulate matter. The atmospheric transport of phosphorus is dominated by mineral dust (82 %), while sea salt, biogenic particles, volcanoes and human activity accounts for the rest. For phosphate mineral dust accounts for 48 %, while the biogenic signal accounts for 38 %. Mineral dust accounts for just 5% of the total pre-industrial source to the oceans. But the atmospheric transport is important for remote ocean sites primary production.

Very little information on the amount of phosphorus in the Arctic exists and even less information is derived on the concentration of phosphorus and phosphate in glaciers. Edwards et al. [2007] are the only ones who have detected phosphorus concentration on the Greenland ice sheet. They found 0.25 ppb P as mean during the last 50 yrs. Detections on glacier run off from smaller glaciers showed concentration of phosphorus between 0.31 ppb and 145 ppb [Chillrud et al., 1994].

Over time the phosphorus cycle has been altered. In glacial times sea level changes have exposed the shelf areas, and thus the P deposited on the shelf is again introduced in the global cycle. The hypothesis is called the shelf nutrient hypothesis and evidence of it has been seen in marine records. In the Holocene a trend of increasing mineral phosphorus was detected indicating cooler conditions, but several short period changes was also observed [Filippelli et al., 2006]. In recent times anthropogenic impact has increased; due to the use of P as fertilizer two times the natural amount is found in rivers and burning of forest also alters the cycle. In the next section information on ice cores use as climate archive as well as some results from ice cores are presented.

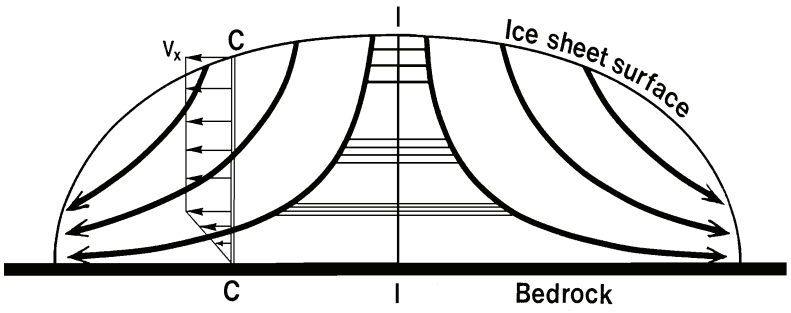

Figure 10: The figure illustrates how the ice flows from the deposition site towards the edges of the ice, making the ice divide (I) an ideal place for drilling, since the snow deposited stays, and as time goes by pressure from the above lying snow thins layers. However bottom melting and bed structures can complicate this picture.

4 Ice cores-a climate archive

This section discusses how ice cores can be used as a climate archive. Processes such as layering and finding the right spot to drill ice cores are explained. Brief information on the dating of ice cores is also presented. Further transportation and deposition effects are discussed, with special focus on the effects related to phosphate and phosphorus. Finally the section compiles information on some of the larger climate variations detected from ice cores as well as the proxies used to detect these climate changes. The information is used as a base for the interpretation of phosphate in ice cores in section 8 and 9.

4.1 Layers - finding the right spot

Using ice cores as climate archives comes down to the fact that yearly layers of precipitation are preserved on the large ice sheets providing a nice chronology, which is drilled and after analysis reveal information on past climate. However some complications are present.

When precipitation falls on the ice sheets of Antarctica and Greenland it only melts when temperatures are above 0 °C. Thus snow is accumulating every year. The imbalance of mass between the region of accumulation and the region of ablation[10] builds up shear stress and eventually the glacier starts to flow from the accumulation zone to the ablation zone. Ideally the flow is hence dependent only on the mass balance, however it is also effected by the height of the ice sheet, the temperature and the slope.

The flow causes the annual layers deposited to stretch under the pressure of the precipitation of the following layers; creating thinner and thinner layers with depth as shown in figure 10. Thus ideally the best place if going for old ice, without flow disturbances, is the ice divide, which is the place where stretching occurs lateral in all directions creating thinner and thinner layers with depth.

However several parameters especially related to the bed complicates the flow. First of all the bed temperature-dependent on the geothermal heat-can cause melting from below, removing layers and increasing the speed of the glacier. A cold bed temperature will reduce the speed, which makes the glacier thicken, insulating the bed, which can cause the bed temperature to raise, again increasing flow velocity, thus thinning the glacier. But basal melting is not necessary a bad thing: if the goal is to have high temporal resolution in a narrow time window, then a place with high precipitation as well as basal melting, reducing the thinning of the ice, can be ideal. Basal melt water can however cause several complications to the drilling.

The geology of the bottom, with obstacles and boulders, can change flow patterns and make bumps that penetrate high into the ice. Besides the shape of the bedrock and the

[10] the melting zone

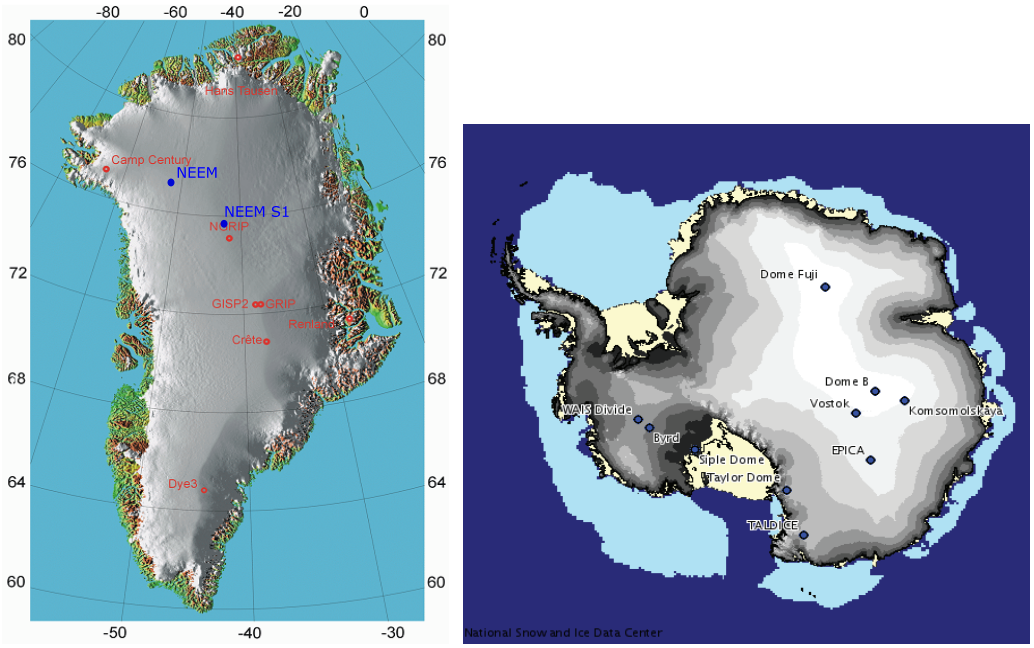

(a) (b)

Figure 11: Positions of deep ice cores. Figure (a) shows Greenland deep ice cores in red and the two ice cores used for this project in blue. Figure (b) show Antarctic deep ice cores.

roughness of the underlying rock influences too. The bumps can cause folding of ice with different age, causing a mixed climate signal in the very deep ice, and one should be aware of this when interpreting ice which originates near the bottom.

Change of the boundary conditions over time should be considered too. *E.g.*, during the last glacial maximum (LGM) the Greenland ice sheet extended onto the outer shelf in Greenland [*Håkansson et al.*, 2007; *Evans et al.*, 2009; *Kelly and Long*, 2009; *Paterson and Cuffey*, 2010]. This has probably also changed the position of the ice divide over time. Thus it can not be assumed that a drilling on the present position of the ice divide will provide the oldest and most undisturbed ice.

Finally climate has changed over time changing parameters such as precipitation rates, and temperature which in turn has changed the viscosity of the ice; the temperature signal is kept in the ice, causing different viscosity of the ice in different depths. Temperature changes can also cause melt layers, erasing some years, making the dating of the ice difficult.

All in all finding the right spot is not easy, but radar measurements are used to find and follow layers in the ice as well as for investigating bed features. Further flow models are used in the process of finding the best position for the desired resolution and time span.

Over the years several deep ice cores have been drilled in Greenland and Antarctica. The position of the cores can be seen in figure 11. The figure also shows the position of the two cores used in this study: The NEEM ice core (77.45°N 51.06°W) and the NEEM S1 shallow core (76.45°N, 44.77°W), a firn core. The NEEM S1 shallow ice core is chosen for phosphate measurements to test the resolution of the phosphate detection method, and the NEEM ice core is chosen, because detection of other parameters were all ready planned. More on the NEEM S1 shallow core and the NEEM core can be found in section

8 and 9.

4.2 Dating the cores

The dating of ice cores is important in order to compare climate information kept in the cores with other ice cores as well as other palaeoclimate records such as marine cores or information from dendrochronology.

The dating of ice cores is done by counting annual layers from various proxies with annual signals such as $\delta^{18}O$, electrical conductivity and some soluble impurities. However as the layers thin, the time resolution deteriorates, requiring another dating method or validation of the counting. A validation can be volcanic signals from huge eruptions, that can be seen on a global or regional scale. Cosmogenic isotopes, such as ^{10}Be, are also used for validation. The validation can help relate dating to other quaternary archives as well as other ice cores.

In places with very thin layers, such as the central Antarctica, the method of layer counting does not work. Here atmospheric gases with long lifetimes, such as methane or diatomic oxygen which varies globally, can be used to compare ice cores world wide.

Older ice can be dated with an uncertainty of 6 kyr by correlating with Milankovich theory (see section 4.4), however this is problematic since the ice core proxies do not correspond directly to sun insolation. Argon gas is depleted of ^{14}Ar over geological time, and can be used to estimate the age of extremely old ice [*Paterson and Cuffey*, 2010].

4.3 Transport and deposition

This section explains some of the processes possibly influencing changes in phosphorus content during transportation between source region and deposition site at Greenland. It also includes general information about deposition and post depositional changes in the ice.

As other aerosols phosphorus is transported to the ice by wind. As explained in section 3.3, most phosphorus and phosphate arrives with dust and thus many of the transport and deposition processes for phosphorus and phosphate relate to dust transport and deposition. However as also explained in section 3.3, phosphorus relates to sea-salt, biogenic material and human pollution such as fertilization and forest fires, too.

When discussing particulate matter in the atmosphere we distinguish between mineral dust, which is non soluble and aerosols, which can contain soluble materials. Aerosols can also be formed in the atmosphere by precipitation, absorption and chemical reactions.

4.3.1 Transportation to Greenland

In order to arrive on the ice from the source, transportation is needed. This imposes different limitations on the source areas of different proxies due to differences in residence time and transport path ways. The residence time in the atmosphere is between 5 and 14 days. The smaller the aerodynamic diameter the longer is the residence time [*Papastefanou and Bondietti*, 1991].

The large cyclone tracks arriving in Greenland in recent times are mainly from the West in summer, while in winter they come in from South-West suggesting source areas west and south-west for Greenland [*Cappelen et al.*, 2001].

In general the aerosols, and thus also the phosphorus and phosphate, that actually make it to the Greenland inland ice is only a fraction of the amount initially coming from the the source. Mixing with other sources, dilution and deposition on the way to

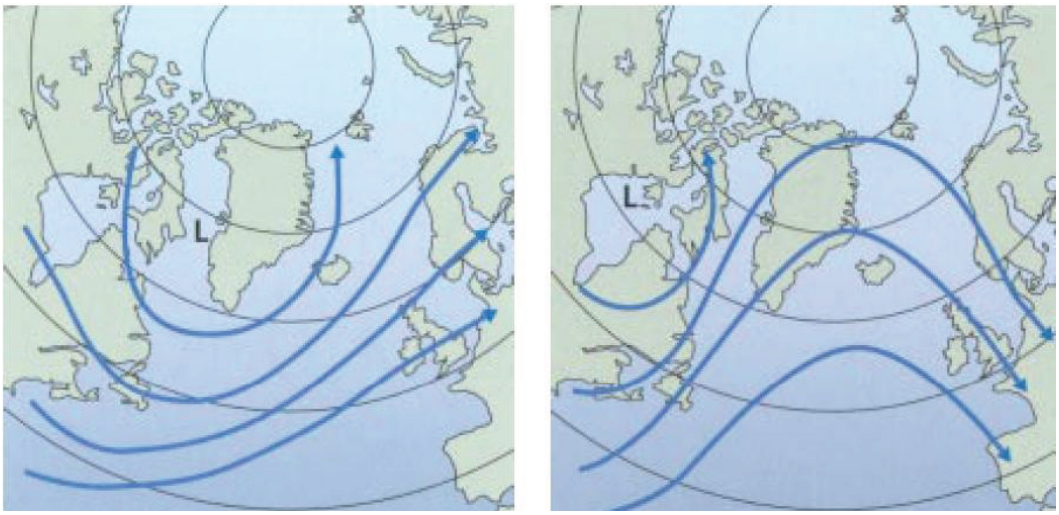

Figure 12: The figure show two typical wind pattern situations nowadays in the area around Greenland [*Cappelen et al.*, 2001].

Greenland changes the original signal from the source and this should be kept in mind when interpreting signals in the ice cores.

4.3.2 Deposition

Figure 13 show the important processes effecting deposition which takes place in the atmosphere, the deposition rate influences on how much of a species actually make it to the ice sheet as well as the amount deposited there. Note that since phosphorus does not have a gaseous phase, the transformation from gas to particulate is not important for phosphorus or phosphate.

The transport of any matter in the atmosphere can be formulated by the global amount of the matter in question in the atmosphere (M), the source strength (SS) and the sink S(M) during transport:

$$\frac{dM}{dt} = SS - S(M) \tag{1}$$

The sink is dependent on global average concentration (C) as well as on the deposition rate (V_d[m/day]). Thus the equation can be written:

$$\frac{dM}{dt} = SS - C \cdot V_d \tag{2}$$

The residence time (T) assuming steady state of any matter in the atmosphere is thus:

$$T = \frac{M}{S(M)} \tag{3}$$

The deposition rate is dependent on several processes, the most important being dry and wet deposition on land and water surfaces. Adsorption on surfaces also influences the amount of phosphate making it to the ice; iron, Mn and Ca does, *eg*, bind phosphate in little soluble compounds. Decomposition by atmospheric chemical and photochemical processes can also occur.

Dry deposition happens by sedimentation. The force of gravity acts on all particles and especially the ones larger than 5 μm will tend to settle fast and they are thus less likely to make it to the interior ice sheets.

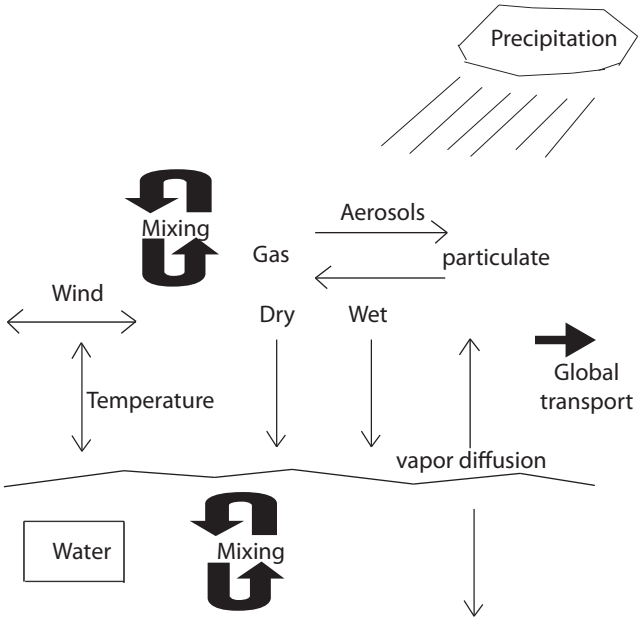

Figure 13: The figure shows the deposition cycle of the atmosphere. Not relevant for phoshorus and phosphate is the phase change between gas and particulates.

Further, electrostatic attraction between particle and surface as well as adsorption and chemical interaction can influence the dry deposition. However these are largest in and near by urban areas.

Wet deposition is removal with precipitation and this includes both snow, rain and combinations thereof. The amount of phosphorus deposited by precipitation is both of particulate matter and dissolved phosphorus in rain droplets. The sodium-(Na_3PO_4), potassium- (K_3PO_4), rubidium- (Rb_3PO_4), caesium- (Cs_3PO_4) and ammonium- ($(NH_4)_3PO_4$)phosphates are all water soluble.

Wet deposition can be either from falling rain droplets containing a solution of phosphate or by droplets or snowflakes scavenging phosphate or phosphor particles on the way down.

A more theoretical approach to wet and dry depositions can be found in appendix A.2.

To account for the different deposition methods, investigation of ions in ice cores is often done both by total concentration [ppb] and flux [$ng/cm^2/year$], which is calculated by multiplying the annual concentration with H_2O accumulation rates [*Kreutz*, 2007].

Chemical reactions are possible between phosphate and others both during transportation and when in the ice. It is suggested that, *e.g.*, Ca^{2+} can bind phosphate in $Ca_3(PO_4)_2$, which is not very soluble. However, in the presence of sulphate and ammonium, phosphate can again come into a soluble form. The reaction can be found in equation 4.

$$Ca_3(PO_4)_2 + 3\,(NH_4)SO_4 \rightleftharpoons CaSO_4 + 2\,NHH_4H_2PO_4 + 4\,NH_3 \tag{4}$$

4.3.3 Postdepositional changes

After deposition on the ice some chemical species can be altered through photochemical reactions. Further diffusion occurs both in the firn and in the ice, and for gases especially the transition between ice and firn is important. However, for all species migration and diffusion occurs in the ice and firn, and when interpreting ice cores these processes should be considered.

4.4 Climate observations from ice cores

In this section major climatic events are described and more detailed information on which proxies are useful for what sort of climatic informations is presented.

Ice cores span a wide range of time scales. The oldest ice core is the Antarctic Dome C, which is assumed to span the last 800.000 yr. In Greenland the oldest core, which was recently drilled, is the NEEM ice core. The NEEM ice core is estimated to span further back than the Eemian, which is the previous interglacial period lasting from 130.000 B.P. to 110.000 B.P.

Before ice cores were measured, climate was believed to be relative stable over time, but ice cores have shown evidence of a highly variable climate, containing rapid fluctuations happening within only few decades. The climate record of the last glacial can be seen in ice cores such as the Greenland North-GRIP ice core (figure 14).

4.4.1 Measurements - what have we learned from ice cores

A variety of climate information can be detected using ice cores. A selection of those will be presented here.

The Milankowich theory hypothesises that the changes between glacial and interglacial periods are caused by change in the solar insolation. Changes in the solar insolation happen due to changes in the orbit of earth around the sun, eccentricity of the orbit and tilt of the earth axis. Variations show periodicity of 19, 23, 41 and 100 kyr and is seen in ice cores. The correlation between the Solar insolation and the Antarctic ice core Vostok can be seen in figure 15.

Holocene is the present interglacial period, which began 11.700 yr ago and is a period of relative stable warm climate. Evidence from palaeoclimate archives suggest that the temperature was highest during a climatic optimum in the period being in the range of 8000 to 6000 B.P. and that it has been slowly cooling since.

Last Glacial Maximum (LGM) took place 20.000 yr ago and evidence from ice core suggest a cooling of 20°C in the north, while marine cores show a cooling of 3-5°C compared to the Holocene. There is evidence of changes in the greenhouse gas concentration, in the insolation, changes in the surface albedo feedback from larger white surfaces, and the highest amount of aerosol and dust are found in this part of the ice [*Paterson and Cuffey*, 2010]. Evidence of a sea level down to 120 meter lower than the current is seen in marine sediment cores.

Heinrich events and Glacial interstadials Heinrich events were first seen in marine sediment cores, and show variations on glacial time scale (65 kyr-14 kyr BP) with a periodicity of 7000-1000 yr. They are believed to correlate with the Laurentide ice sheet surges, sending large floods of ice bergs into the ocean. It is suggested that the Heinrich events started with a slow growth of the Laurentide ice sheet over time making the bed temperature increase. At some point bed melting point was reached and fast flow started a surge. The surge made the ice thin, creating a steeper temperature gradient and eventually the melt water refroze to the bottom, stopping the surge [*Paterson and Cuffey*, 2010]. Glacial interstadials (GI), or Dansgaard-Oeschger-events as they are also called, are very rapid variations having a close to 1500 yr cycle, visible in the Greenland ice cores. It is evident from the ice cores that the GI's start of very quickly with a warming as fast as a temperature change of 8 °C in only 40 yr, however changes of 5 °C during a period of 30-40 yr is more common.

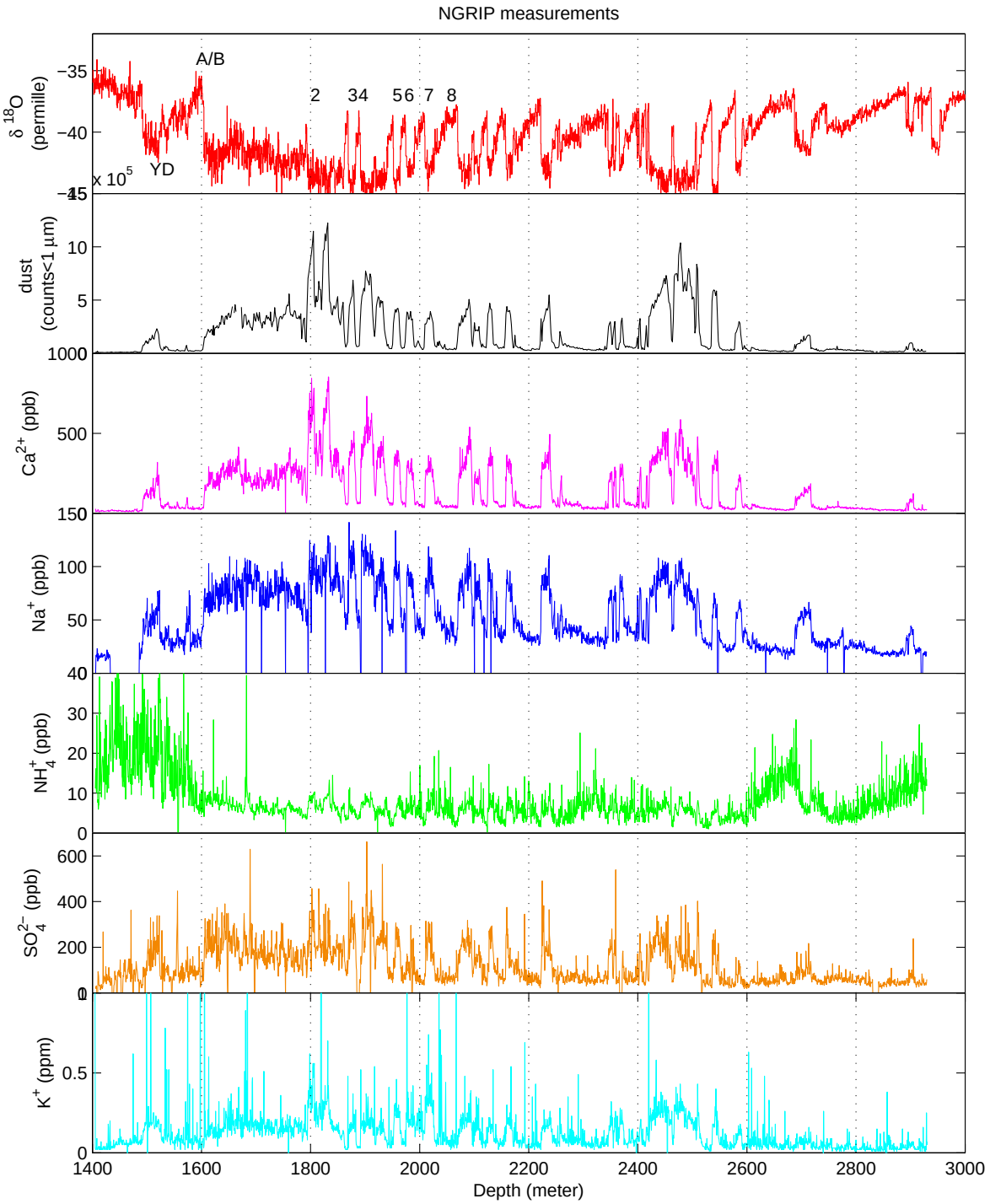

Figure 14: Measurements from the Greenland North-GRIP ice core. Top: $\delta^{18}O$, which is believed to be a proxy for temperature. Then dust (black) and Ca^{2+} (pink), which is believed to show dust signals. In blue Na^+ a sea salt proxy. NH_4^+ is a tracer for biogenic land sources (green). In orange SO_4^{2-}, which has various sources including volcanic eruption and finally K^+, which represents a mixture of dust and sea salt and possibly also some biogenic signal such as forest fire. The period covers the last glacial. YD denote the younger dryas and A/B is the Alling-Bollerod warm period. The numbers denote periods of glacial inter-stadials, more than 8 are present, but the rest are not numbered here [*unpublished*, 2004; *Ruth et al.*, 2003].

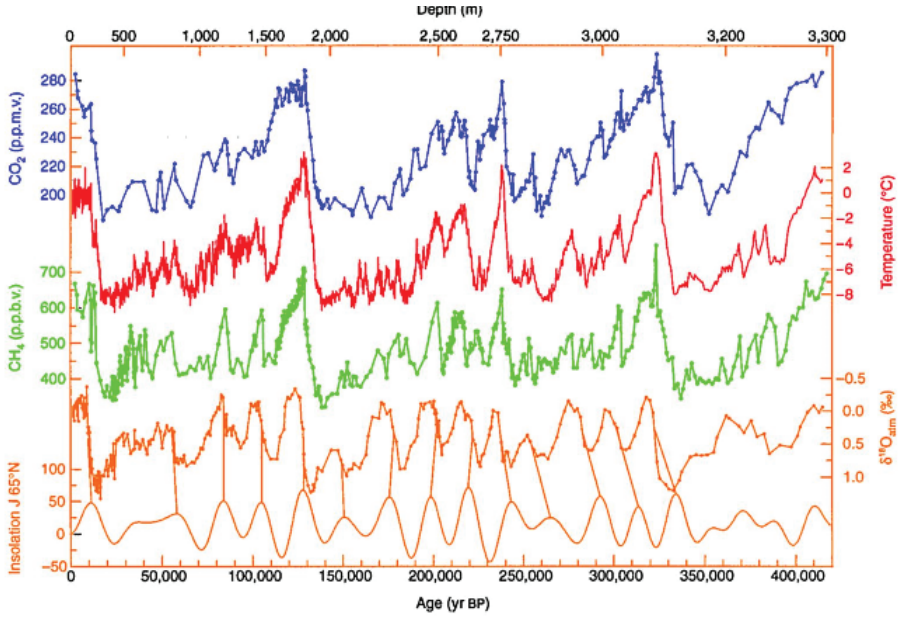

Figure 15: CO_2, temperature, methane, and δ^{18}O from the Antarctic ice core Vostok, and the solar insolation changes. The section shown covers 4 glacial periods.

It is suggested that the GI's are caused either by solar radiative forcing changes or by deep ocean circulation changes. GI's correlate with the Heinrich events and it is therefore believed that the same mechanisms drive the two. The GI's are represented by numbers in figure 14, note that more than 8 are present in the section shown, but not numbered.

Measured species, sizes and interpretation from Greenland ice cores

Many species have more than one source, and the interpretation is not always straight forward. Here I aim to shortly discuss the interpretation of various species.

δ^{18}O and δD δ^{18}O is given by $\delta^{18}\text{O} = \frac{^{18}O/^{16}O_{sample}}{^{18}O/^{16}O_{SMOW}} - 1$, where SMOW a measurements made in a standard mean ocean water. To a first approximation the $\delta^{18}O$ show a linear dependency on temperature. When the $\delta^{18}O$ is low temperatures are low and when the $\delta^{18}O$ is high temperatures are high. The effect is due to the rain out of heavy isotopes, which means that there is also an effect as a function of height above sea level and how far north the ice core is positioned. The same is essentially the case for δD.

Sea salt Sea salt is enhanced in cold periods and is anti correlated to δ^{18}O. On a sub annual scale sea salt is enhanced in winter time. This has led to speculations, because one would expect sea salt concentrations to be high, when the ocean is near by and not when sea ice covers the ocean. The high sea salt concentrations in cold periods is explained by stronger winds or brine in newly formed sea ice or frost flowers, both of which have increased amounts of salt relative to sea water [*Kreutz*, 2007]. Many of the species which represent sea salt also represent other natural phenomenons, hence the non sea salt component is calculated by $[X_{nss}] = [X_{tot}] - [X_{ss}]$, where $[X_{tot}]$ is the total amount of the species in question and $[X_{ss}]$ is the sea salt part calculated by assuming that all Cl^- is from sea salt and using the ratio normally

found in sea water between Cl^- and the species in question. The bulk ratio between Na^+ and Cl^- often is the same as found in sea salt suggesting that both are mainly sea salt signals. Species which have a partial sea salt signal are for example, Ca^{2+} (7%), SO_4^{2-}(12%), Mg^{2+}(51%) and K^+(27%), where the percentages denote the percentage related to sea salt in the Renland ice core [*Hansson*, 1994; *Kreutz*, 2007]. The sea salt variation between Glacial stadials and inter stadials is approximately a factor 3.

Dust Dust is wind borne minerals. These affect climate both direct and indirect: Direct by scattering and absorption of solar radiation. Indirect by changing cloud properties, which then affect the radiation budget. Another indirect effect is the fertilizing of the ocean with Nitrate and Iron. The dust source for Greenland ice cores is the East Asian desert in Western China and the inner Mongolia [*Svensson et al.*, 2000]. In recent times mineral dust arrives from west, which exclude Sahara as a source. The dust can be divided into a soluble part, which is measured by the Ca^{2+}, and a nonsoluble part which is measured by counting particles seen by an Abakus (see section 5.1.3). The two normally correlate to a high degree. All of the non sea salt part of Ca^{2+}, Mg^{2+} and Na^+ is believed to be a dust signal as is part of the non sea salt K^+, SO_4^{2-} and NO_3^-. Maximum concentrations of dust in Greenland ice cores are found during spring months. Changes in the amount of dust found in ice cores can be due to changes in the mobilization in the source area, transport changes, loss properties *en route* and deposition effects. This means that the amount of dust deposited on the Greenland ice sheet can represent changes in the chemical and physical weathering at source area or wind speed changes, changes in vegetation as well as terrain changes as for example sea level changes. The amount of dust has been highly variable during time. The flux of dust is two to five times larger in the glacial than in the interglacial [*Maher et al.*, 2010]. In the Holocene non-soluble dust concentrations of 33 μg/kg was found in the Greenland ice core GRIP, and levels of 0.72 μeq/kg Ca^{2+} [*Steffensen*, 1995][11]. In the NGRIP the amount of dust is found to be 100 time larger in the glacial while stadial (GS)-interstadial (GI) transitions show changes of approximately a factor of ten. The amount of large dust particles is found to increase by 10% in the GS's compared to the GI's, this is suggested to indicate shorter transportation times because of higher wind speeds [*Ruth*, 2005] further it is believed that glacial periods are much dryer than inter glacial periods. For the last glacial maximum the GRIP core showed a level of 7600 μg/kg nonsoluble particles and 31.02 μeq/kg Ca^{2+} [*Steffensen*, 1995] and particles larger than 2 μm increased by 25 % [*Ruth*, 2005].

Biogenic . Biogenic emmisions play a large role in the SO_4^{2-} cycle. Measurements of SO_4^{2-} in the presence of methane sulfonic acid (MSA) is believed to show evidence of the marine biogenic signal of phytoplankton. Such measurements in the Vostok ice core, Antarctica, have proven larger marine productivity during the LGM. However correlations have also been found to sea ice extent suggesting algae production within and on top of the sea ice [*Kreutz*, 2007]. Land emissions are believed to be evident in the NH_4^+ record. NH_4^+ is believed to show both soil and vegetation emissions as well as biomass burning. Biomass burning can also be detected from NO_3^-, which however also has an atmospheric source. Another biomass burning proxy is vanillic acid. There is also the possibility that an increase in K^+ can be found related to biomass burning [*Hansson*, 1994; *McConnell et al.*, 2007a]. Nitrate and ammonium

[11] μeq times the molar weight times the charge gives the concentration in grams

are among the very few species which drop to low values in the glacial. Ammonium drops by a factor of 5. It is suggested that the minimum ammonium content during the period 21 kyr-18 kyr B.P. is due to the maximum extent of the Laurentide ice sheet, inhibiting soil and vegetation emissions over large parts of North Amerika [*Fuhrer et al.*, 1996]. The biogenic signals show spring peaks [*Hansson*, 1994].

Volcanic Volcanic eruptions are shown by a highly elevated signal in non sea salt SO_4^{3-} and H^+, but also species such as F^- and Cl^- can show signs of volcanic eruptions. Significant volcanic layers are used for cross dating ice cores [*Hansson*, 1994; *Kreutz*, 2007]

Anthropogenic Increases in SO_4^{2-} and NO_x during the last 50 to 100 years have been seen in Greenland ice cores suggested to resemble the increased industrial processes and fossil fuel use. The amount heavy metal (Pb) has also been shown to increase until it became obligatory that cars had a filter and Pb was removed in gasoline. The black carbon signal had a seven fold increase in the period 1850-1950, suggested to be a sign of the industrial revolution [*Kreutz*, 2007; *McConnell et al.*, 2007a;b].

Ice cores provide valuable information on past climate. Climate variations covering the time periods back to and including the last interglacial using Greenland ice cores and covering the last 800 kyr using Antarctic ice cores can be detected. The temporal resolution is dependent on the amount of annual precipitation. When choosing where to drill an ice core, parameters such as annual precipitation, bottom features and ice flow should be considered. The ice cores can be dated using annual layer counting and cross references such as volcanic layers can be compared to other ice cores as well as to other palaeoclimate records. The two Greenland ice cores used for this study are the NEEM S1 shallow ice core and the NEEM ice core. When interpreting proxies detected in the ice, one should be aware of transport mechanisms and deposition rates. For Greenland most weather arrives from west, and deposition can occur as either dry or wet deposition. One should also be aware of post depositional changes, including both diffusion and migration. Ice cores have given proof of a very variable climate in the past. In Antarctic ice cores, several interglacial cycles are evident. Greenland ice cores show large variability within the last glacial period, having mild glacial interstadials in between the cold glacial stadials. The cold periods have higher loads of almost all impurities. Glacial and interglacial stadials show changes of a factor 10 for dust proxies, while sea salt proxies only show a change of a factor 3. Dust load is especially high during last glacial maximum, probably due to a combination of lower sea level and increased wind speed. In the next section information on the continuous flow analysing systems used to detect various ions in ice cores are presented.

5 Continuous flow analysis (CFA)

In the previous section information on why we can use ice cores for getting a climate record for the past was presented as well as some climate signals detected in the ice. This section gives general information on continuous flow analysis (CFA) of ice cores, which is an analysis method providing the opportunity of fast, continuous measurements of chemical species, combined with high resolution. Discussion of the core preparation and melting as well as the methods used for conducting CFA measurements, with special focus on the absorption method is presented. More specific information on the differences between the CFA system in Copenhagen and the CFA system in Bern, the two systems used for this project, is provided through out the section but is summarized in section 5.3.

5.1 CFA measurement methods

The Continuous Flow Analysis (CFA) method for ice cores is a system developed for measuring ions in a continuous flow. The advantage of such a system is, compared to discrete measurements, a higher spatial resolution combined with reduced handling of the core minimizing the time consumption as well as the contamination risks.

The CFA system consists of a melt head, which continuously melts the ice splitting it in two streams; an inner part going to analysis and an outer part going to waste, in order to avoid contamination from handling.

The liquid from the inner part is debubbled to remove air from the water and make the flow steady. The flow is split into different detection lines, and each line typically has a flow rate of 1 mL/min. These low flow rates are necessary because of the small quantities of ice available. Dust and conductivity is measured directly in the water stream, while different ions are measured after adding reagent and buffer using an absorption or a florescence method [*Sigg et al.*, 1994; *Röthlisberger et al.*, 2000; *Kaufmann et al.*, 2008].

A schematic illustration of a CFA system for measuring ions can be seen in figure 16.

5.1.1 Preparing the ice

The ice core has a diameter of between 7 cm and 10 cm and each piece has a length of close to three meters when drilled. It is split into pieces of 55 cm for transportation (a so called bag). The CFA only gets a part of the ice; the rest is used for measuring other proxies. The ice core is split as seen in figure 17 and only the middle part, which has not been touched is used for CFA measurements. It has a size of about 3.5 cm·3.5 cm.

To avoid contamination end parts and places that have breaks are removed before measuring. At NEEM it was removed using a planer, which means approximately 0.2 to 0.5 cm were removed of the ends, and at breaks 0.2-0.5 cm was removed, too. For the NEEM S1 shallow core an automatic saw is used to remove the end and break parts. It removes at least 0.5 cm. In the bottom of the NEEM and Copenhagen cores approximately 3 cm of milli-Q ice[12] is added to make the change from water to ice measurements as smooth as possible. A schedule of how breaks are removed can be seen in figure 18.

At the NEEM camp the breaks are removed from the ice in the room where the melt head is standing, at a temperature of -25°C and after cutting the ice is put directly into a holder that fits the melt head. Each core prepared for melting has a length of 110 cm (2 bags).

In Copenhagen the freezer facilities are in the basement and the cores are cut in the freezer at -15 °C and then put in plastic bags to avoid evaporation while moving the bags

[12] milli-Q ice is ice made from water highly de-ionized in a milli-Q plant (milli-Q water)

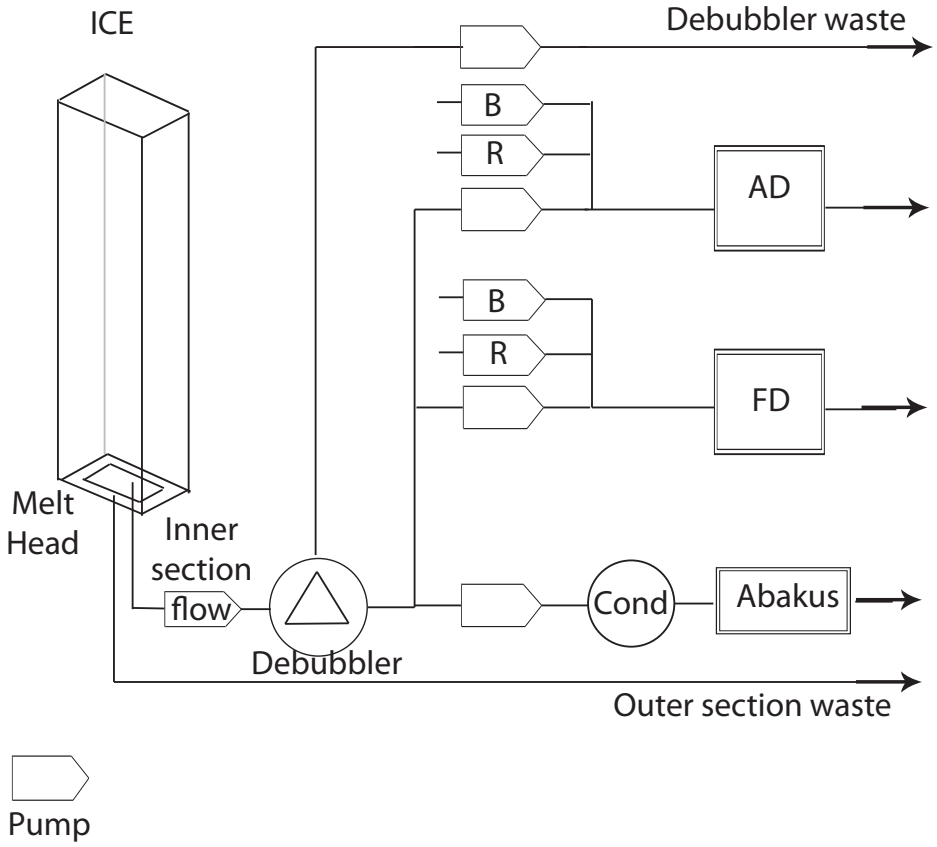

Figure 16: Schematic of automatic flow analysis system. The ice is melted and the melt water split in an inner and an outer flow. The inner flow goes through a debubbler and is split into various detection lines. Conductivity (cond.) and dust (Abakus) are measured. Other lines are added reagent (R) and buffer (B) before detection with absorption (AD) or florescence (FD) takes place.

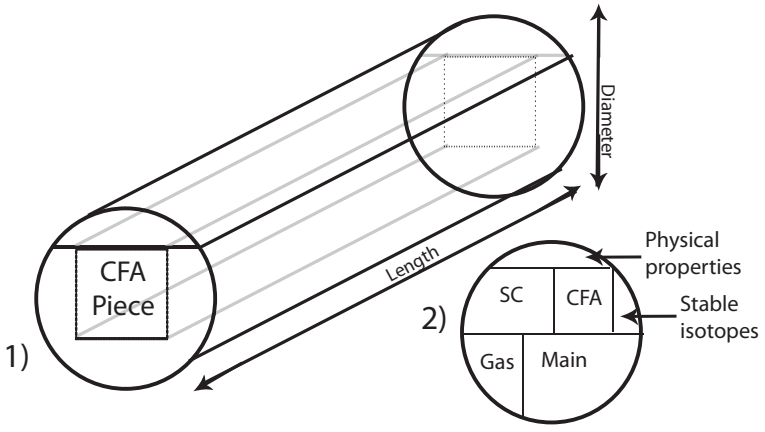

Figure 17: The figure shows how only the central parts of an ice core is used for CFA measurements to avoid contamination. 1) shows the cutting prescription used for the NEEM S1 shallow core, it has a diameter of 7.62 cm and 2) show the cutting sheet for the NEEM deep ice core, which has a diameter of 10.2 cm. The deep core is split into a CFA piece, a piece for discrete gas measurements, a piece for stable isotope measurements, a piece for physical properties and a steering committee piece, of which measurements yet to be decided should be conducted and finally the main piece, which is saved for better ideas in the years to come.

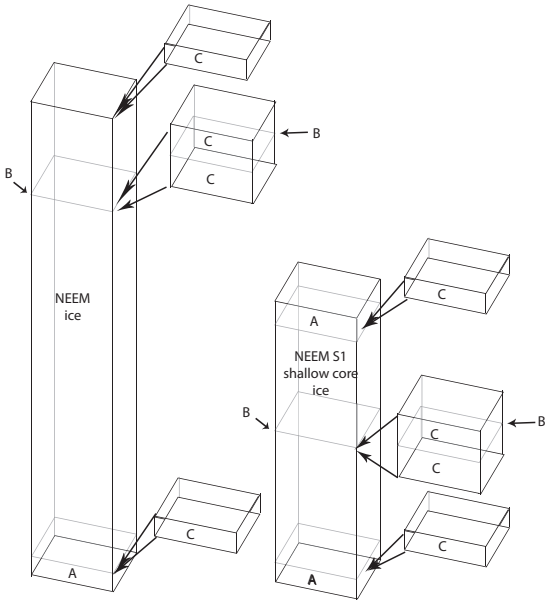

Figure 18: The figure shows how the ice is prepared for CFA measurements. To the left illustration for preparation of the NEEM ice core. To the right preparation of the NEEM S1 shallow core. A is a piece of milli-Q added in the ends, B is the position of a break and C illustrate removed ice, due to risk of contamination at break position and in ends.

to the 2nd floor where the CFA laboratory is positioned. The melt head is in a small freezer and 1-2 cores are prepared at a time in the basement freezer and moved to the laboratory. Those, which is not melted directly, is kept in the plastic bags in the small laboratory freezer. The ice in Copenhagen has been moved in boxes from the Greenland ice sheet and due to the size of the boxes each piece of ice is only 55 cm long.

5.1.2 Melting the ice

The melt head should provide a non reactive chemical surface, and have a design, which ensures that as little mixing as possible occurs and at the same time avoids contamination from the outer part of the core.

One of the fundamental ideas of the melt head is that it splits the outer possibly contaminated ice core from the clean inside. A schematic of a melting device can be found in figure 19.

The ice is placed vertically on top of the melt head and pressed down by its own weight and by an extra load weighing approximate 100 g.

The melt head is heated to a temperature sufficient to maintain the flow needed for all parameters to be measured. Usual temperatures are between 15 and 48 °C depending on the amount of detectors attached and on the desired time resolution [*Sigg et al.*, 1994; *Röthlisberger et al.*, 2000; *Kaufmann et al.*, 2008].

The melt unit can be made from many different materials and have many different shapes as well. *Sigg et al.* [1994] and *Röthlisberger et al.* [2000] used a melt head made in aluminium and surface coated with PTFE, while *Kaufmann et al.* [2008] made a chemical inert surface on the melt head with a copper plated, electroless nickel covered and then gold covered surface.

When the ice is melted the melt head splits the melt stream from the outer part of the core from that from the inside of the core. It is important that only the necessary fraction of the outer part is removed, to keep the amount of water for measurements high. The diameter of the inner melt section can be from 10 $mm^2 \cdot$ 10 mm^2 to 26 $mm^2 \cdot$ 26 mm^2. The soak in the inner section is smaller than the amount from the ice actually melted in the inner section making sure no water from the outer section is sucked to the measurement side. Recent melt heads have several wholes for the water to be soaked through rather

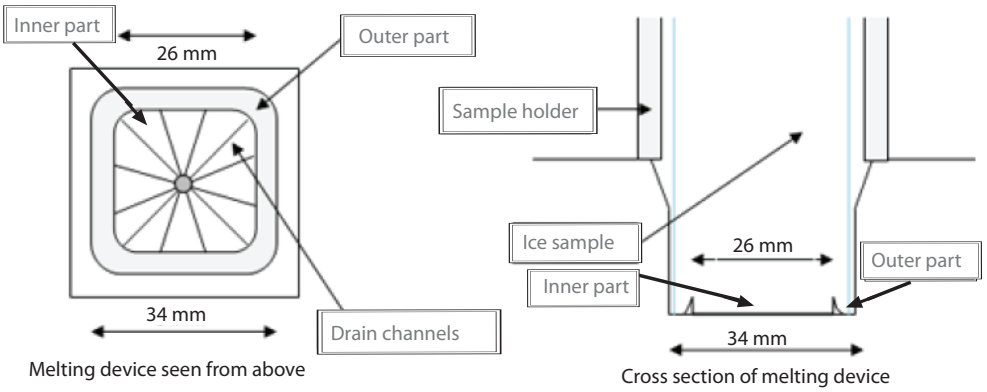

(a)

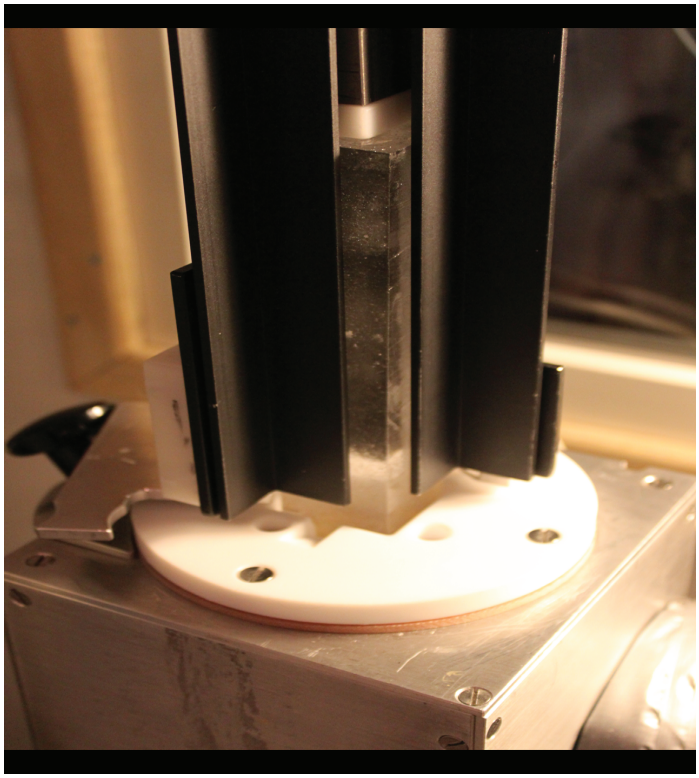

(b)

Figure 19: (a) is an illustration of the melting device used in the Copenhagen set-up. Note how the inner and outer parts are separated to avoid contamination *Nielsen* [2009].(b) is a picture of the melting at NEEM.

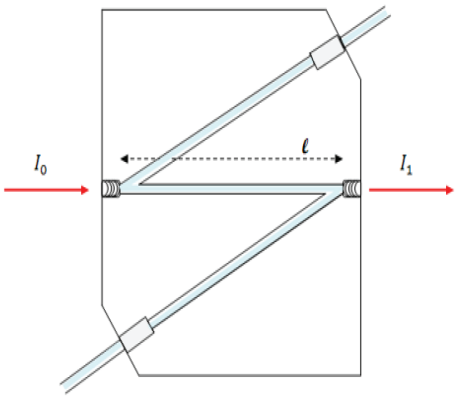

Figure 20: The figure show an example of an absorption cell [*Nielsen*, 2009].

than one, to make the mixing on the melt head lees pronounced, but this at the same time requires that the lines and suction on the lines are similar.

For firn ice melting it is important to keep a relative high soak because of capillary forces in the ice dragging the water up into the ice during melting and thus diminishing the temporal resolution of the measurements. A melt head with several radial narrow slits can make the capillary force in the melt head larger than those in the ice [*Röthlisberger et al.*, 2000].

5.1.3 Detection methods

In the following different methods used for detection of species in the ice using CFA is presented. After melting, the water is measured for different ions by absorption or fluorescence methods. This usually requires mixing with different chemicals. Dust and conductivity is measured, too. Further combinations of CFA melting methods and ion chromatography (IC), Gas measurements and ICP-MS has developed in the recent years. In the following a presentation of the different detection techniques used in combination with CFA is presented.

Absorption. Absorption detection methods all have in common that the fluid concentration of the species in question is measured by the absorption of light. The fluid is led into a waveguide of length l and the intensity of incoming light (I_0) is absorbed so only a smaller fraction makes it through (I). Figure 20 illustrates such a waveguide.

Absorbance is given by the Beer-Lambert equation:

$$A = \beta \cdot \varepsilon \cdot l \cdot c = -log_{10}(\frac{I}{I_0}) \tag{5}$$

where ε is the wavelength dependent molar absorptivity ($M^{-1}cm^{-1}$) and β is the absorption coefficient of the liquid wave cell used, l is the path length (cm) and c is the molar concentration (M)[*Adornato et al.*, 2007]. I_0 is the light emitted by a lamp and I is the intensity measured on the other side of the liquid. The equation can also be written:

$$I(l) = I_0 \cdot 10^{-\varepsilon \cdot \beta \cdot l \cdot c} \tag{6}$$

Note that an increase in length of the cell gives a better limit of detection.

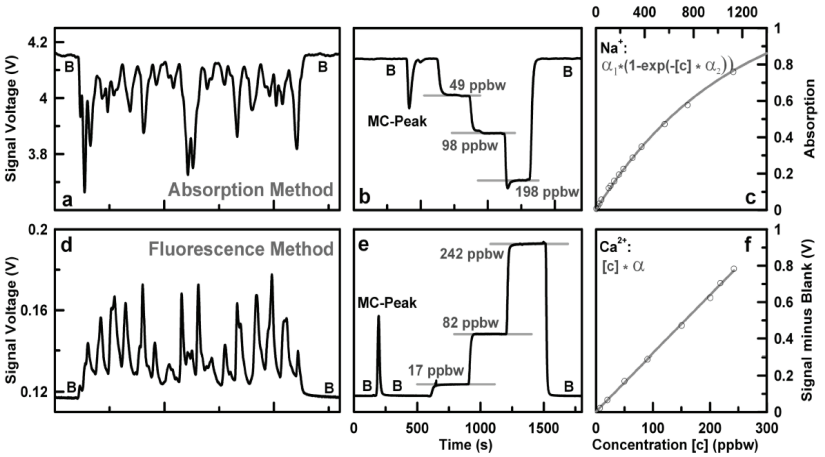

Figure 21: The top row shows absorbance (a,b,c) and the bottom row (d,e,f) shows flouresence. a) and d) is examples of raw signals measuring a 110 cm ice core. B denotes blank-sample without the species of interest. b) and e) is example of standards used for calibration. c) and f) show typical calibration series *Kaufmann et al.* [2008].

The combined factor of $\varepsilon \cdot \beta \cdot l$ can be calculated using standards of known concentration. The absorption is found by the difference between detected light in a sample without the species to be detected and sample with the species we want to detect. Thus concentration can be found using equation 5.

In figure 21 (top) examples of an absorption signals are shown.

Examples of species measured in ice cores using a CFA method in combination with absorption detection techniques are Na^+, NO_3^- and SO_4^{2-}.

Flourescence. Fluorescence detection techniques are also dependent on a light source. If a molecule is excited by a beam of light to a higher energy state by absorbing a photon and the molecule decays to the ground state a photon is again emitted. The emitted light will have same or a lower energy as the absorbed light and thus the detection can be done at a different wavelength from the wavelength used to excite the molecule. The emission is fluorescence which can be detected after using a filter to make sure that only of the emitted light is detected.

In figure 21 (bottom) examples of a florescence signal is presented.

Examples of species measured in ice cores using fluorescence detection are Na^+, Ca^{2+} and NH_4^+.

Mineral dust. Mineral dust, particles that are insoluble, is measured using an Abakus. The water stream that enters the Abakus has to go through a very narrow split and the idea is that only one dust particle at the time can enter the split, making all the dust line up nicely. A laser is mounted orthogonal to the flow and a detector is on the other side of the flow. Detection of mineral dust is made by counting the time the laser is shut off due to particles blocking the light. The size distribution is determined by detecting the scattered light and using a comprehensive algorithm made by comparing Abakus measurements to a coulter counter[13]. The Abakus produces results in [counts/sec] however it is needed recalculated to [counts/cm]. Thus the exact flow through the Abakus must be known and for that purpose a flow counter is positioned right after the Abakus.

Conductivity. The electrolytic conductivity gives a bulk signal of all the major ions. It will often resemble the dust signal, because the Ca^{2+} ion is the most predominant.

[13] A coulter counter is another and more precise way of measuring particles.

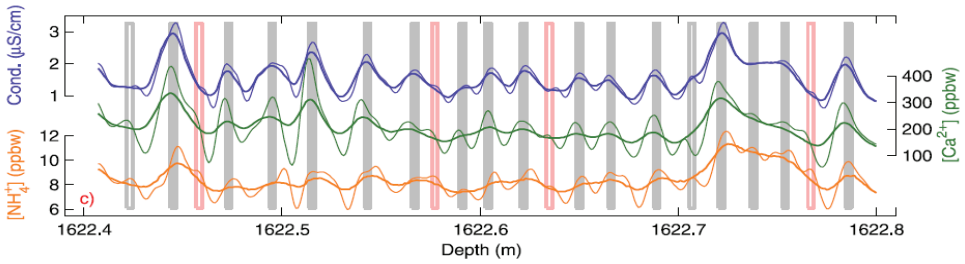

Figure 22: The figure show an example of original (thick lines) and deconvoluted (thin lines) data [*Rasmussen et al.*, 2005].

The conductivity also resembles volcanic signals since the SO_2 emitted by the volcano will show up as H_2SO_4. Further biogenic signals and organics is visible.

ICP-MS, FIC and CFA-Gas. CFA systems can also be set up to detect using inductively coupled plasma mass spectrometry (ICP-MS), Ion Chromatography (IC) or detect gas using a PICARRO detection cell. These methods are not used for this study, but a description of them can be found in appendix A.3. Neither the IC or the ICP-MS actually detects continuously: A two way valve is set up to allow one sample into the ICP-MS or IC at the time, while a second system gets sample while the first detects, thus creating semi-discrete measurements. When two systems run simultaneously this way a high time resolution can be accomplished.

5.2 Treatment of CFA data

In order to enhance the data acquired by CFA methods a deconvolution procedure can be applied. An example of such can be seen in figure 22.

Deconvolution is an algorithm based tool used to calculate back the signal of dispersion that happens in the measurement system. The algorithm require that the shape of a delta peak or a step function in ones system is known, this is used for creating a filter that can be applied for the data.

In the case of most of the above mentioned detection methods, some standard calibration is done, this calibration essentially provides the step function necessary for doing the deconvolution. However, the standards used for calibration are not introduced at the same position as the ice. Hence only restoration of details lost through mixing coming in the part after standard introduction can be accounted for [*Rasmussen et al.*, 2005].

After deconvolution the ionic balance can be investigated. The ionic budget in ice cores can generally be written as the sum of all ionic species present. However some species, *e.g.* phosphate, contributes very little to the ionic budget. The most important ions accounting for 95 % should in principle balance when in the atmosphere and thus they are also expected to balance when trapped in the ice. Checking up on the balance of the ions can be done by equation 7.

$$[Na^+] + [NH_4^+] + [K^+] + [Ca^{2+}] + [Mg^{2+}] = [Cl^-] + [NO_3^-] + [SO_4^{2-}] \quad (7)$$

If assuming an atmosphere in ionic balance over time The ionic budget provides a method for checking if the measurements of the ions seem plausible [*Kreutz*, 2007].

Table 2: The table show the difference between the Bern CFA system used for the NEEM deep ice core on Greenland, which is optimized for many species and the Copenhagen CFA system used for the NEEM S1 Shallow core, which is optimized for high resolution.

CFA system		**Bern**	**Copenhagen**
Melt head	*material*	Copper, electroless nickel (5μm), gold (2μm)	Aluminium
Inner section	*size*	24 mm x 24 mm	26 mm x 26 mm
	suction wholes	6 concentric	one central
Outer section	*size*	36 mm x 36 mm	34 mm x 34 mm
	suction wholes	6 concentric	4 concentric
Melt speed		3.5 cm/min	1.5 cm/min
Overflow		20 %	10 %
Sample length		110 cm	55 cm
Measuring time	*per sample*	32 min	37 min
Water flow rate		15.2 mL/min	6.7 mL/min
Conductivity		Yes	Yes
Dust particles		Yes	Yes
Total air content		Yes	No
Species		Na^+, NH_4^+, SO_4^{2-}, Ca^{2+}, NO_3^-, H_2O_2, HCHO	Na^+, NH_4^+, SO_4^{2-}
Gases		Yes	No

5.3 CFA systems used in this project

Two different CFA systems were used for this project. One is the Copenhagen CFA system, used for testing and optimizing of the method and for detection of phosphate in the NEEM S1 shallow core. The second system was the Bern set-up, which was used in the field on Greenland for detection of phosphate in the NEEM deep ice core.

The goal in the Copenhagen system is to achieve very high temporal resolution. Thus the melt speed and flow is kept relatively small, but still sufficient that all detection units get enough water. The Copenhagen CFA system measures 55 cm at a time and takes approximately 35 minutes. The mean melting speed is about 1.57 cm/min. The set-up detects Na^+ using an absorption detection method, NH_4^+ using a fluorescence method as well as dust and conductivity. The Copenhagen melt head is 34 x 34 mm large and is divided in two sections. The inner section used for detection is 26 x 26 mm.

The Bern set-up used for the NEEM ice core is made for detecting many species rather than achieving high temporal resolution. In the NEEM set-up 110 cm ice was melted in about 32 minutes. The NEEM system measures 7 different ions (excluding phosphate) as well as total air content, dust, conductivity, black carbon and some gases. Further the water from the outer part is divided in 6 samples and used for IC measurements, Tephra measurements [14] and others. The melt head used at NEEM is the melt head by *Kaufmann et al.* [2008], with a chemical inert surface and 6 concentrically positioned drain off holes for the inner part as well as six for the outer part.

In table 2 comparison of technical details between the two CFA systems can be found.

[14] Tephra is ash from volcanoes

In this section information on Continuous Flow Analysis (CFA) is provided. When using CFA for ice cores, the ice is cut to fit a melt head. To avoid contamination the melt water from from the outer side of the ice core is separated from the inner side, which is used for detection. Several detection methods have been combined with CFA; these include absorbance and fluorescence techniques for detection of ions, detection of mineral dust using an Abakus and conductivity detections. Semi continuous detections can be done using the melt system in combination with IC and ICP-MS. Further gas systems have been developed in recent years for CFA systems. A better resolution of the detected species can be obtained by deconvolution of data, which will remove some of the dispersion coming from the detection system. Further assuming a neutral atmosphere in time the ionic balance can be used to check the size of measurements for the major ions present in the atmosphere.

In this thesis two CFA systems have been used. The Copenhagen CFA system was used for optimising the system chosen for phosphate detection and for detecting phosphate in the Greenland NEEM S1 shallow ice core. The other system, the Bern system, was used for detection of phosphate in the Greenland NEEM ice core. The Bern CFA system is optimized for many species, while the Copenhagen CFA system is optimized for high resolution. Thus the melt heads in the two systems are different: The Copenhagen CFA system has a larger inner section and a small overflow from inner to outer section and the water flow is kept low about 6.7 mL/min, while the Bern set-up runs with 15.2 mL/min. The preparation of ice cores in the two systems are slightly different, for both ice cores Milli-Q ice are added in the end and melted first, and breaks and ends are removed. Exactly how much is removed and how it is removed varies in the two CFA systems. The next section presents methods available for the detection of phosphate. When choosing a method it was important that it fulfilled the requirements coming from the CFA system.

Table 3: Left: Different aspects that should be considered when choosing methods or instruments is present. Right: Examples of options.

Sensitivity	picomolar, millimolar
Specificity	unequivocal species identification
Range	picomolar, millimolar
Accuracy	relative % error
Precision	relative % error
Measurement frequency	seconds, hours
Endurance	hours, months
Versatility	single analyte, multiple analytes
Sample requirements	microliter, deciliter
"Intelligence"	adaptive sampling, periodic sampling
Power requirements	milliwatts, kilowatts
Cost	cost/instrument, cost/measurement

6 Methods available for phosphate detection

In the previous section continuous flow analysis was presented. This section presents available methods for detection of phosphate. The method which is chosen should meet the constraints given by continuous flow analysis and be capable of detecting the low concentration of phosphate expected to be present in ice cores.

When choosing a method for measurement of phosphorus (P) or phosphate (PO_4^{3-}) in ice cores several issues should be considered. The section contains a list of criteria, which in general should be considered when choosing a detection method.

Special attention is given to spectral methods because they have the advantage that they are easy to implement in continuous flow. Optimization approaches for lowering the limit of detection is presented.

Finally I explain in detail the absorption method using a 2 meter long liquid waveguide by *Zhang and Chi* [2002], which is the method chosen as base for implementing measurements of PO_4^{3-} in continuous flow for ice core measurements. I also look at draw backs and interferences using the method by *Zhang and Chi* [2002] combined with a presentation of optimization possibilities of parameters such as concentrations, pH and mixing time.

6.1 Restrictions on the method

When deciding on a detection method all the issues in table 3 should ideally be considered.

However for measuring P or PO_4^{3-} in ice using Continuous Flow Analysis (CFA) the most difficult and limiting constraints was to find a method with the necessary sensitivity. From *Edwards et al.* [2007] it was known that the level of P in Greenland ice in recent years was no larger than 0.25 ppb. At the same time CFA has a high measurement frequency, making steps such as preconcentration difficult, and very little sample is available, only of order 1 mL/min. Further for detection of PO_4^{3-} in ice cores a robust method is desirable, so transport to and from the ice does not adversely affect equipment.

6.2 Available continuous methods for measuring phosphate in water

The methods available for P and PO_4^{3-} detection can be split between optical methods and electrochemical methods. The optical methods comprise visible spectrometry, florescence spectrometry, chemiluminescence photometry and more.

The electrochemical methods, such as potentiometry, voltammetry and amperometry, all have high limit of detection (LOD$\geq$0.1 ppm) and since with these methods not many

optimization methods are available, they are not suitable for detection in ice.

6.2.1 Absorption detection

Absorption methods in general have been discussed in section 5.1.3. The spectrophotometric method for PO_4^{3-} detection uses the fact that ortophosphate combined with molybdate will form 12-molybdophosphoric heteropolyacid in an acidic medium. Wavelengths, which detects the 12-molybdophosphoric heteropolyacid can then be measured and the absorption is proportional to concentration as discussed in section 5.1.3. This method detects, however, not only phosphate but also the soluble fraction of phosphorus [*Estela and Cerdá*, 2005; *Mahowald et al.*, 2008].

Molybdate blue method. The molybdate blue method uses the fact that molybdate reacts with PO_4^{3-} to create a blue liquid and the absorption of red wavelengths is thus phosphate dependent [*Murphy and Riley*, 1958; *Gimbert et al.*, 2007]:

$$PO_4^{3-} + 12\,MoO_4^{2-} + 27H^+ \rightarrow H_3PO_4(MoO_3)_{12} + 12H_2O \tag{8}$$

where $H_3PO_4(MoO_3)_{12}$ er phosphomolybdate blue.

The absorbance is measured somewhere between 660 nm and 885 nm. Shorter wavelengths are used when using a long waveguide because the transmission of the long wavelengths is limited by water absorption [*Gimbert et al.*, 2007; *Patey et al.*, 2008].

A buffer is used to stabilize and enhance the reaction. As buffer an **ascorbic acid** solution can be used, but also methol, hydrazine and tin(II)chloride buffers are sometimes used. It was early discovered that ***methol*** had to be used at about 100 °C for colour formation to occur [*Murphy and Riley*, 1958]. ***Hydrazine*** minimizes the coating effect[15] compared to ascorbic acid, thus stabilizing the baseline [*Li et al.*, 2008]. ***Tin(II) chloride*** has the advantage of high sensitivity, but is very unstable and should be remade every day, and observations show that different batches of molybdate tend to give different extinction coefficients. Further, negative interference can come from iron(III), aluminium, calcium and chloride. The first three due to competitive complexation with the phosphate while the chloride probably inhibits the reduction of phophomolybdate [*Nollet*, 2007]. According to *Murphy and Riley* [1958] and *Nollet* [2007] ascorbic acid is the best buffer because the buffer and reagent can be added at the same time, which is not possible using the stannous chloride method.

Antimony tartate if added serves as a catalyst [*Estela and Cerdá*, 2005]. The molybdenum blue method normally shows limit of detection of about 2.85 ppb PO_4^{-3} [*Patey et al.*, 2008].

The main interferences on the absorption method using molybdenum blue are silicate, arsenate and germanate. They form heteropolyacids, which on reduction form a molybdenum complex with absorption in the same wavelengths as phosphate. However *Murphy and Riley* [1958] concludes that concentrations equal to those of seawater (Ar$\leq$ 1 ppm and Si $\leq$10 ppm) are negligible.

Yellow vandomolybdo phosphate complex. In the yellow vanadomolybdo phosphate method the reagent is made of ammonium heptamolybdate tetrahydrate

[15] see section 6.3.1

($(NH_4)Mo_7O_{244}H_2O$) and ammonium monovanadate (NH_4VO_3) in HCl acid. It has a lower sensitivity than the molybdenum blue method, but it has some advantages for continuous flow. It consists of only one reagent and it is very stable, making it useful for unmonitored measurements; and finally it does not have any fine precipitation accompanying the blue color formation as has the molybdenum blue method [*Neves et al.*, 2008].

Ionic pairs of molybdophosphate or vanodomolybdophosphate. Other methods are based on the formation of ionic pairs of either molybdophosphate or vanadomolybdophosphate with basic dye compounds such as Malachite Green, Rhodamine B, Fuchsine red, Methyl Violet, and others.

Liang et al. [2007] found that cetyltrimethylammonium bromide can form an ion pair compound with molybdenum phosphate that can be detected after enrichment. LOD was 0.15 ppb PO_4^{-3} and the method showed linear detection between 0.30 and 3.08 ppb.

6.2.2 Fluorescence detection

Florescence detection is discussed in general in section 5.1.3. Generally, florescence techniques are more sensitive than absorption techniques, obtained LOD for PO_4^{3-} is between 0.3 and 100 ppb, though LOD down to 0.06 ppb was obtained using Malachite green combined with flow injection analysis [*Estela and Cerdá*, 2005].

Determination of ortophosphate is possible by adding thiamine to the vandomnolybdo phosphate complex, forming highly florescent thiochrome; however silicate and arsenate again cause interference, but levels of Si/P up to 70 and Ar/P up to 50 is tolerated [*Estela and Cerdá*, 2005].

Perez-Ruiz et al. [2005] used a method for investigating organophosphorus pesticides where detection relied on the photolysis of the organocompounds by irradiation with a low pressure mercury lamp in the presence of peroxydisulfate. Reaction with molybdate took place and finally thiamine reacted to create thiochrome. Measurements were taken at 440 nm and excitation at 375 nm. LOD was found to be 4 ppb.

Huang and Zhang [2006] used a malachite green method combined with an anion surfactant (Ultrawet 60 L) and found a detection limit of 0.076 ppb PO_4^{-3} and a linear calibration range between 0.075 ppb and 3.08 ppb. But the reaction is slow and it takes 40 minutes to gain full color.

Li et al. [2005] used a combination between Rhodamine B and molybdophosphate and measured with fluorescence a LOD of 0.095 ppb PO_4^{3-} with linearity in the range of 0-9.50 ppb.

6.2.3 Chemiluminescent detection

Chemiluminescence is a chemical reaction, which releases excess energy as light. Oxidisation of luminol (3-aminophthalhydrazide) by heteropolyacid results in emission of blue light (λ =440 nm) and this is the basis for phosphate chemiluminescence photometry analysis [*Yaqoob et al.*, 2004]:

$$PO_4^{3-} + 12\,MoO_4^{2-} \xrightarrow{H_2SO_4} H_3PO_4(MoO_3)_{12} \tag{9}$$

$$H_3PO_4(MoO_3)_{12} \xrightarrow{OH^-} Light \tag{10}$$

However a preconcentration step is necessary to remove compounds such as Mg^{2+} and Ca^{2+}. The method provides high sensitivity (LOD=0.19 ppb PO_4^{3-}) because the background noise is low and further it provides the possibility of measuring other organic compounds in the sample. Poor accuracy (12 % RSD for 3.99 ppb PO_4^{3-}) combined with the preconcentration process makes it less attractive [*Patey et al.*, 2008]. Further the reaction process is very fast and light is emitted instantly. This calls for the photomultiplier window to be large and hence the cost of the instrument is significant [*Dallas and Dasgupta*, 2004].

Yaqoob et al. [2004] constructed a chemiluminescence flow system and found a LOD of 0.93 ppb P and linearity between 1.00 and 309.60 ppb P. They removed the interfering cations by passing the sample through an in-line iminodiacetate chelating column. Mg^{2+} however still had an enhancing effect when concentrations were above 100 ppm and Cu^{2+} showed a diminishing effect if concentrations were above 2.5 ppm.

6.2.4 Other methods for detecting phosphate and/or phosphorus

Atomic spectroscopy has a poor sensitivity; in *e.g.* a method using malachite green and in which the solution was flotated in an aqueous diethyl interface and dissoluted in methanol, further burned with a nitrous oxide flame the LOD was 20 ppb. Of course this method has way to many steps to be used for continuous flow.

Inductively coupled plasma-atomic emission spectrometry (ICP-AES) achieved a LOD of 200 ppb at wavelength 177 nm.

ICP-MS can also be used, here the optimum wavelength for P detection is 215 nm. LOD is low, only 0.7 ppb P [*Nollet*, 2007; *Worsfold et al.*, 2008]. *Edwards et al.* [2007] however as all ready mentioned found a ppt detection level, but i do not know if they used some sort of methods for enhancing such as the ones described below.

6.2.5 Enhancing detection of small concentrations

Few of the above mentioned methods does detect concentrations as small as 0.25 ppb PO_4^{3-}. Three things can be done to enhance detection limits. Either do preconcentrations, which is difficult when working with continuous flow, lengthen the cell in the case of absorption or optimize the chemistry. Often the chemistry is already optimized and how chemistry can be improved to enhance detection varies between methods, thus how to improve on the chemistry is not described here.

Preconcentration. Preconcentrating is a method for increasing the amount of phosphorus in the sample. It involves techniques of anion exchange resins [*Nollet*, 2007]. The MAGIC method uses magnesiumhydroxide to precipitate the inorganic phosphorus out of the sample by increasing pH using a strong base. After centrifugation the magnesium precipitation can be dissolved in a clean acid and measurements of dissolved reactive phosphorus can be undertaken using the molybdenum blue method [*Anagnostou and Sherrell*, 2008; *Patey et al.*, 2008]. *Anagnostou and Sherrell* [2008] found limit of detection (LOD) to be 4.65 ppt, while others have found the LOD to be 6.20 ppt P.

Another method of preconcentrating is to concentrate after formation of chromophore, for example by using an organic solvent such as hexane to extract the molybdate or malachite-green ion pair complex [*Patey et al.*, 2008]. Finally preconcentration can be done by filtering the sample on acetate or cellulose filters and dissolving in an organic solvent prior to analysis [*Patey et al.*, 2008].

Motomizu et al. [1995] used a Malachite Green method and preconcentrated using a membrane filter. They found a detection limit of 3 ppt P and linearity between 0.018 and 1 ppb P using a florescence method.

Susanto et al. [1995] also used a malachite green method. The ion associate was filtered through a membrane and dissolved in methyl cellosolve. LOD was found to be 60 ppt and linearity was good up to 18 ppb. However the sample size was large: 10 cm^3.

Enlengthen the cell path. For absorption detection the path can be enlengthened to obtain a better detection limit. According to Beer-Lamberts law the concentration is inversely proportional to the path length. Enhancing the path length lowers the detection limit. However the longer the path length the shorter is the linear range of detection [*Zhang*, 2006].

The company World Precision Instruments produces **long waveguide capillary cells** (LWCC-see figure 23a), which consists of a material that enables light introduced into the capillary core to be totally internally reflected through the cell, down to the detector. The refractive index of the cell (1.29 or 1.31 depending on the material) is lower than that of water (1.34). Cells with these special refractive properties are available in lengths between 2 cm and 500 cm with an internal volume spanning 5 μL to 1250 μL, thus keeping time resolution low even for very long cells with low detection limits.

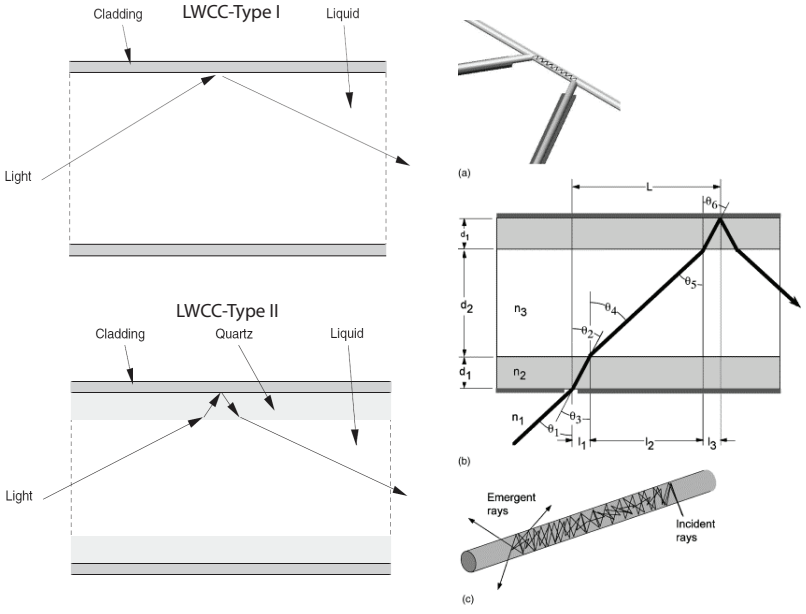

(a) LWCC (b) Refractive cell

Figure 23: (a) shows the path of totally reflected light in the liquid waveguide capillary cell, top type I and bottom type II [WPI, 2009], this type of cell assumes has are very narrow and thus it is assumed that the wave path is equal the length of the cell. While (b) shows how the refractive cell works, refracting the light several times before detection, thus increasing path length by including the path perpendicular to the length of the cell [*Ellis et al.*, 2003].

The longer the waveguide the more difficult it is to work with, because bubbles and particles may get stuck inside. Thus cleaning is important. For rinsing the LWCC

flushing with ultra pure water followed by 1 M NaOH and 1 M HCl *Gimbert and Worsfold* [2007] suggested.

The waveguide comes in two types. Type II has both a silica capillary and a Teflon-AF cladding, which makes it easier to clean than Type I, where the sample is in direct touch with the Teflon-AF cladding [*Gimbert and Worsfold*, 2007].

Recently many people have used the longer cells for detection of soluble reactive phosphorus in seawater. *Zhang and Chi* [2002] and *Ma et al.* [2009] used a 2 meter LWCC in combination with the molybdate blue method using ascorbic acid as buffer and found LOD of 0.049 ppb and linearity between 0 and 18.94 ppb PO_4^{3-}. They found no silicate interactions with silicate levels below 6.74 ppm Si and no interaction from arsenate below 2.13 ppb Ar. *Patey et al.* [2008] find a LOD of 0.075 ppb using a similar method.

Neves et al. [2008] used the vanadomolybdophosphate detection method in combination with a 1 meter LWCC and find a LOD of 17 ppb P and linearity up to 500 ppb.

Adornato et al. [2007] found linearity from 0.95 ppb to 95 ppb PO_4^{3-} using a 50 cm path length with a molybdenum blue method.

Another method for enhancing wavelength is using **multi reflective flow cells** (see figure 23b), where the light is introduced with an angle and several reflections take place before detection. These flow cells is estimated to increase detection 2.5 times compared to normal flow cells. They are different from the LWCCs, because these flow celles are broader cells including the length perpendicular to the cell size as wave path, requiring larger samples. While the LWCC is very narrow cells, which assumes that the wave path is equal the length of the cell.

Gentle et al. [2010] used an refractive wave cell in combination with the molybdenum blue method and found LOD of 30.97 ppb P and linear detection range between 0 and 6194 ppb P.

6.2.6 Filters

Filters are used in various methods to filtrate samples and thus remove particulate phosphorus so that only dissolved phosphorus and phosphate is measured. *Adornato et al.* [2007] use a 0.4 μm filter for sea water and find that it provides stable measurements. *Neves et al.* [2008] use a 0.45 μm Whatman cellulose acetate membrane to filter groundwater samples before introducing the samples into a LWCC. *Adornato et al.* [2007] used a 0.4 μm filter in an *in situ* instrument used in an estuarine environments and obtained results without drift. *Li and Hansell* [2008] investigated the effect of different filter types on measurements of dissolved phosphorus. They measured concentrations of inorganic phosphorus[16] (IP) of 1.55 ppb after filtration and concluded that filters made of glass material should be avoided, because they removed up to 66% of IP and that the best ones were made of polycarbonate (2%) or cellulose ester (1.6%), a Versapor membrane was also tested and did have some influence on the amount of IP detected (13%).

[16]inorganic phosphorus is any phosphorus-containing compound which does not also contain carbon

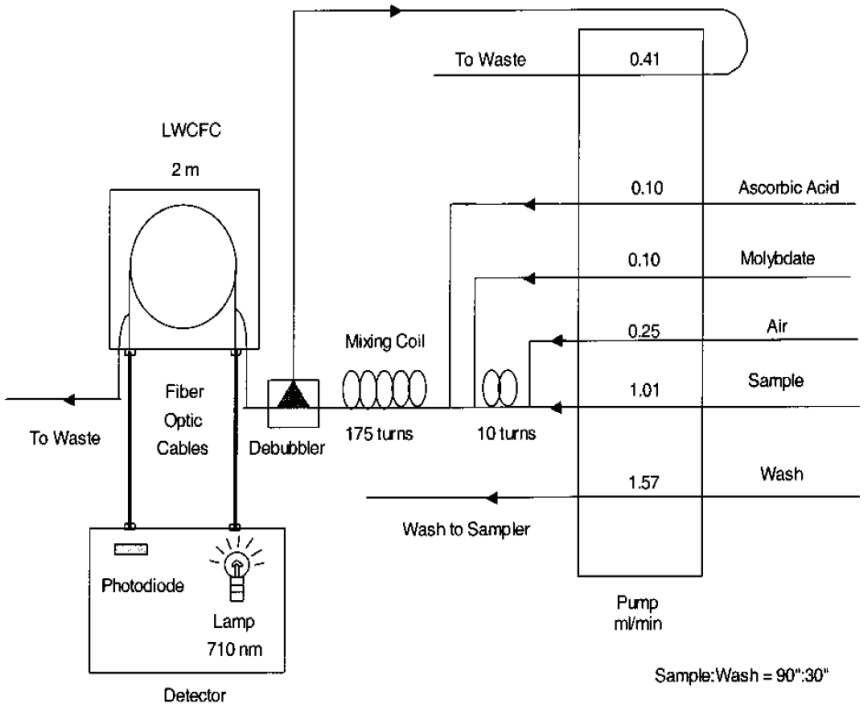

Figure 24: The figure show the flow diagram for phosphate detection using a LWCC as suggested by *Zhang and Chi* [2002]. The detection wavelength is 710 nm and flow rates are in mL/min.

6.3 Molybdate blue method using a two meter LWCC by *Zhang and Chi* [2002]

I found that the method by *Zhang and Chi* [2002] was the most promising method for obtaining high resolution in combination with a convenient daily use and providing the necessary limit of detection. This section presents in detail the method by *Zhang and Chi* [2002]. The possible interferences on the method are explained and finally different ways of optimizing the method to limit negative interferences and speed up color formation are presented.

When using CFA systems preconcentration is not an option to enhance sensitivity, therefore I choose to use a LWCC method. *Zhang et al.* [1999] obtained some chemical detection enhancement by optimizing concentrations in reagent and buffer. This was also done with the purpose of minimizing silicate interference. In the article *Zhang and Chi* [2002] they combine these optimizations with a 2 meter LWCC, creating a method with a detection limit of (three times standard deviation) 0.049 ppb of reactive soluble phosphate, which is well below the expected level of 0.25 ppb P in ice known from *Edwards et al.* [2007] and *Zhang and Chi* [2002] finds a linear range up to 18.94 ppb.

The set-up used by *Zhang and Chi* [2002] can be seen in figure 24. Air is introduced with a speed of 0.25 mL/min to a sample with flow rate 1.01 mL/min. The air is introduced to avoid dispersion in the mixing. The air-liquid is mixed for 10 turns corresponding to 0.53 meter. Then the molybdate reagent is introduced at a flow rate of 0.10 mL/min and immediately after ascorbic acid is introduced at flow rate 0.10 mL/min. After 175 turns of mixing corresponding to 9.34 meter, the flow goes through a debubbler, which removes all the air and a little bit of water mixture with a speed of 0.41 mL/min, before the rest enters the 2 meter LWCC with an internal volume of 0.5 mL and detection takes place at a wavelength of 710 nm.

In the method by *Zhang and Chi* [2002] no heater is used; this choice was made to minimize silicate interference (see section 6.3.1).

Below the recipe for the molybdate reagent and the ascorbic acid buffer can be found:

Molybdate reagent recipe:

1. Dissolve 0.23 g antimony molybdate in 20 mL 5N H_2SO_4 [17]
2. Add 5 mL of stock antimony potassium tartrate

   Stock antimony pottasium tartrate recipe

   Dissolve 0.3 g antimony potassium tartate in 100 mL of milli-Q-water. Keep below 5 degrees.
3. Dilute the mixture in 100 mL milli-Q-water

Ascorbic acid buffer:

1. Disolve 0.5 g ascorbic acid in 100 mL milli-Q-water
2. Add 7 g sodium dodecyl sulfate

If kept in refrigerator when not used, according to *Drummond and Maher* [1995], the molybdate blue reagent can live for 6 months, while the ascorbic acid buffer has a life time of just 14 days. *Ma et al.* [2009] find that a concentration of ascorbic acid of 10 g/L gives the highest absorbance and *Drummond and Maher* [1995] found that a concentration of 0.009 M ascorbic acid reduced reaction time to 1.5 minutes and that the antimony molybdate should be 0.03 mM to obtain the fastest reaction time. Further *Huang and Zhang* [2008] looked at the ascorbic acid concentrations and found no advantage by increasing them: 0.5, 1, 2, 5 and 10% ascorbic acid caused the percentage of full color formation after 10 minutes to be 69, 78, 79, 66 and 51 % respectively. *Huang and Zhang* [2008] also investigated the effect of persulfate on formation time and found that persulfate rates of 2.5 mg/mL gave 3 minutes for full formation, while higher concentrations took much longer: 5 mg/L took 10 minutes and 20.0 mg/mL took 34 to 38 minutes.

Zhang and Chi [2002] found that it did not improve measurements if mixing was introduced between the introduction of reagent and buffer, rather introducing mixing on this position would decrease precision and linearity.

Furthermore they found that the linearity up to 200 nM (18.94 ppb) PO_4^{3-} can be described by equation 11. Above this limit absorbance is lower than predicted using the linear trend.

$$Absorbance = (0.0016 \pm 0.0006) + (0.001391 \pm 0.000006)[PO_4^{3-}](\text{nM}) \tag{11}$$

6.3.1 Interference and other problems in the molybdate blue method

In the following interferences on the molybdenum method is presented. When using the molybdate blue method for detecting phosphate interferences can be caused by silicate and arsenate forming molybdenum complexes, micro bubbles and particles such as dust in the detection cell can limit the light penetrating the cell by direct absorption as well as cause refraction, hydrolysable dissolved organic phosphorus can react with the molybdenum, so that not only phosphate but all reactive phosphorus is measured. Further problems is coating of cell or tubing, which creates a memory effect in the detection.

[17] N is the normality defined as gram equivalent of a solute per liter of solution.

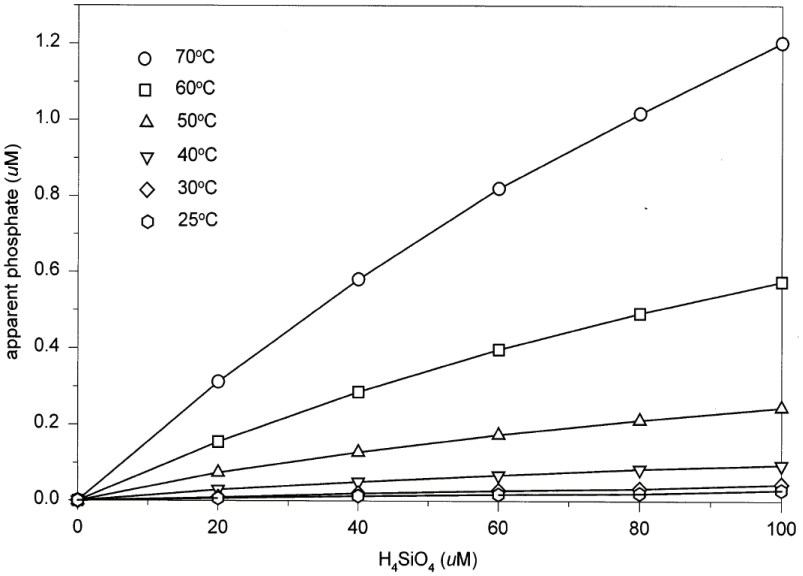

Figure 25: The graph shows the interference of silicate on the molybdenum method as seen in [*Zhang et al.*, 1999]. Measurements were conducted at pH 0.78 and $[H^+]/[Mo]$ ratio of about 70.

Silicate: Silicic acid (SiO_4^{4-}) can react with the molybdenum and create silicomolybdenum, that has a broad spectrum, with maximum at 790 nm, overlapping the 710 nm used for detecting PO_4^{3-} in the method by *Zhang and Chi* [2002].

The reaction of silicate with molybdenum is much slower than that of phosphate and thus the interference increases with time so in order to avoid silicate interference reaction times should be kept short [*Zhang et al.*, 1999; *Ma et al.*, 2009].

Silicate reactions are favoured at 40°C to 65 °C, therefore temperature should be kept below these temperatures. Temperatures below 15 °C, however, can cause PO_4^{3-} measurements to be too low. In several articles it is suggested to keep room temperature to avoid the formation of silicamolybdate [*Zhang and Chi*, 2002; *Gimbert and Worsfold*, 2007]. pH should be low and *Zhang et al.* [1999] found that the sensitivity of the molybdate method was constant for pH between 0.3 and 1.5 and that very low pH (0.19) reduced the sensitivity by 40 %. Tartaric acid masks the silicate by 47 % at temperature of 70 °C and oxalic acid does the same [*Zhang et al.*, 1999; *Gimbert et al.*, 2007; *Nollet*, 2007; *Ma et al.*, 2009].

Zhang et al. [1999] find that using the molybdate blue method the interference of silicate can be calculated using the equation:

$$[PO^{3-}_{4\text{-false}}] = (24594 \cdot 10^4[\text{Si}] - 661951[\text{Si}]^2)(\frac{(\frac{1000}{T})^{-23.6653}}{0.1587})e^{\frac{(pH-0.78)^2}{0.05037}} \quad (12)$$

where $[PO_4^{3-}]$ is the apparent phosphate concentration and [Si] is the silicate concentration in the sample in μM, T is the temperature in kelvin and pH is the value in the final solution.

Silicates interference with temperature is also presented in figure 25. *Adornato et al.* [2007] finds using the same method as *Zhang and Chi* [2002] that 2.8 ppm silicate does not interfere with 95 ppb PO_4^{3-}.

Arsenate. The isomorphy between the arsenate ion (As(V)) and phosphate allows it to form similar molybdate complexes with absorption in the same wavelengths.

Further the reaction rate of arsenate-molybdenum is similar to that of phosphate-molybdenum.

As(V) can be reduced to As(III), which does not react with molybdenum blue, in the presence of thiosulfate or sulfite [*Zhang et al.*, 1999; *Adornato et al.*, 2007; *Anagnostou and Sherrell*, 2008]. By the MAGIC and LWCC-molybdenum blue methods *Li and Hansell* [2008] found the same concentration of phosphorus in samples added arsenate suggesting that they either have the same interference from arsenate or both have none.

Micro bubbles. Micro bubbles cause the measurements to fluctuate. They form from dissolved air in samples and reagents and when stuck in the detection cell they can block the light completely or just cause some refraction unexpected. The longer the cell the larger is the risk that bubbles will be stuck inside [*Gimbert and Worsfold*, 2007; *Patey et al.*, 2008]. *Zhang* [2006] investigated the effect of an online degassing system made by Alltech (Deerfield, IL, USA) in combinations with different LWCC lengths, while measuring nitrite and found that the baseline was more stable using this product, due to minimizing of micro bubble effects.

Dust. Dust can cause scattering as well as direct absorption of light. The problem is that while normal flow cells, do not retain scattered light due to the material they consist of, the LWCC retain all light, also the scattered. Backscattering by small ($< 1\mu$m) particles is wavelength dependent, with stronger effect on shorter wavelength [*Floge et al.*, 2009; *Anagnostou and Sherrell*, 2008]. *Floge et al.* [2009] investigated the effect of colloidal material in LWCC's of length 0.5 meters and concluded that particles with a diameter of 120-270 nm caused a small bias in the absorption, but scattering will be more noticeable with a longer path length.

Hydrolysable dissolved organic phosphorus (DOP). Hydrolysable dissolved organic phosphorus (DOP) can interfere with the molybdenum blue method. *Li and Hansell* [2008] conducted an experiment to test whether DOP had influence on PO_4^{3-} measurements in seawater. He compared the MAGIC and the LWCC method and found that both had equal interference from DOP, suggesting that either both are equally influenced by it or there is no influence at all.

Coating Being electrically charged, PO_4^{3-} tend to get stuck on almost everything, which causes a direct memory effect. Further coating of optical surfaces by the phosphomolybdenum complex may occur, *e.g.*, Quartz and silica surfaces can be coated by surface silanol formation from aqueous solution [*Adornato et al.*, 2007].

Coating can be readily seen in continuous flow, since the ideal peak will become asymmetric, with excessive tailing. Coating effects can be minimized by cleaning the cell carefully after use. *Zhang et al.* [1999] and *Li et al.* [2008] have suggested the coating effects may be further minimized if hydrazine sulfate is used as reducing agent instead of ascorbic acid.

6.3.2 Optimization of the molybdenum blue method

To avoid interferences and obtain a good limit of detection some issues should be considered, which can optimize the detection. These include the amount of molybdenum blue present in the solution, the pH, which effects reaction rates, the flow rate and mixing time, which effects how much of the possible reaction has taken place before detection and the

temperatures, higher temperature enhances the limit of detection, but can enhance the interference with silicate.

Mo over H^+ ratio In the article by *Zhang et al.* [1999] the optimal reaction conditions were found using a ratio of $[H^+]/[Mo]$ of 70. Here the time for color formation would be only 2 minutes. *Drummond and Maher* [1995] suggested once full reaction is reached and that a ratio between 45 and 80 gives a constant response oand that a ratio between 50 and 70 gives the fastest reaction rates at any pH, while ratios below 20 has high blank absorbance.

pH *Zhang et al.* [1999] found that any pH between 0.3 and 1.5 provided high sensitivity, but at pH 0.19 sensitivity was reduced by about 40 %. They explain this by the fact that at low pH there needs to be a high level of [Mo] in order to satisfy the $[H^+]/[Mo]$ of 70. pH should be kept above 0.7 according to *Nollet* [2007] since lower pH can cause the Mo(VI) to form molybdenum blue even in the absence of reactive phosphorus. *Zhang et al.* [1999] also found that the coating effect was close to linear for pH ranging from 0.5 to 1.5. *Drummond and Maher* [1995] found that the fastest reaction rates of 0.8 to 1 minute occurred using pH between 0.36 and 0.88. *Huang and Zhang* [2008] investigated the effect of pH on time for formation. pH was varied between 0.64 and 10 and a formation time below 3 minutes was found using pH between 1.3 and 10.

Flow rate and mixing time The necessary mixing time is closely correlated with the time needed for color formation, because increasing mixing time will increase the time available for the colour formation to take place and will thus influence how far the color process has come when measuring the absorption. In the same way increasing flow rate, can shorten the available color formation time. Increasing flow rate can also influence memory effects caused by coating.

Ma et al. [2009] investigated mixing coil lengths between 43 and 250 cm, positioned after the input of both reagent and buffer, using a flow of 1 mL/min, and concluded that the more mixing the higher the sensitivity. They also investigated flow rates and found flow that rates between 0.8 and 1 mL/min were best for minimizing dispersion.

Temperature *Zhang et al.* [1999] found a positive temperature dependence in the molybdenum method with no added potassium tartrate, while in the presence of potassium tartrate absorbance was high all ready at temperatures of 30 °C. They found that the temperature, absorbance curves with and without potassium tartate cross at about 70 °C. They conclude that adding potassium tartrate is advantageous. They also discovered that coating decreased with increasing temperature.

In this section available methods for measuring phosphate have been presented. The methods include detection of absorbance; detecting either molybdenum blue phosphate or yellow vanadomolybdo phosphate complex. Both methods can be combined with basic dye compounds so ionic pairs are detected. Florescence detection and chemiluminescent detection are also available for detection of PO_4^{3-} in continuous flow. All the measurement methods have problems getting the required limit of detection, for detection of PO_4^{3-} in ice cores, if not using longer path ways or including pre concentration steps, which are difficult in continuous flow, and which if included in continuous flow only makes semi continuous detections.

Enhancing the length of the detection cell is what is done in the method by Zhang and Chi [2002], who uses the molybdenum blue absorption method using ascorbic acid as buffer and combines it with a two meter LWCC-a cell with special optical features. They gain a limit of detection of 0.05 ppb.

When using the method one should be aware that some interferences are possible: Interferences can be caused by silicate and arsenate reacting with the molybdenum blue; micro bubbles and particulate matter in the cell can change the optical properties and thus the absorbance detected; dissolved organic phosphorus reacts with the molybdenum blue too, so that not only phosphate but also the soluble fraction of phosphorus is measured; Further coating of the inside of the cell can alter baseline and introduce a memory effect. Several parameters can however be optimized to avoid interferences. Enhancing the ratio of molybdenum blue over sample, the pH, the flow rate, the mixing time and the temperature can minimize interferences. The method by Zhang and Chi [2002] was found to show best prospect for detecting PO_4^{3-} in ice cores. In the next section experiments conducted to optimize the method for measurements in ice cores are presented and discussed.

7 Optimizing the method by *Zhang and Chi* [2002] for measurements of ice cores

In the previous section the methods available for detecting PO_4^{3-} using continuous flow was presented. The method by *Zhang and Chi* [2002] had best prospects. In the following I present results of optimization experiments conducted in this study to improve the molybdenum absorption method by *Zhang and Chi* [2002] using a two meter liquid wave guide capillary cell for detection of PO_4^{3-} in ice cores. The set-up used for optimization was changed many times: Flow lines including air, debubblers and filters of various types were tested. Furthermore concentrations of chemicals in reagent and buffer were varied to detect whether this could improve the absorption detected for low concentrations of phosphate.

7.1 Description of the instruments used for optimizing

The set-up is basically the same as shown in figur 24, but it is modified between almost every experiment. A six port valve was used to switch the input sample from milli-Q to standards of known PO_4^{3-} concentration. The sample was pumped at a flow rate between 0.98 and 1.78 mL/min and mixed with reagent, buffer and in some cases air, which was included to prevent dispersion. Then the mixture of sample, reagent, buffer, and air was mixed in a heat bath, which could be set to various temperatures in the different experiments, before a debubbler (sometimes used) removed air and excess water and a filter (some times used) positioned in front of the LWCC removed particles, which could cause optical interference. Finally detection was done in the 2 meter LWCC at a wavelength of 710 nm. Further details on the instruments used can be found in Appendix (A.4). For each experiment details on the set-up is explained. Absorption is calculated using equation 5, where I_0 is the maximum counts of the baseline and the signal during detection of a standard I is found using the minimum counts shown during detection of the standard.

7.2 A small flow cell - first try out

To investigate whether the method by *Zhang and Chi* [2002] would work at all, an experiment was conducted using the set-up as explained, but in order to make the set-up as simple as possible, no air was introduced and thus no debubbler was used. Further the mixing length was reduced to 3.25 meters of mixing in a tubing of diameter 0.5 mm. Sample was introduced at a rate of 1 mL/min, while reagent and buffer were introduced with at speed 0.1 mL/min each. The set-up did not have any temperature control and this caused some degree of fluctuation. Finally, but most important, the length of the detection cell was only 3.5 cm. The 3.5 cm cell (shown in figure 20) was produced at the Center for Ice and Climate.

Standards with concentration of 9891.1, 998.0, 97.9 and 9.9 ppb PO_4^{3-} were prepared in glass bottles. The data obtained can be seen in figure 26. The set-up using the small flow cell had a detection limit close to 9.9 ppb, but some variation from background can be seen at 9.9 ppb. The highest concentration show some variability, this could be due to ageing of the standards. As time passes PO_4^{3-} will tend to stick on the side of the glass bottles, depleting the aqueous solution of PO_4^{3-}. Another issue is the highest standard being out of the linear range and thus a lower value of absorption than linear is to be expected.

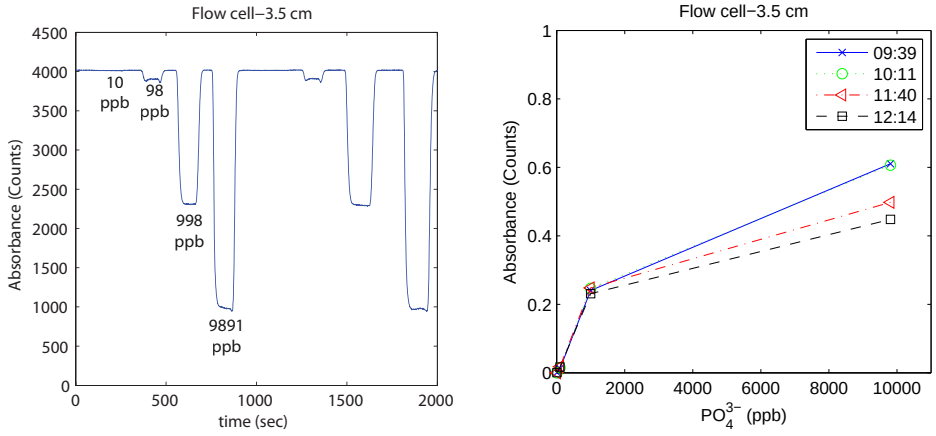

(a) (b)

Figure 26: Small flow cell

(a) Raw data acquired using the method by *Zhang and Chi* [2002], without heat control and debubbler and using only a small 3.5 cm flow cell. Mixing length is 3.5 meters. (b) The relationship between concentration and absorption. The color coding indicates the time of day the measurements were taken; the later the time the older the standards.

The small flow cell was not adequate for measuring the low concentrations expected in ice.

7.3 Long Waveguide Capillary Cell (LWCC)

The small flow cell was replaced by a 2 meter Long Waveguide Capillary Cell (LWCC)-type II purchased from World Precision Instruments, Inc with an internal volume of 0.5 mL in the following (figure 27). Further information on the LWCC is provided in section 6.2.5.

7.4 Chemistry

Experiments were conducted to test the dependency of the limit of detection and of the extent of the linear range dependency on the concentrations of molybdenum blue, 5N H_2SO_4 and ascorbic acid used for the buffer. Since according to literature ascorbic acid is the buffer showing the least interference and keeping color for the longest time, it was chosen not to investigate other types of buffer.

All chemistry tests were conducted using 300 ms integration time and a boxcar value[18] of 15 at wavelength 710 nm, flow rates were 0.98 mL/min, 0.14 mL/min and 0.14 mL/min for sample, reagent and buffer respectively. The heat bath was set at a temperature of 35 °C.

All the chemicals are of analytical grade and purchased from the company Merck, except for ascorbic acid, which is purchased at the company Sigma-Aldrich.

Concluding a recipe for the reagent using 0.37 g molybdate blue, adding 25 mL 5N H_2SO_4, 5 mL stock antimony pottasium tartate and 100 mL water gave optimum conditions combined with the original buffer suggested by *Zhang and Chi* [2002].

In section 7.4.1 to 7.4.3 these results are presented.

[18]Boxcar is a measure for the integration length used, see section 7.8

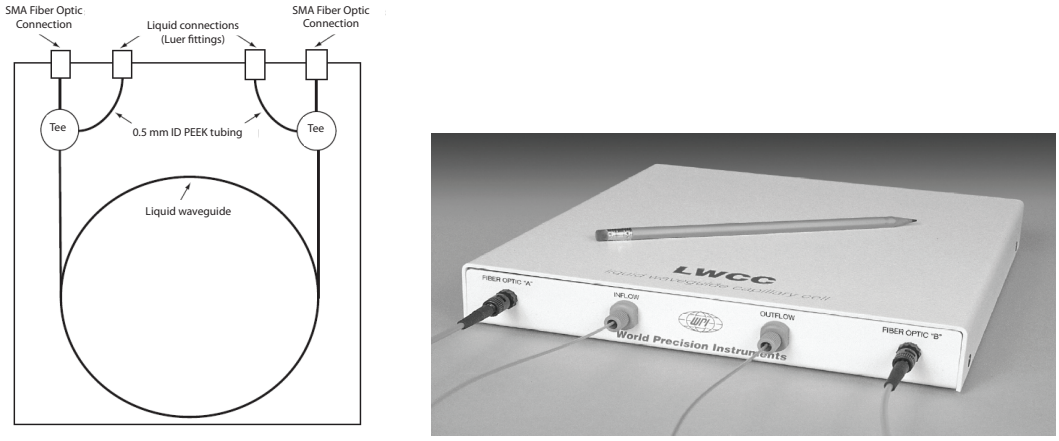

(a) (b)

Figure 27: (a) A sketch of the LWCC (b) A picture of the 2 meter LWCC.

7.4.1 Molybdenum blue

Concentrations of molybdenum blue of 0.170 g, 0.290 g, 0.375 g, 0.510 g, 0.735 g, 0.895 g and 1.100 g per 20 mL 5N H_2SO_4, 5 mL Stock antimony potassium tartrate and 100 mL water were tested. The results are presented in figure 28.

The background level (signal for pure milli-Q water) was found peaking at 0.375 g molybdenum blue, but in general the signal was above 3200 counts between 0.170 to 0.375 g. The higher molybdenum blue concentrations gave a very low background level. The reason is that the molybdenum, when in excess, starts color formation by the pure contact with water, thus making background low.

Absorption increased with the concentration of molybdenum blue. However linearity was lost above 0.375 g molybdenum blue. The non-linearity could also have been caused by the ageing of the standards (see section 7.4.4).

A concentration of 0.375 g molybdenum blue was chosen for optimum conditions.

7.4.2 5N H_2SO_4

The amount of 5N H_2SO_4 and molybdenum blue added is known to affect the time for colour formation (see section 6.3.2).

The volume of 5N H_2SO_4 added was varied from 20 to 35 mL using a set-up as described above and the original recipe for buffer and reagent by *Zhang and Chi* [2002].

The amount of 5N H_2SO_4 influenced the absorption and linearity by giving high absorption at 20 mL and highest at 25 mL, but 25 mL had the lowest baseline value (see figure 29). Finally 25 mL 5N H_2SO_4 was chosen to enhance the sensitivity of the method, thus accepting a lower baseline.

7.4.3 Ascorbic acid

Tests of the amount of L-ascorbic acid used in the buffer was conducted. The amount of L-ascorbic acid dissolved in 100 mL Milli-Q water and added 7 g sodium dodecyl sulphate was varied between 0.5 g and 2.5 g. The results are shown in figure 30.

It was found that 1.0 g L-ascorbic acid per 100 mL water yielded the highest baseline. Higher concentrations of L-ascorbic acid decreased the baseline by some 100 counts. Again

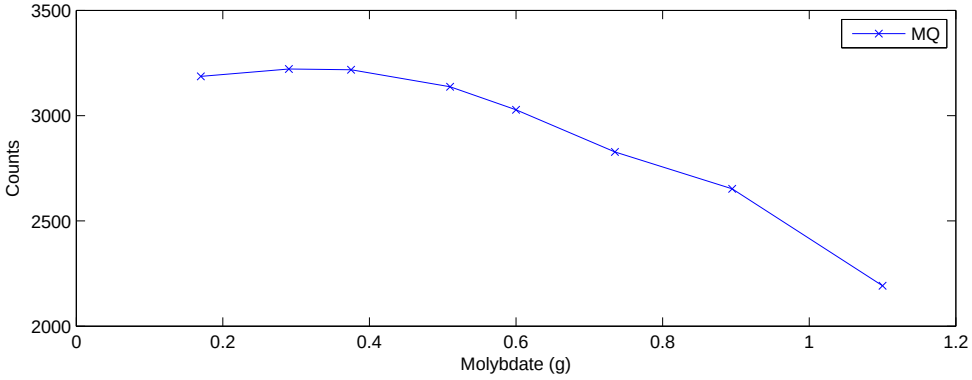

(a)

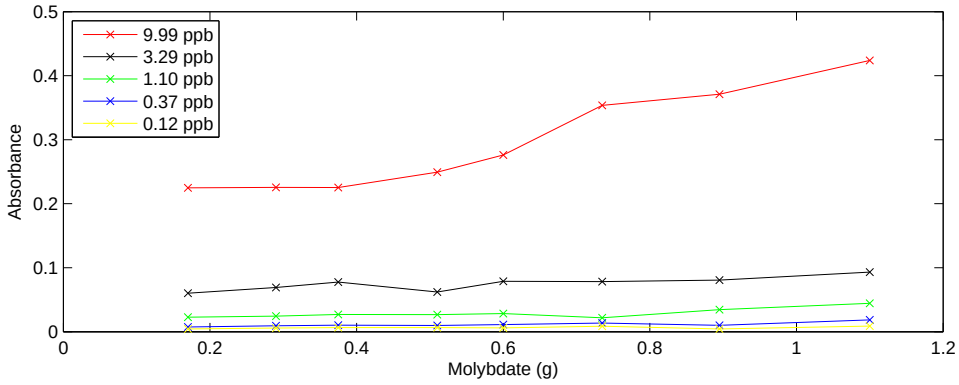

(b)

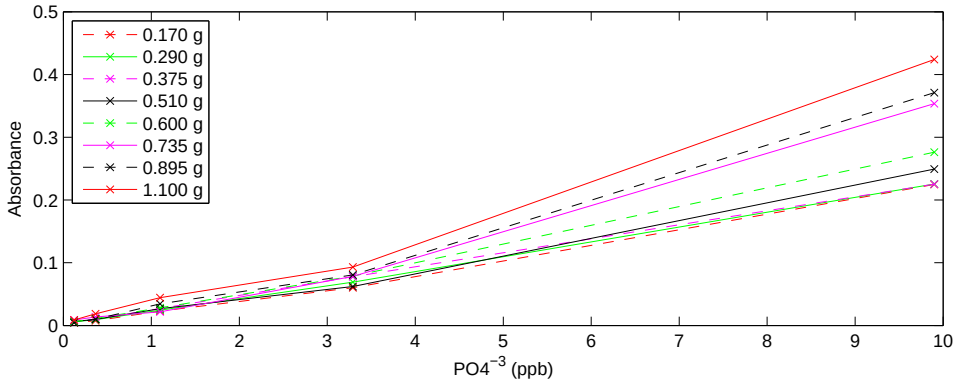

(c)

Figure 28: Dependence of Molybdate blue concentration

The dependence of molybdate blue:(a) show the variation of the amount of counts in baseline as a function of the concentration of Molybdenum blue in g per 125 mL solution. The concentration of molybdenum blue is seen to effect the baseline. The maximum signal for milli-Q occurs for a concentration of 0.37 g molybdenum blue;(b) The absorbance is plotted as a function of concentration of molybdenum blue for various concentrations of PO_4^{3-}. The concentration of molybdenum blue is seen to affect the absorption non-linearly for various concentrations of PO_4^{3-}; In (c) absorption is shown as a function of PO_4^{3-} for different concentrations of molybdenum blue. Note again the non-linearity for high molybdenum blue concentrations. Note that (b) and (c) show the same data in two different ways.

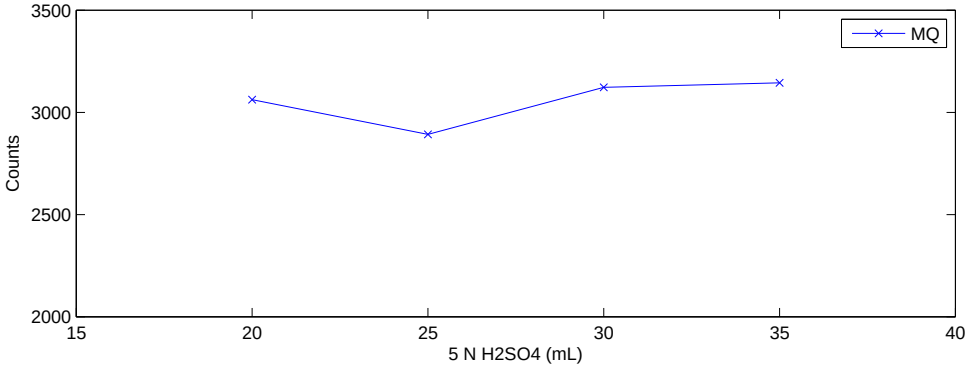

(a)

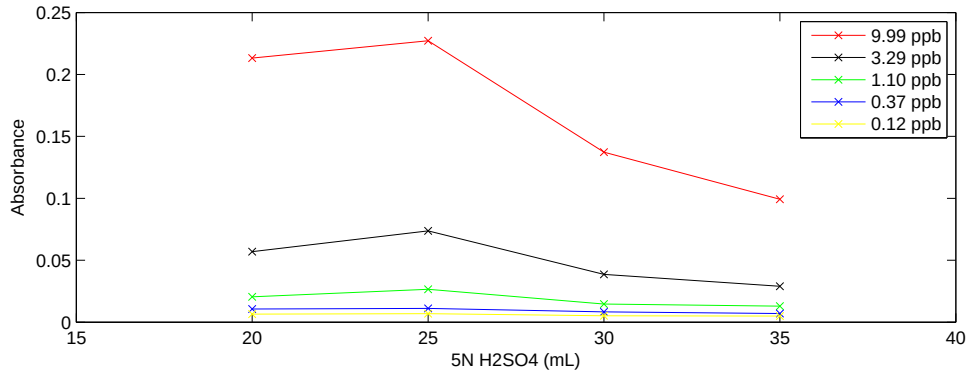

(b)

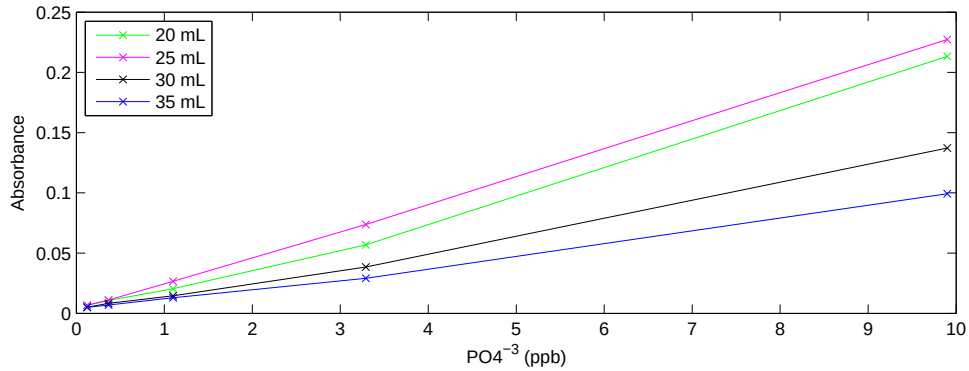

(c)

Figure 29: Dependence of H_2SO_4 concentration

The dependence on H_2SO_4:(a) the variation of the baseline signal as a function of the volume of 5N H_2SO_4 [mL] added to 100 mL solution. The highest baseline was found using 30 or 35 mL;(b) The absorbance is plotted as a function of 5N H_2SO_4 using various concentrations of PO_4^{3-}. The highest 5N H_2SO_4 absorbance occurs for 25 mL 5N H_2SO_4;(c) Absorbance vs. concentration of phosphate showing good linearity for all H_SO_4 concentrations.

the reason for this is probably that the ascorbic acid influences the speed of the reaction with molybdenum blue. For high concentrations of ascorbic acid, the molybdenum will be more willing to react, causing reaction also when only milli-Q and no PO_4^{3-} is present.

The linearity was affected at low concentrations. But I suspect that lack of linearity is due to the experiments being conducted using glass bottles causing concentrations of phosphate to vary over time.

The decision was reached to keep the original recipe by *Zhang and Chi* [2002] for the buffer using 0.5 g L-ascorbic acid per 100 mL water and 7 g dodecyl sulfate.

7.4.4 Standards

The standards were made from a 999 ppm PO_4^{3-} solution, bought from Merck. First the phosphate concentration is diluted to a concentration of 1 ppm and hence diluted further to the lower concentrations. Concentrations were calculated using equation 13, where C_2 is the concentration in the second dilution, C_1 is original concentration and V_1 is the volume of C_1 diluted in the volume of V_2.

$$C_2 = \frac{C_1 \cdot V_1}{V_2 + V_1} \tag{13}$$

Some linearity problems, as allready shown in the previous section, were found using glass bottles. This is most likely due to PO_4^{3-} sticking on the side of the glass, due to the relatively high charge density. It is likely that the concentration of phosphate in a glass bottle would change over time as PO_4^{3-} was either stuck to the side of the glass or present in the water.

In order to avoid this problem, polytetrafluoroethylene (PTFE) type bottles were used instead. The material makes the bottles catch less PO_4^{3-}. Making the same standard concentration (4.94 ppb) and running it three times showed that the variation in standards corresponds to 0.30 ppb (see figure 31). The variation is partly caused by the fact that the three standards were made in two different ways. First a dilution of concentration 9891.1 was made from diluting 200 μL stock standard of concentration 999 ppm in 20 mL milli-Q, then one standard was made from diluting 40 μL in 80 mL Milli-Q water and the other two were made by diluting 20 μL in 40 mL Milli-Q water. But part of the effect is probably due to PO_4^{3-} also sticking to the side of the polypropylene bottles.

Another way to avoid the sticking of PO_4^{3-} to the side of the glass is to rinse the bottles with HCl or H_2SO_4 before using them for standards [*Nollet*, 2007]. This was not done in this study, because the effect probably is small.

7.5 Temperature dependence

The temperature dependence was investigated using the original recipe from *Zhang and Chi* [2002]. A heat bath was included, heating 4.25 meter mixing tubing. Flow rate was 1.02 mL/min for the sample and 0.08 mL/min for buffer and reagent. No air was introduced and hence no debubbler was used. The boxcar value was set to 15 and integration time was 300 ms. Temperature was varied between 35 and 70 °C. The results are presented in figure 32.

At constant phosphate concentration a clear dependence of absorbance on temperature is observed: The higher the temperature the larger the absorbance. This is most likely due to faster reaction rate, when increasing temperature making the not fully ended reaction at low temperature come closer to full reaction at high temperature.

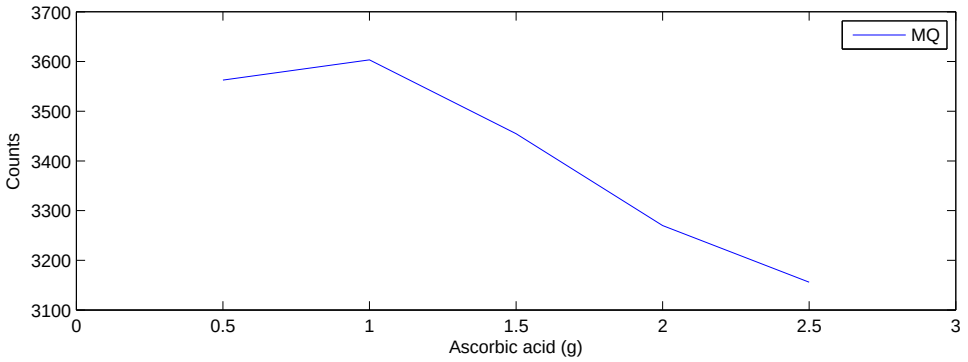

(a)

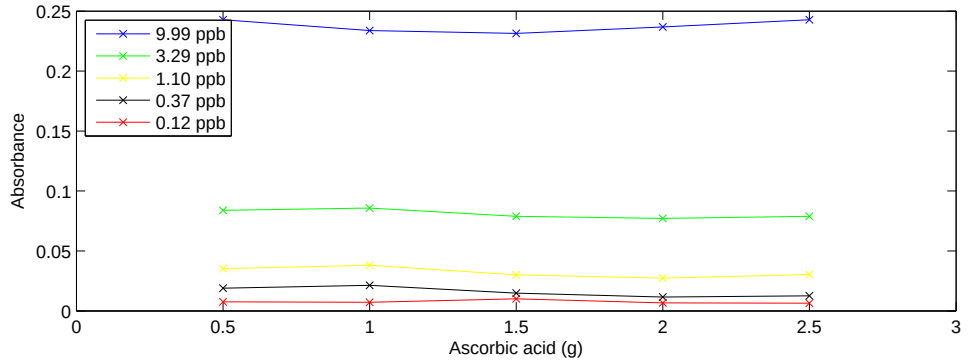

(b)

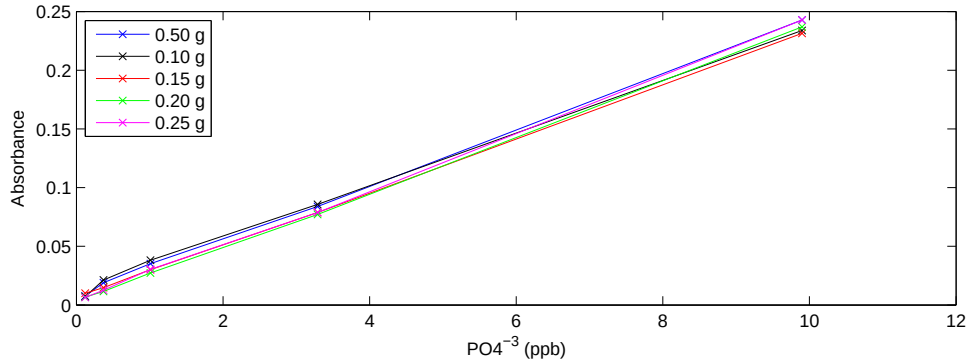

(c)

Figure 30: Dependence of L-ascorbic acid concentration

Dependence on L-ascorbic acid concentration:(a) Baseline signal as a function of ascorbic acid concentration in g per 100 mL buffer solution;(b) Absorbance variation with the concentration of L-ascorbic acid in g per 100 mL for different PO_4^{3-} concentrations; and,(c) Absorbance vs. PO_4^{3-} concentrations is not significantly influenced by the concentration of L-ascorbic acid in the buffer.

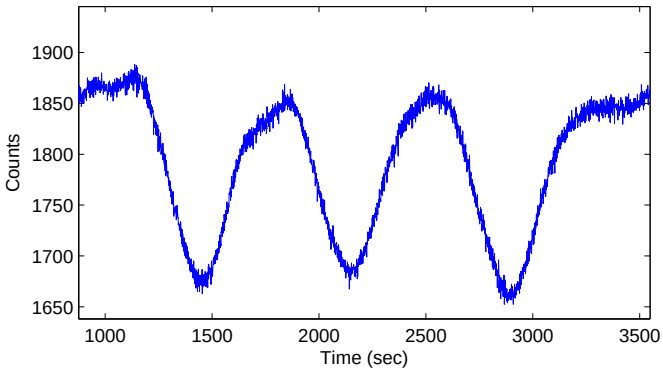

Figure 31: Counts as a function of time. The dips is three times the same size standard with a concentration of 4.94 ppb. The first standard was made diluting in another way than number two and three.

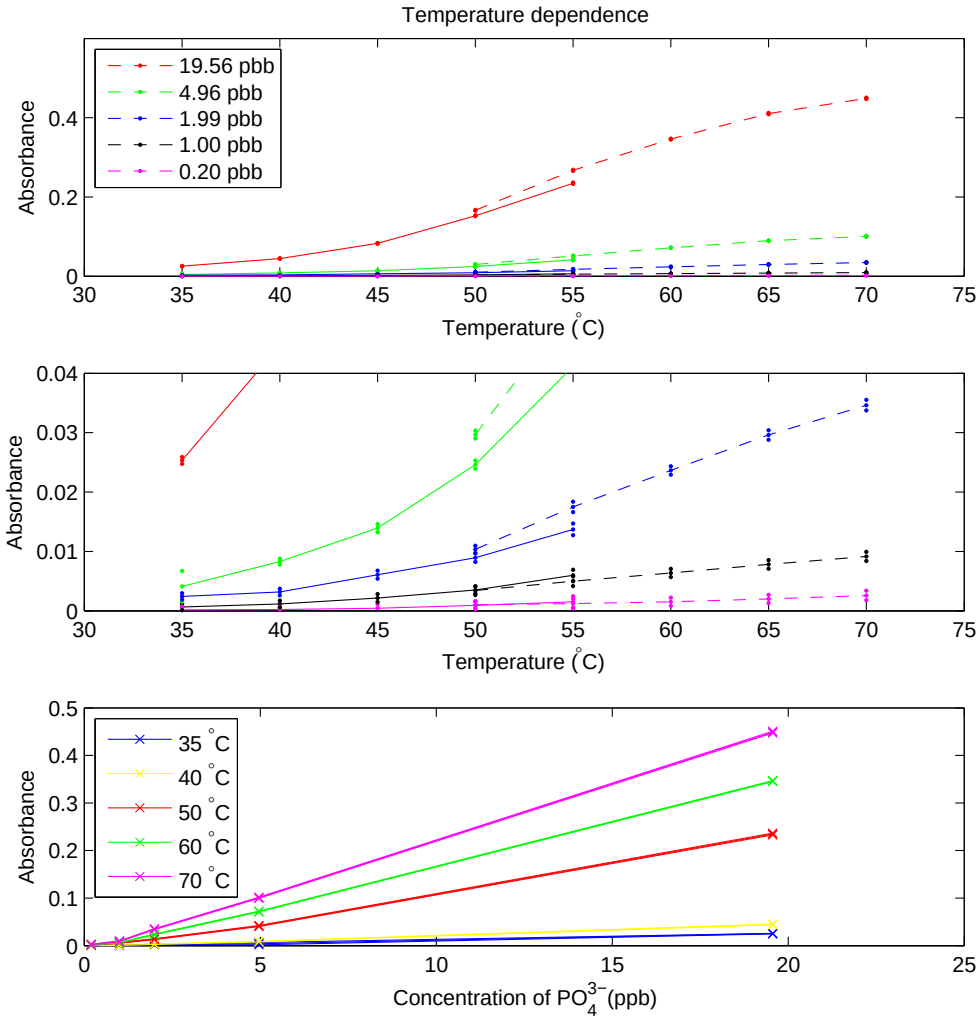

Figure 32: Top: Absorbance as a function of temperature. Middle a zoom-in on the same data. Bottom the absorption as a function of phosphate concentration. Measurements were done over two days for 35 to 55 °C on day one and 50 to 70 °C on day two. The concentrations in the standards seem to have been slightly different on the two days, leading to the discrepancies.

Table 4: Parameters describing the linear relationship between phosphate concentration and absorbance (Abs), by the equation $Abs = a*Conc+b$, where $Conc$ is the concentration in ppb. R^2 is the correlation between data and fit; the closer R^2 to unity the better the linear fit.

Temp ($°C$)	**a** (ppb^{-1})	**b**	R^2
35	0.0013	-0.0080	0.9960
40	0.0023	-0.0014	0.9960
50	0.0123	-0.0880	0.9974
60	0.0121	-0.0106	0.9992
70	0.0234	-0.0106	0.9996

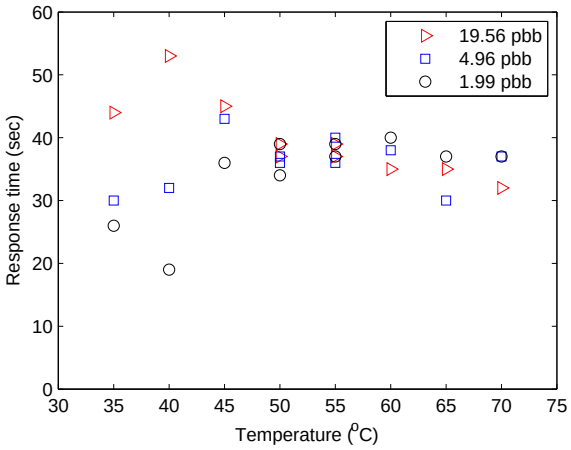

Figure 33: The temporal resolution, calculated as the time it takes for the response to a step function to rise from 10 % to 90% signal is presented as a function of temperature and phosphate concentration.

The results of fitting the linear equation $Abs = a \cdot conc+b$, where Abs is the absorbance and $conc$ is the concentration of phosphate (ppb), can be found in table 4. From the table it also clear that the absorbance was higher with higher temperature and that there was no significant effect on the linearity.

The response time or temporal resolution is a measurement of the time it takes for the response to a step function to rise from 10 % signal to 90 % signal. In this case a step function could be a switch from baseline (milli-Q-water) to one of the standards [*Kaufmann et al.*, 2008]. In figure 33 the temporal resolution as a function of temperature is presented for phosphate concentrations of 1.99, 4.96 and 19.56 ppb. It is clear that for low temperature the noise is higher and thus the variability for the response time is high, while for temperatures above 50 °C, noise does not influence so much on the response times, because the signal to noise ratio is much higher. No clear trend in the response time with temperature is observed and thus the temperature does not seem to influence coating effects.

All though there is a risk of silicate interfering with the method for temperatures above 40°C it was decided that a high temperature during mixing would be best for detection in ice, due to the low phosphate concentrations expected.

7.6 Flow rate and mixing length

The **flow rate of the reagent** was varied between 0.070 and 0.352 mL/min to investigate the effect. In table 5 flow rates and the corresponding color coding and type of pump tubing can be seen. The heat bath temperature was kept at 35 °C, boxcar value was 15, detection was done using a wavelength of 710 nm, integration time was 300 ms and the improved reagent described in section 7.4 was used. Results of the experiment are presented in figure 34.

The baseline signal does not show any trend. However for the highest flow rate baseline went down, probably again due to the fact that excess molybdenum blue can create blue

Table 5: The table provides information on the pump tubing used to investigate the effect of reagent flow rate

Colour code	**Wall thick-ness**	**iØ [mm]**	**Tygon®LFL**	**iØ [mm]**	**Tygon®ST**	**Measured flow rate [mL/min]**
Orange/blue	0.91 mm	0.25	SC0397	0.27		0.070
Orange/green	0.91 mm	0.38	SC0398	0.38		0.152
Green/yellow	0.91 mm	0.44			SC0052	0.198
Orange/yellow	0.91 mm	0.51	SC0399	0.49		0.236
Orange/white	0.91 mm	0.64	SC0397	0.59		0.352

color formation. Neither did the absorbance of the various phosphate concentrations show a clear trend. Orange/green (0.152 mL/min) and orange/yellow (0.236 mL/min) pump tubing for reagent provide the best sensitivity. Linear range was not good for any of the pump tubing most likely the standards were somehow contaminated. A flow rate of 0.152 mL/min was chosen for optimal conditions.

The **flow rate of sample** was not directly investigated, but sample flow of 1.689 mL/min combined with reagent and buffer flow of 0.148 mL/min and air introduction of 0.198 mL/min, removal of air and liquid from a debubbler with a flow rate of 0.353 mL/min and thus a total flow though the LWCC of 1.830 mL/min gave good results.

Mixing length was also investigated. The mixing length was varied between 75 cm and 500 cm. Detection was done at 710 nm with an integration time of 200 ms and a boxcar value of 2. The temperature in the heat bath was 65 °C. It was found that the mixing length had an effect on the limit of detection. Mixing lengths less than 300 cm did not show any difference between 0.12, and 0.37 ppb (see figure 35).

When the mixing length was less than 200 cm micro bubbles interrupted several times, ruining detection (not shown). This was probably due to a low back pressure, which for longer mixing is higher preventing micro bubbles from dissolving in the liquid.

The mixing length should not be shorter than 300 cm, but values of 350 or 500 cm do not make significant difference.

7.7 Wavelength

Tests of the optimal wavelength was conducted using an integration time of 50 ms and only one snap shot of the absorbance at the wavelength in question, hence there can be some effects due to noise. Further no filter was used. The concentration of phosphate was 97.30, 48.96, 24.48, 12.24 and 6.12 ppb. The effect of wavelength choice on the linearity between concentration and absorption is presented in figure 36. Note that above above 50 ppb the linearity is lost.

The optimal wavelength would be in the range 680 to 700 nm, which all show high absorbance. However when looking at the spectra for PO_4^{3-} absorption (see figure 39, right, bottom, green and blue lines) it becomes clear that for low concentration of PO_4^{3-} the peak is exactly at 710 nm. Since we expect low concentrations of PO_4^{3-} to be present in ice cores, a detection wavelength of 710 nm was kept as initially suggested by *Zhang and Chi* [2002].

7.8 Boxcar-spectrum integration

To investigate the signal to optimize on the signal to noise ratio part of the spectrum around 710 nm is integrated. The boxcar setting defines how much of the spectrum is

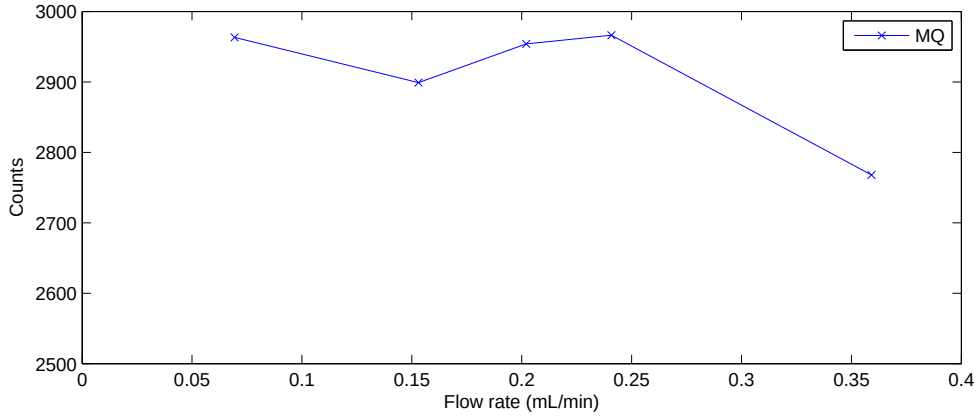

(a)

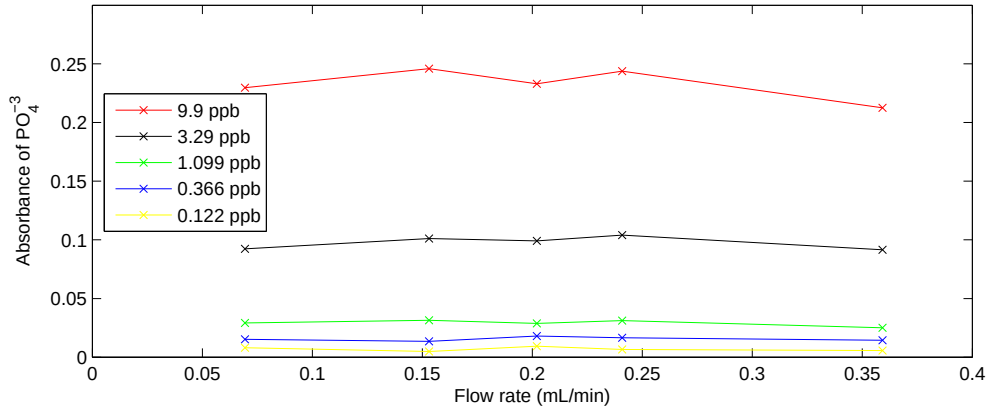

(b)

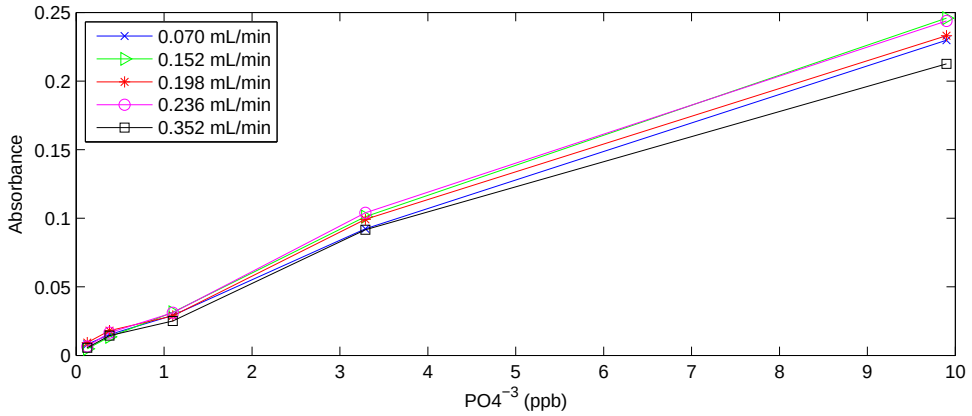

(c)

Figure 34: Reagent flow rate

The figures illustrate the effect of changing the flow rate of the reagent. ((a)) The baseline as a function of flow rate for the reagent;((b)) Absorbance vs. flow rate of reagent for different PO_4^{3-} concentrations; and ((c)) Absorbance vs PO_4^{3-} concentrations, showing a linear dependence slightly dependent on reagent flow rate.

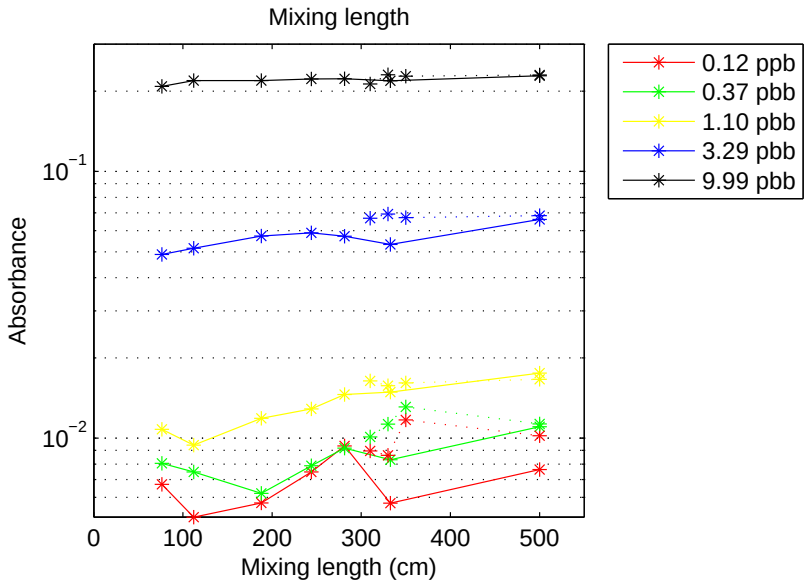

Figure 35: Absorption as a function of mixing length for PO_4^{3-} standards concentrations between 0.12 and 9.99 ppb, shown on a ylog axis. Dotted lines represents measurements conducted on another day than full drawn lines; changes in flow or standards concentrations can account for the discrepancies between the two.

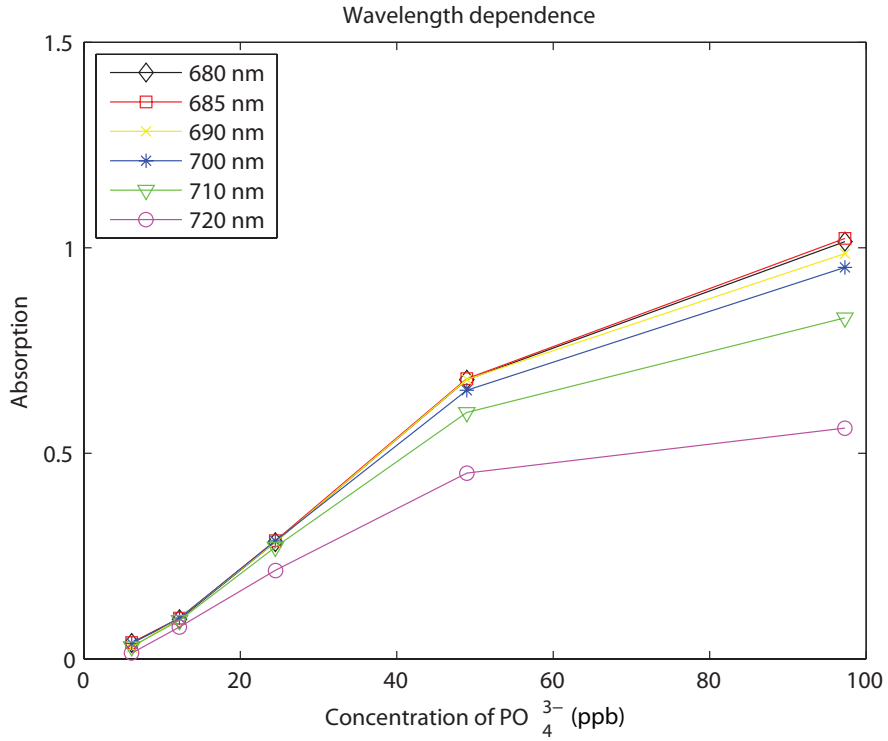

Figure 36: Absorbance as a function for phosphate concentrations is presented for various wavelength used for detection. Note how linearity is lost for high concentrations.

Table 6: Boxcar values reference to wave number integration. Integration is done between the start and end value.

Boxcar		0	2	4	6	8	15
Wavenumber	begin(nm)	709.980	709.305	708.637	707.695	707.292	704.938
	end(nm)	709.980	710.652	711.323	711.994	712.665	715.012

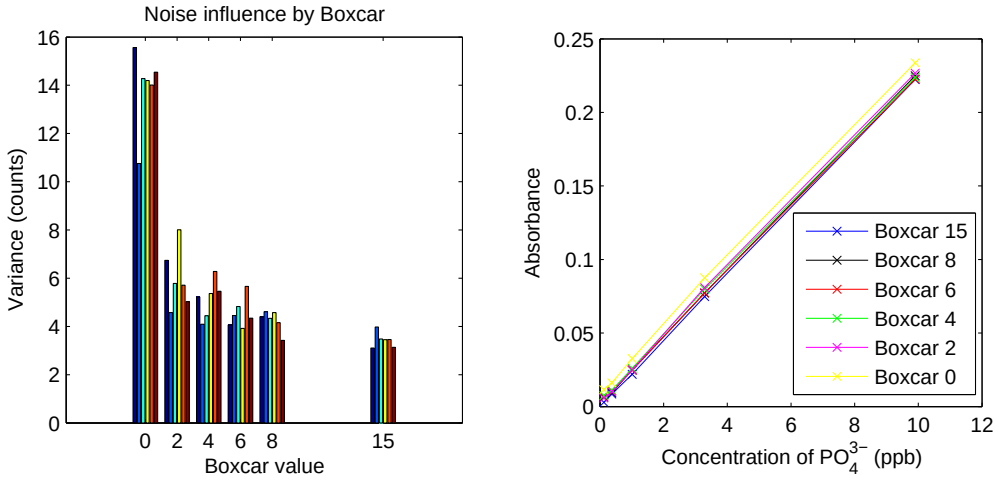

(a) (b)

Figure 37: The figures show the dependence on Boxcar values:(a) is the variance for different values of Boxcar. The colours refers to different concentrations of PO_4^{-3};(b) shows how the absorption of different amounts of PO_4^{-3} changes with Boxcar.

integrated around the central 710 nm. In table 6 the relation between the Boxcar value and the spectra integrated can be found. The higher Boxcar value the larger part of the spectra is used.

When the boxcar parameter is small, integration is done over a very short part of the spectrum, which gives a high standard deviation (STD). However, for large boxcar, not only the top in the spectrum from the molybdenum PO_4^{3-} reaction is measured, but also the sides of the top as well, which reduces the signal. A test was performed to see, which boxcar values gave the most stable, but at the same time the most precise data. The test was conducted using the original method by *Zhang and Chi* [2002] at temperature 35 °C, integration time 300 ms, with no air introduced and no debubbler and a mixing length of 4.25 meter.

In figure 37 the standard deviation (STD) in counts can be seen. The STD was calculated using a relatively flat part of the raw data. Note that the STD is fairly low as long as the boxcar is not 0, suggesting that as long as the mean is taken over some part of the spectra, rather than at just one wavelength, detection is stable.

The lower the boxcar value the higher the absorption as can be seen in figure 37. Therefore a boxcar value of 2 is suggested.

7.9 Dust and filter types

Dust particles are present in the ice and though the concentration of particles is low, they were found to highly effect the optical properties inside the LWCC. Filters for removing the dust were tested. A filter made of a glass capillary filled with glass wool had the desired effect. The filter tests conducted are presented below.

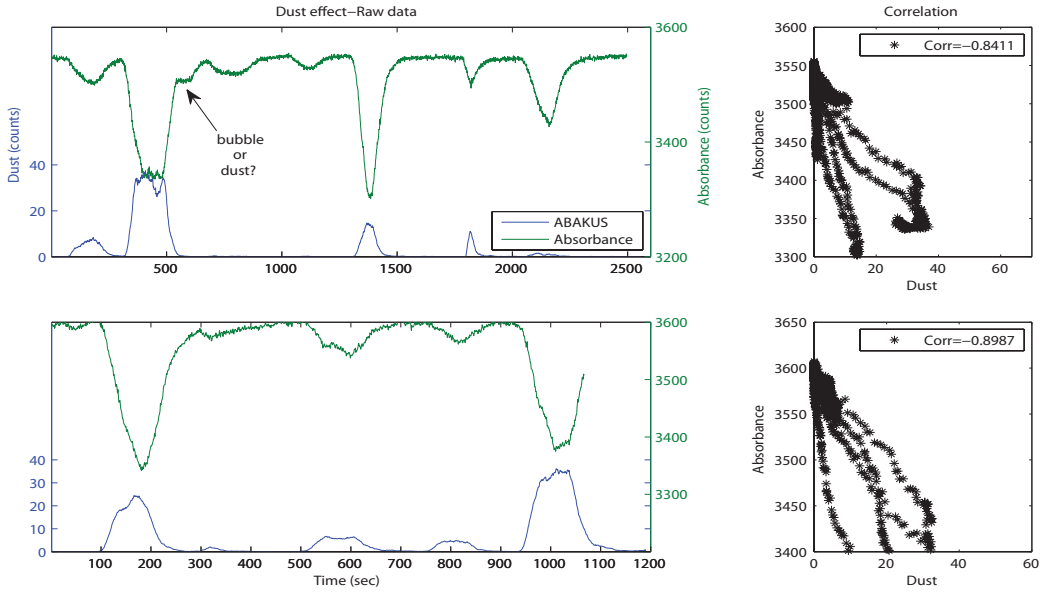

Figure 38: Left: Two examples of raw data showing dust measured by Abakus and optical effects of dust measured by LWCC. The data are smoothed over 20 seconds. A correction of the timing is made by eye, so that the measurements from the Abakus giving dust and the measurements from the LWCC giving the optical absorbance from dust start at the same time. Right: Plots of corresponding correlation between smoothed dust measured by Abakus and the absorbance in the LWCC from optical interference from dust. The correlation coefficient is corrected for the time lag between the Abakus and the LWCC and is based on the smoothed data.

First, to test if **dust** had any effect at all, the Abakus[19] was set up on the sample line to detect dust particles. Approximately one year old ice samples from the NGRIP ice core were used as dust contaminated samples and measurements were conducted using chemistry as described earlier but without molybdenum blue. Using chemistry with molybdenum blue would show both dust and phosphate effects, but the experiment without molybdenum blue shows only the result of optical interferences by dust. The results are presented in figure 38. Temperature was kept at 35 °C and integration time was 300 ms, no air was introduced and no filter was used. Flow rates were 1.00 mL/min, 0.08 mL/min and 0.69 mL/min for sample, reagent and buffer respectively.

It is clear that dust has an optical effect on measurements in the LWCC and that there is not a linear dependence between the counts measured by the Abakus and the dust interference detected in the LWCC. However between single events there seem to be some sort of linear correlation. Unfortunately this is not enough for devising a correction scheme for the LWCC using Abakus measurements.

Further, in the first example in figure 38 at time 600 seconds, an optical interference is visible in the LWCC, but not presented in the Abakus dust counts. This is either some dust, which was stuck inside the cell or an air bubble stuck inside the cell.

To further investigate the effect of dust in the 2 meter LWCC, the spectra of pure milli-Q water, melted ice water from the NGRIP core, that had been resting for a year and spectra of different standard PO_4^{3-} solutions were compared. The hope was that there was a wavelength at which the dust interference was not significant, but for which PO_4^{3-} was detectable: or two frequencies at which the dust effect was approximately the same, but PO_4^{3-} signal was detectable and different at the two wavelengths. 50 ms integration

[19] see section 5.1.3

Figure 39:

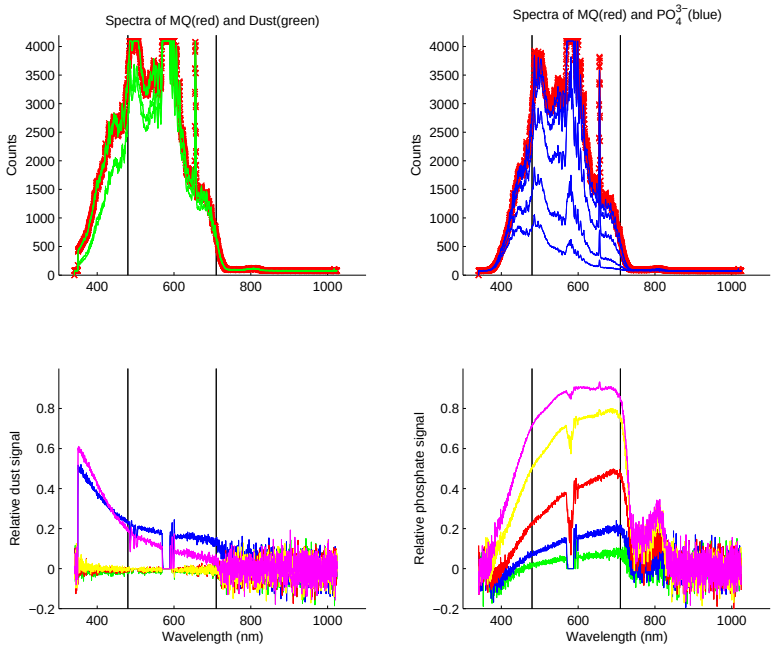

Spectra measured using an integration time of 50 ms at temperature 35 degrees are shown. Top left: For Dust (green) and milli-Q (red) measuring without molybdenum blue in the reagent. Right: For phosphate concentrations (blue) varied between 97.30 ppb and 6.12 ppb and milli-Q water (red) measured using molybdenum blue in the reagent. Bottom (left) and phosphate (right) relative to milli-Q water values is presented. The vertical black lines mark 710 nm and 480 nm.

time was used for detection, no air was introduced and thus no filter was used.

The spectra are shown in figure 39. The figures, which show $\frac{\text{Milli-Q}-\text{Sample}}{\text{Milli-Q}}$, makes it clear that there are not two wavelengths for which the dust has the same influence, neither are there two wavelengths at which the absorbances by PO_4^{3-} are similar. Further it can be noted that for high wavelength ($\geq$750 nm) almost no light gets through due to the absorbance of light in water.

In conclusion it was impossible to find a wavelength where the optical effect of dust was negligible, combined with a high PO_4^{3-} absorbance response. Thus a method was necessary for removing the dust from the flow.

To correct for the effect of dust different **filters** were tested. The filter types tested were three conventional type a green 2 μm frit in PCTFE (Polychlorotrifluoroethylene) material [20] and two PEEK (organic polymer thermoplastic) filters, blue 0.5 μm and green 2 μm[21]. The advantage of the conventional filters is that they are easy to change. Further the extra volume introduced by this kind of filters is usually very low. The PEEK filters introduce only an extra volume of 1.4 μL. The filters can be seen in figure 40.

The green **2 μm frit** and the **2 μm filter** was tested first. The hope was that due to their relative large pore size, they would not affect the flow rate and at the same time be useful for removing dust. The two types were tested on milli-Q water and ice core samples from NGRIP melted the previous year and kept in refrigerator. The samples were shaken before they were introduced. Reagent and buffer were replaced with water, so no PO_4^{3-} would be seen. Figure 41 show the raw data. It is clear that neither the frit nor the filter of 2μm succeeded in removing dust. They both show clear dips in the signal, when ice sample was led in. Further the baseline seems unstable, probably due to dust getting stuck inside the LWCC, changing its optical properties. In conclusion 2μm filters are not small enough to remove all dust.

[20] Bought from IDEX-Health and Science, product P372x

[21] Bought from IDEX-Health and Science, products A701 and A702, respectively

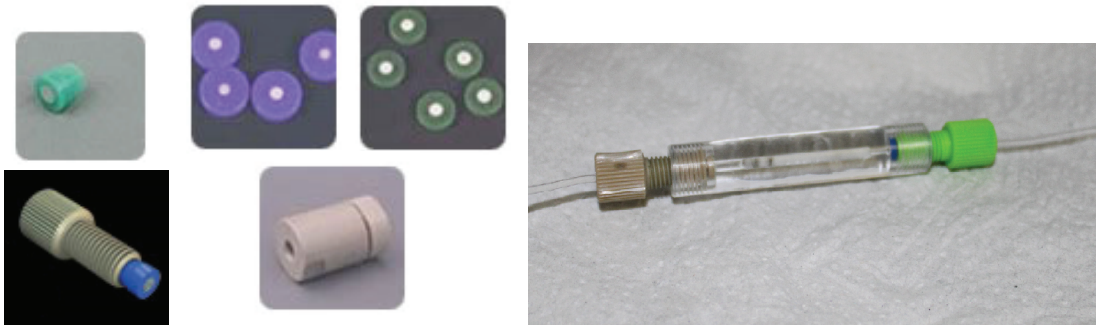

(a) (b) (c)

Figure 40: The images show the various filter types tested; (a) The frit, which is a conventional filter made of PCTFE material and stopping colloidal material larger than 2 μm;(b) Another type of conventional filters. The small colored filter is inserted in the grey holder and can thus easy be replaced. The filters come in sizes keeping 0.5 μm and keeping 2μm colloidal material out and are made of PEEK; (c) A home made glass filter, which is two-thirds filled with glass wool keeping nearly all dust out. This was the filter found optimal for the set-up.

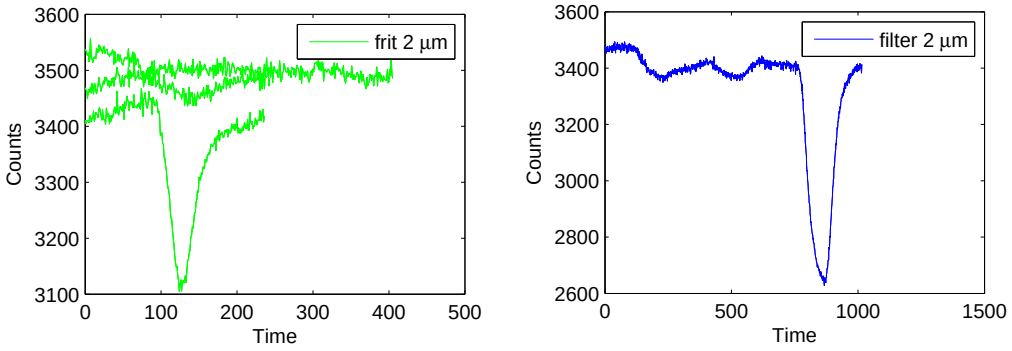

(a) (b)

Figure 41: The figures show raw data using an old NGRIP ice sample and milli-Q water, without reagent added. This means that the raw data from the LWCC shows only dust effects. (a) The effect of a 2 μm frit inserted before the LWCC, for three different experiments using samples with varying dust concentrations;(b) The effect of a 2μm filter. Though the ice sample is the same, the sizes of the peaks are not comparable.

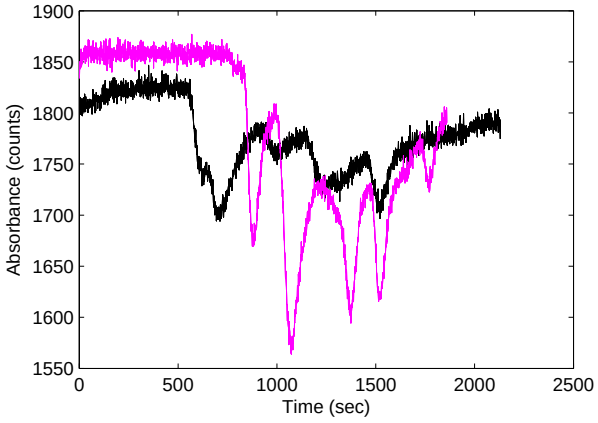

Figure 42: The figure shows ice core NEEM S1 shallow, bag 28 (pink) and 29 (black), measured replacing reagent and buffer with milli-Q water, and using a 0.5 μm filter to investigate the effects of dust.

As shown in figure 42 the effect of the **0.5 μm filter** was investigated measuring bag 28 and 29 from the NEEM S1 shallow core. Again buffer and reagent were replaced by water. Clearly the dust is seen using the 0.5 μm filter, too. Yet another effect is visible using the small filter; a flow difference from the beginning of the detections of the ice core to the end producing lower baseline after each core. This is due to the back pressure build up, when the filter gets more and more clogged with particles, making the flow through the LWCC slower and thus the molybdenum has longer time to react, colouring the water. In conclusion the 0.5 μm filter can not be used.

Finally, a filter home made by filling a glass capillary with glass wool was tested. Before being filled with glass wool the glass capillary has a length of approximate 29.6 mm, giving an internal volume of close to 0.2 mL. Thus the internal volume of this sort of filter is much higher than in the commercial ones, but since it is still lower than the internal volume of the LWCC (0.5 mL), which can be thought of as our measurement resolution, it is acceptable. Thus we can introduce it without significant loss of resolution.

Using old samples from NGRIP the effect of how much glass wool was needed in the filter was investigated. The set-up had an integration time of 200 ms, a temperature of 65 °C, wavelength 710 nm. Air was added and a debubbler of circular type was used. The Abakus instrument was inserted before the phosphate system. Results are presented in figure 43.

It is clear that it is necessary to compress the glass wool in the glass capillary and in order to completely avoid dust getting through, the filter needs to be at least 2/3 full. The drift seen in the measurements from the 2/3 filled filter is a coating effect, which I expect is not related to the filter.

Finally the glass wool filter was tested on bags 13 and 14 (7.15 to 8.25 meters depth) as well as on bags 53 and 54 (29.15 to 30.25 meters depth) from the NEEM S1 shallow core. This test was done using a reagent with all chemistry except molybdate and buffer as described in section 7.4.3. The reason for using chemistry except for molybdate was the belief that some of the dust particles could be water soluble and thus go into solution by the very acid chemistry (pH=1.5), so the chemistry it self might move some dust.

Sample was introduced at a speed of 1.68 mL/min, first passing the Abakus, then reagent and buffer was introduced at speed 0.15 mL/min and air was added at a speed of 0.20 mL/min. Mixing length was 500 cm. From the debubbler waste water and air was removed using a speed of 0.35 mL/min. Thus resulting in a flow of 1.83 mL/min through the filter positioned right before the LWCC. Detection was done at 710 nm and integration time was 200 ms. Results are presented in figure 44. It is obvious that the filter has a good effect. Almost no dust is seen even though the Abakus reads high values. However it

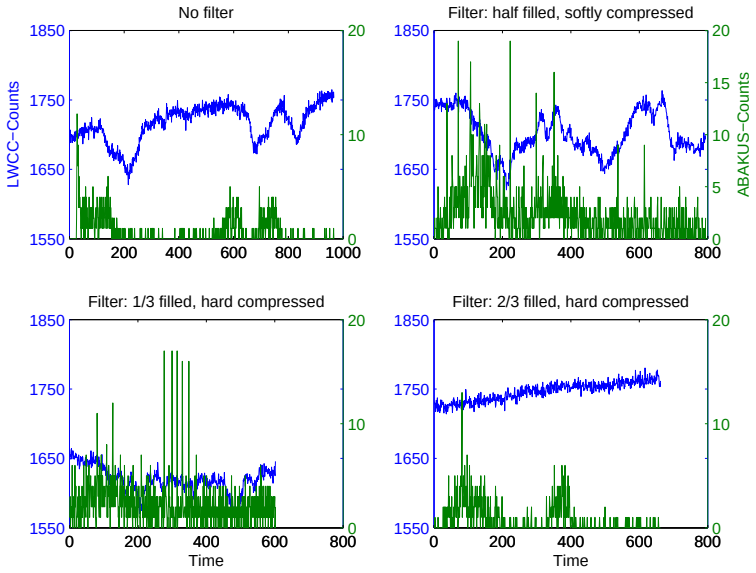

Figure 43: The figures show dust (green) and Absorption detection caused by dust (blue). In the top left, no filter is used. In the top right, a filter half filled with only softly compressed glass wool was used. In the bottom filters containing compressed glass wool were used, left 1/3 filled and right 2/3 filled. The very high single Abakus spikes are water bubbles. Note that the absorption (blue) is shifted relative to the Abakus detection (green) due to the sequence of detection with Abakus (green) first and absorption detection afterwards.

seems that there is a small bump in the LWCC absorption measurements in the beginning of bag 53 and 54 as well as half way through bag 53, where a break was present. This could be a dust signal coming from contamination from ends and from breaks. The reason that this type of contamination is not present higher in the firn (bag 13 and 14), could be due to capillary pressure, dragging the melt water into the more porous firn cores, thus smoothing the contamination from the ends.

A capillary filled with compressed glass wool was chosen as the best working filter. Though it is not perfect it is the only filter, which seems to work at all.

7.10 Bubbles

As explained in section 6.3.1 micro bubbles can cause measurements to fluctuate and larger bubbles can completely block the cell and be extremely hard to get rid off. An example of a bubble is shown in figure 45. But even worse, air bubbles in combination with a filter create a soap foam, due to the buffer, which is very sticky and hard to get rid of. Thus, avoiding bubbles in the set-up is essential for stable measurements.

To avoid bubbles an **accurel**[22] was inserted in the system right before the LWCC- However due to the amount of sodium dodecyl sulfate reducing the surface tension in the water, the liquid penetrated through the permeable holes in the accurel, too. Once the liquid was on the outside the very low pH caused the holes to get bigger. Thus over time dripping from the accurel occured. The accurel was moved further up system, so it was positioned before reagent and buffer. But when including filters after the accurel, back pressure was increasing and the water again penetrated through the accurel. Further, at this position it did not successfully remove tiny air bubbles coming from the reaction of sample with reagent and buffer during mixing. In conclusion an accurel at this position does not help-if on purpose we introduce air to avoid mixing as initially suggested in the set-up by *Zhang and Chi* [2002].

Hence another debubbler type was investigated. This debubbler consisted of a **pipette tip**, into which the liquid dripped (see figure 46(b)). A pump was sucked the liquid through the narrow end of the pipette tip. The pipette tip solution succeeded in removing

[22] Accurel is small piece of micro porous membrane allowing air but not water to penetrate

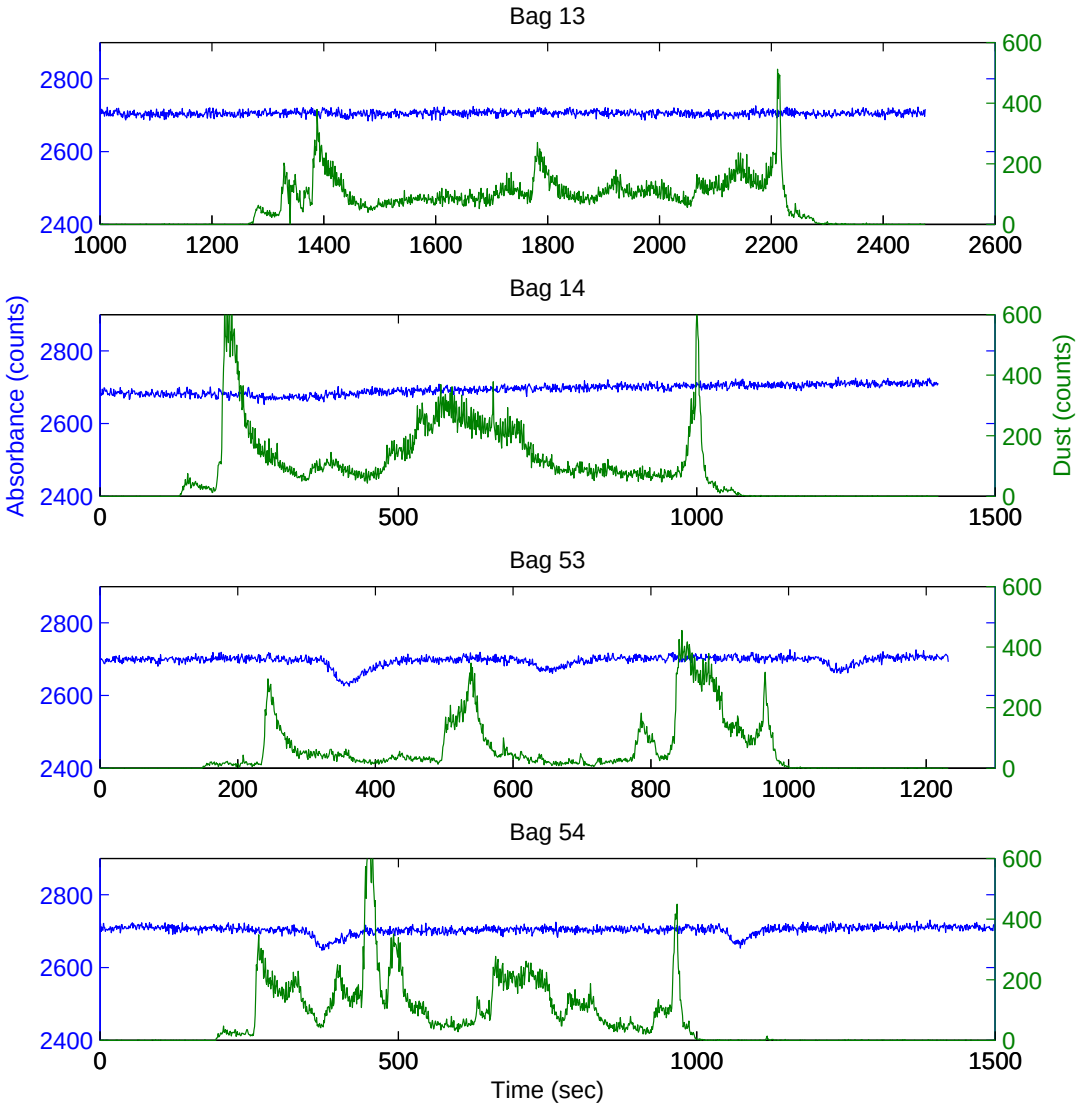

Figure 44: Measurements of dust using Abakus(green) and LWCC without molybdate in the reagent (blue) using a completely filled, hard compressed glass wool filter. The measurements are of bag 13 (top), 14, 53 and 54 (bottom) of the NEEM S1 shallow core. Note that there is a time lag between Abakus dust measurements and absorption of dust.

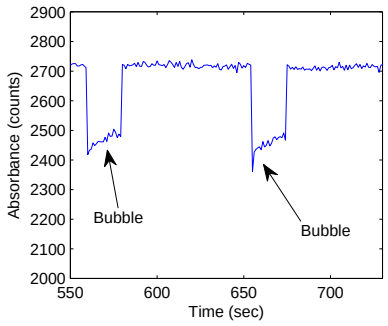

Figure 45: The figure show a measurement in which bubbles interfered.

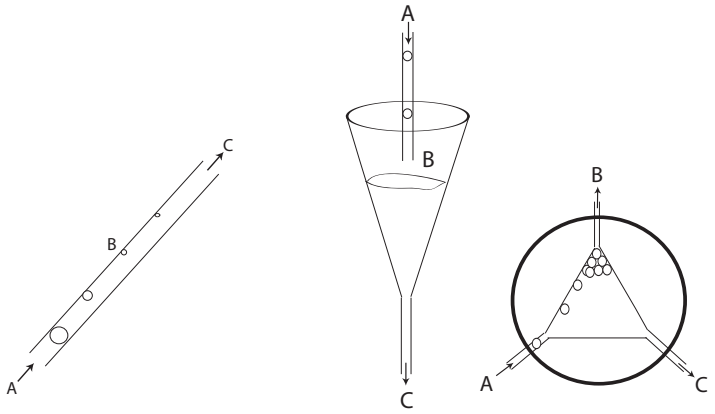

Figure 46: Different types of debubblers. A is the ingoing flow containing a mixture of liquid and air, B is the air removed and C is the liquid that continues to detection: (a) shows the idea of an accurel, which is permable for air but not for liquid. (b) show that a pipette tip can be used to debubble and in (c) the normal debubbler used in a CFA is shown. Note that it is very similar to (b), except that it is closed off.

air bubbles-however there are some disadvantages to this kind of solution. First of all open access to air can contaminate the sample. This could be remedied by closing the air part and flushing with a gas, minimizing contamination risks. Second, it is very difficult to get flow rates equal between the ingoing dripping and the outgoing suction and only a little difference between the two will cause the pipette tip to be either emptied or filled over time, creating a time dependent mixing. If a lot of air is introduced, the mixing volume in the pipette would change, changing the effective mixing time of the water solution and thus creating difference in absorption, because the system is running so a full reaction never happens. The reaction time and mixing must ideally be the same at all times.

Finally a debubbler of the type used in the normal CFA set-up was chosen (round type). The debubbler was positioned before the LWCC as suggested by *Zhang and Chi* [2002]. This debubbler consists of three connected lines and is a closed system, thus contamination from the outside is avoided. The debubbler had the ingoing mixture of sample, reagent and buffer at a flow speed combining the three, while air was removed by a pump set at a sufficient speed remove all air as well a small part of the liquid. This was so to ensure that if any larger air bubbles made it that far in the system they would be removed, too. The third side going to the LWCC has a flow rate, which is the difference of the two others. This last type of debubbler was chosen and positioned before the filter

and the LWCC. It does still have the issue that the mixing time can be changed depending on the amount of air inside, but since the internal volume of the debubbler is only 0.5 mL, depending on the exact type, this is not a huge problem. This type of debubbler was found to be the best of the three.

The three types of debubblers are shown in figure 46.

7.11 Cleaning the LWCC

Though the set-up is optimized for avoiding that bubbles or dust particles get stuck inside, nevertheless this does happen from time to time. Some coating can also occur. Hence a cleaning process is needed.

To clean the LWCC for bubbles and dust particles the best result is obtained by using a syringe to flush with Milli-Q water, then flush it with air and then flush with Milli-Q water again. This procedure has proved successful for removing air bubbles as well as small particles stuck in the LWCC. It is also useful to remove soap foam micro bubbles.

However coating of the cell requires a different approach. The LWCC cleaning manual suggests that it is useful to flush first with a solution of soap, then methanol and the HCl acid. I found that this approach was extremely time consuming and extensive flushing of water was needed to gain full counts again afterwards. Thus cleaning only by flushing with water should always be tested first.

I found that leaving a solution of sodium hydroxide in the LWCC cell for 5 minutes was the best way to get rid of coating effects from the molybdenum blue, and thus get the baseline up again. But I do not know the effect of using this approach over long times. There is a risk that it could cause small fractures in the surface coating of the LWCC, thus permanently changing the optical properties of the LWCC.

7.12 Ice samples

Some changes can happen to the phosphate content detected using the method described during freezing conditions. According to *Nollet* [2007] in general freezing of phosphorus samples can rupture cells and release phosphorus into solution. Thus filtered measurements can not be compared to filtered samples of not frozen water. However the method I use seeks to measure the total reactive phosphorus[23] and as long as I am aware, when analysing data it is not a problem. If calcite is present in the ice matrix, some co-precipitation of phosphorus with the calcite can occur.

7.13 Optimum conditions

The optimal conditions for detection of phosphate in ice cores, obtained from the above presented experiments, are described below: The reagent should be mixed by dissolving 0.37 g molybdenum blue in 25 mL 5N H_2SO_4 adding 5 mL tartaric acid and diluted with 100 mL milli-Q water. The buffer should be made by dissolving 0.5 g L-ascorbic acid and 7 g sodium dodecyl sulfate in 100 mL milli-Q water. Standards should be made in polypropylene bottles to avoid that the PO_4^{3-} sticks on the glass walls.

The optimum set-up is shown in figure 47. Optimal flow rates are 1.68 mL/min for sample, 0.15 mL/min for reagent and buffer and the flow rate for air should be 0.20 mL/min. Air is introduced to limit dispersion. It is recommended that mixing occurs over at least 300 cm of tubing of a diameter

[23] reactive phosphorus is phosphate and soluble phosphorus

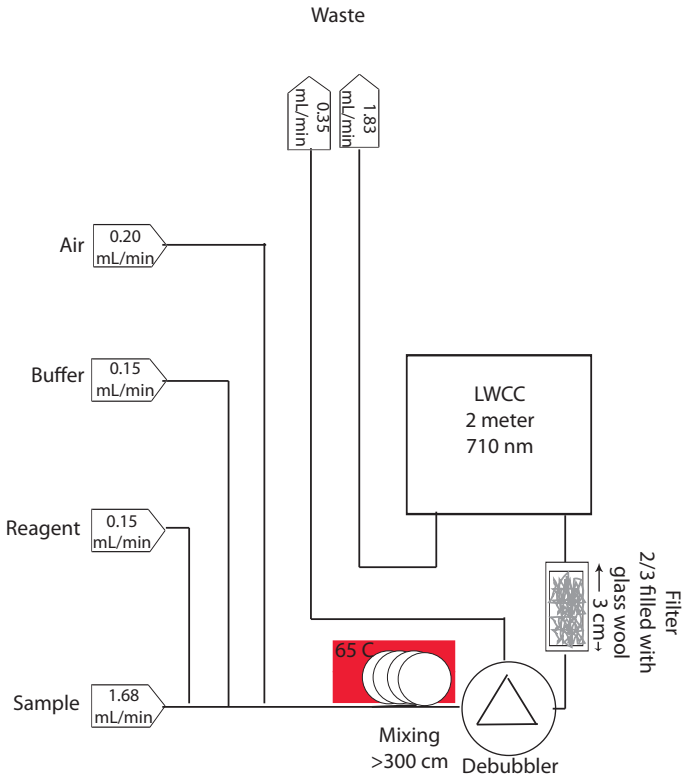

Figure 47: Optimized set-up for the detection of phosphate in ice cores.

of 0.5 mm, in a heat bath with a steady temperature of about 65 °C. Air should be removed using a sealed debubbler to avoid bubbles in the detection cell.

A filter made of a 29.6 mm long glass capillary, with an internal volume of 0.2 mL should be at least 2/3 filled with compressed glass wool and positioned before the entrance of sample to the 2 meter long LWCC to prevent optical interference from dust.

Detection at a wavelength of 710 nm using a boxcar value of 2 corresponding to an integration from 710.305 to 710.652 nm with an integration time of 300 ms yielded the highest limit of detection.

Using this set-up concentrations below 0.1 ppb can be detected and the noise is about 15 counts corresponding to about 0.18 ppb PO_4^{3-} when baseline is 3000 counts. There is good linearity below approximately 50 ppb. An example of detection of standards using the optimum conditions is presented in figure 48. The response time is between 37 and 43 seconds-but as can be observed in the raw data, some coating effects is present causing more smoothing for the high concentrations. Further there is a risk that silicate might interfere, due to the high temperature chosen. The next section presents the detection of phosphate in the NEEM S1 shallow ice core using the optimized method.

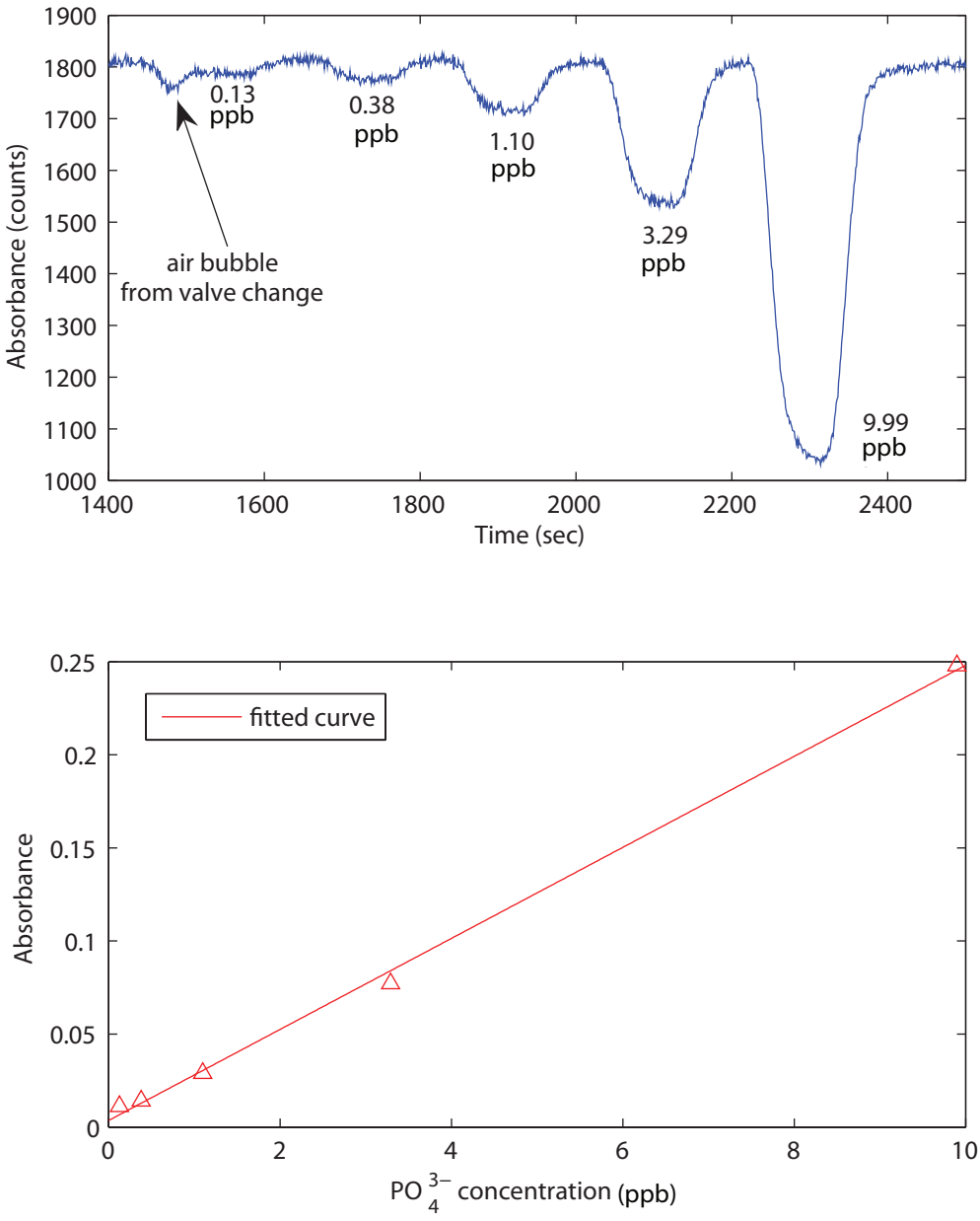

Figure 48: Top: Raw data obtained using the optimum conditions. The figure graph shows as a function of time counts detected for different concentrations of phosphate. Bottom: Linearity. The reason for the not completely linear relationship is most likely difficulties with standards.

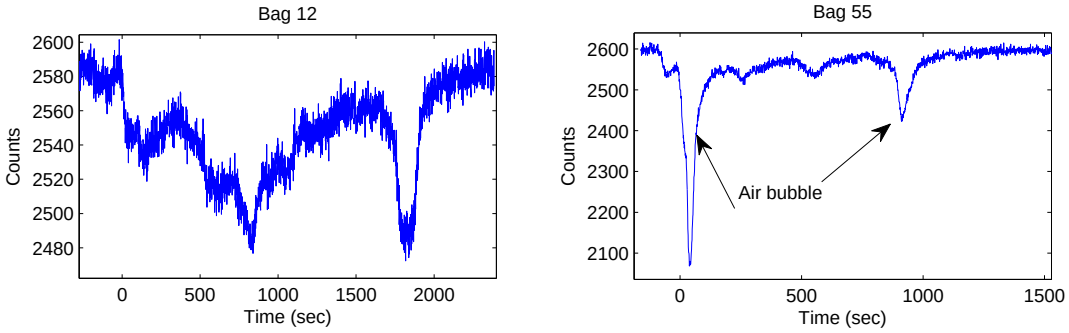

(a) (b)

Figure 49: Raw phosphate detection in counts per second showing (a) bag 12 from the NEEM S1 shallow ice core and (b) bag 55.

8 The last 120 yr - NEEM S1 shallow core

A presentation and analysis of phosphate detected in the NEEM S1 shallow ice core are presented in this section using the optimum conditions found in the previous section.

The NEEM S1 shallow core is a firn core from Greenland 76.45°N, 44.77°W, 2771 meter above sea level. It was retrieved during the NGRIP-NEEM traverse expedition in 2007. It has a diameter of 7.62 cm. Detection of PO_4^{3-} was done between 6 and 35 meters depth. The detection of PO_4^{3-} covers parts of the last 120 yrs. In total 15 bags of 55 cm were analysed in this work.

8.1 Description of the set-up used for the NEEM S1 shallow core

The Copenhagen CFA system was used for measurements of the NEEM S1 shallow ice core. Melt head temperature was kept close to 35 °C corresponding to a melting rate of about 7 mL/min. The rate of melt of the ice core was measured by a decoder in cm/min. The melt water was debubbled before being divided between 4 lines: Conductivity, Ammonium and a combined dust-phosphate line- further a sodium line was attached, but no useful sodium signal was produced at the same time as PO_4^{3-} was detected. For more info on the Copenhagen CFA set-up see section 5.1.

Ammonium was detected using a fluorescence method. Standards had a concentration of 16.5 and 33.1 ppb Ammonium. Unfortunately the system did not work well and thus only the shape and not the absolute values can be trusted.

The dust-phosphate line went through the Abakus combined with a flow counter that was inserted in order to gain information for calculating dust in counts/mL rather than counts/sec. The line then continued to the phosphate system at a rate of 1.83 mL/min and PO_4^{3-} detection was as explained in section 7.13; except that 5 meters of mixing was used to ensure that no bubbles were introduced due to lack of back pressure.

8.2 Calibrating phosphate

Phosphate is detected in counts per second. Examples of raw data are shown in figure 49.

Raw data were calibrated using standards of concentration 0.1, 0.49, 0.99, 2.99 and 9.99 ppb PO_4^{3-}, which were kept in polypropylene bottles and were run after every 2nd to every 4th bag. The calibrations used can be found in table 7 together with the bag

Table 7: The linear relationship between phosphate concentration ($Conc$) and absorbance (Abs), by the equation $Abs = acdotConc + b$, where $Conc$ is the concentration in ppb. R^2 denotes the correlation between data and fit and the closer to unity the better the fit. All fits are reasonable.

Bag	depth (meter from surface)	a (ppb^{-1})	b	R^2
11,12	6.05-7.15	0.02045	0.0009487	0.9941
16,17,18	8.80-10.45	0.02021	0.001247	0.9945
51,52	28.05-29.15	0.02445	0.003595	0.9980
55,56	29.15-30.25	0.02163	0.0002769	0.9964
57,58,59	30.25-31.90	0.02094	-0.00216	0.9957
60,61,62	31.90-33.50	0.01916	0.001639	0.9949

numbers and corresponding depths. Not all bags were detected for PO_4^{3-}; some bags were used for optimization of the phosphate detection method.

The phosphate data were transformed to concentration vs depth(cm) using the encoder information which provided the melting speed in cm/second.

Breaks were set into the record and contaminated parts and parts with bubbles were removed. As shown in figure 44 both ends and breaks can be contaminated by dust, not removed by the filter. Hence at all ends and breaks a piece of size 25 mm was removed from the PO_4^{3-} signal.

Finally the cores were inserted at the correct depth.

A time scale was found by *Sauer* [2010] and can be seen in equation 14 [*Paterson and Cuffey*, 2010], where t is the age of the core in years, the mean annual layer thickness in meter of ice equivalent is $\lambda_{ice} = 0.166m$, the density of the ice is $\rho_{ice} = 917kg/m^3$, the density of snow is $\rho_{snow} = 315kg/m^3$, $C = 0.03026m^{-1}$ and z is the depth measured from the top. The age is then given by subtracting the year t from the year in which the core was drilled-in this case 2007. The age model has an uncertainty of 13 years for the uppermost 224 yrs[24].

$$t = \frac{1}{\lambda_{ice} \cdot \rho_{ice}} \int_0^z (\rho_{ice} - (\rho_{ice} - \rho_{snow}) exp(-C \cdot z)) dz \tag{14}$$

Flux measurements was calculated only for the bags 55 to 62 using the accumulation rates for the NEEM S1 shallow core found by *Sauer* [2010], who used the NH_4^+ to detect the beginning of summer each year. The flux was calculated using equation 15, where $\Delta PO_4^{3-}[\mu g/kg]$ is the mean PO_4^{3-} concentration for the depth from summer start of one year to summer start of the next year, $Acc[m]$ is the accumulation rate and $\rho_{ice} = 917[kg/m^3]$ is the density of ice.

$$PO_{4\text{flux}}^{3-}[ng/cm^2/yr] = \Delta PO_4^{3-}[\frac{\mu g}{kg}] \cdot Acc[\frac{m}{yr}] \cdot \rho_{ice}[\frac{kg}{m^3}] \cdot 10^{-3}[\frac{ng}{\mu g}] \cdot 10^{-4}[\frac{m^2}{cm^2}] \tag{15}$$

8.3 Results from the NEEM S1 shallow core

Phosphate detected in the NEEM S1 shallow core can be seen in figure 50. The mean level of PO_4^{3-} is 0.32 ppb. For the 2 mm resolution phosphate data the standard deviation is 0.27 ppb and the variance was 0.07 ppb^2. The maximum of detected PO_4^{3-} was 4.18 ppb at a depth of 30.3 meters (1903 A.D.).

Figure 51 is a histogram of the phosphate detected in the NEEM S1 shallow ice core.

[24]There is a volcanic signal from the eruption of Laki in 1783-1784 A.D. *i.e.* 224 yrs ago

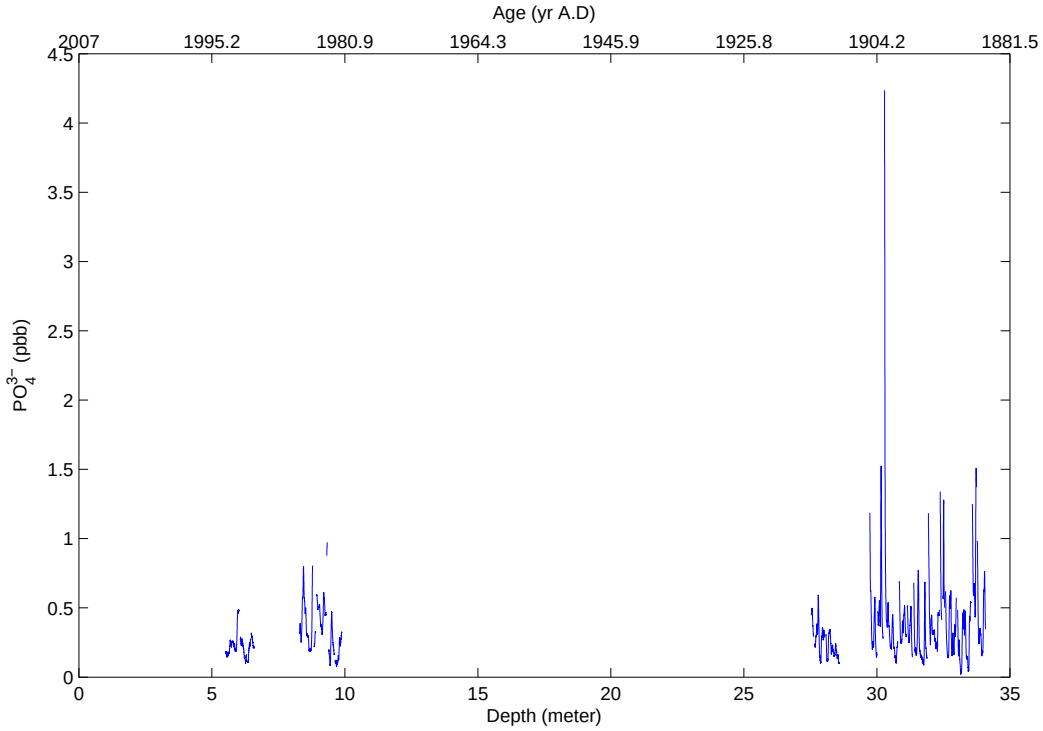

Figure 50: Phosphate detected in the NEEM S1 shallow core is shown (using a 2 cm smoothing) vs. depth (bottom) and age (top) calculated using equation 14. Note that the age axis is not linear.

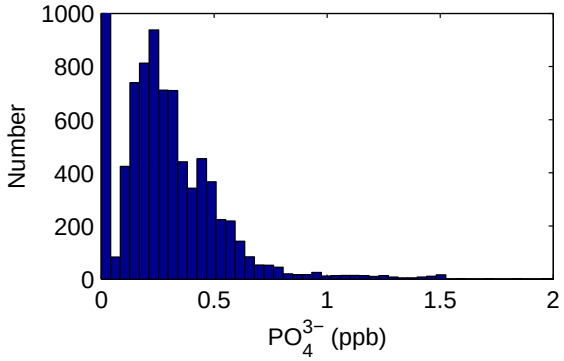

Figure 51: The distribution of phosphate found in the NEEM S1 shallow ice core.

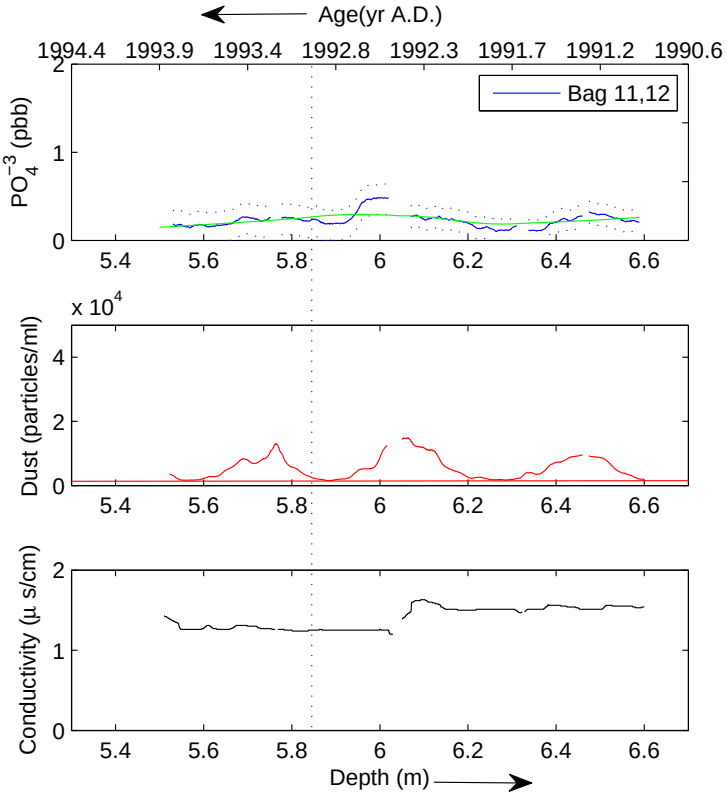

Figure 52: Measurements from bag 11 and 12. In the top graph solid blue represents phosphate and dotted blue is the amount of phosphate found using maximum and minimum baseline values. Green is smoothed phosphate. Middle graph (red) is dust measurements and in the bottom solid black is conductivity. Measurements are shown *vs.* depth as well as *vs* age. Note that the age scale is not linear.
The vertical black dotted line marks a small bump in the phosphate, which does not show in the dust signal.

In figures 52 to 55 dust, conductivity and ammonium detection are presented together with the phosphate using a 2 cm smoothing on all parameters, in order ensure that the higher resolution data is on a comparable scale as the phosphate measurements. For phosphate both the most likely amount and the minimum and maximum deviations are presented, calculated using the minimum and maximum count of baseline instead of the mean is shown to give an idea of the uncertainty, which is about 0.3 ppb.

The correlation coefficient between the series of raw dust and phosphate was 0.72 and between ammonium and phosphate 0.09 using only bag 55 to 62, because they are the only ones in which ammonium signal can be trusted. No convincing linear correlation between phosphate and dust or phosphate and ammonium was found (analysis not shown).

A spectral presentation of the data is shown in figure 56. The analysis was performed for five different sections of length of 110 cm (2 bags) each. Annual layer thickness was between 0.12 and 0.15 meter. The cut-off length found as five times the noise was between 1.3 cm and 2.9 cm. No trend between depth and cut off length nor between depth and annual layer thickness was found.

The flux of phosphate together with the phosphate concentrations detected is presented in figure 57 for bags 55 to 62. The mean value was 5.86 ng/cm^2/yr.

8.4 Discussion of phosphate in the NEEM S1 Shallow core

In the following the observations from the NEEM S1 shallow ice core are discussed. First levels and trends are compared to data from other sources (referring to section 3), then phosphate is discussed in relation to dust, combined phosphate-ammonium sources are suggested, some special layers are discussed and finally the spectral analysis is considered.

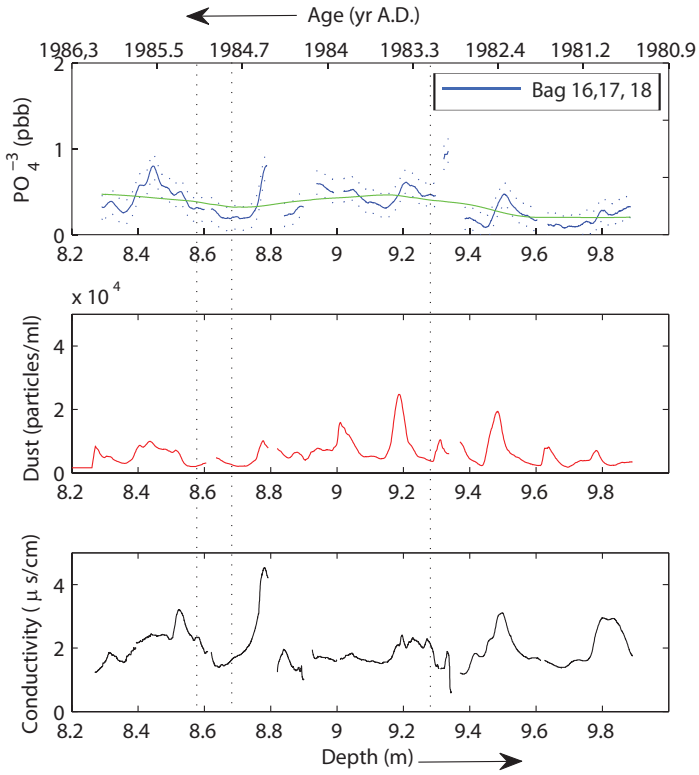

Figure 53: Measurements from bag 16, 17 and 18. For details see caption to figure 52.

8.4.1 Level and trends

The average level of PO_4^{3-} found in the NEEM S1 shallow core (0.32 ppb) is higher than the level of phosphorus in Greenland detected using ICP-MS by *Edwards et al.* [2007] (0.25 ppb). The two results are of comparable size, even though the ICP-MS measures the total phosphorus content and the method used in this study only detects the reactive part of phosphorus and phosphate, expected to be approximately 35 % of the total phosphorus. Thus the PO_4^{3-} level detected in the NEEM S1 shallow ice core is higher than expected by a factor 3.66 or the detection done by *Edwards et al.* [2007] is to low. This can be due to the different sites of the ice cores and the difference in detection method. Further the discrepancy could be explained if there is not a large amount of nonreactive phopshorus on the ice, since then the detections of phosphate and reactive phosphorus found in this study would be comparable to that of total phosphorus by *Edwards et al.* [2007].

The concentration of PO_4^{3-} found in the NEEM S1 shallow ice core is much lower than the results found by looking at PO_4^{3-} in melt water streams from glaciers (see section 3.4). It is expected that Greenland would have lower values of phosphate due to the ice sheet being very remote and high in the north and further in high elevation causing rainout of all species before reaching the central ice sheet.

The distribution of the phosphate concentrations (figure 51) show an excessive tail towards the higher concentrations. This looks like a log normal distribution. It was not feasible to put the detected phosphate on a log scale, because there were too few data points to get a meaningful looking distribution on a log scale.

No trend was visible in the PO_4^{3-} data over the last 120 yr, though some higher spikes are present in the older part of the ice. There is no evidence of any **anthropogenic change**. It could have been expected that there would be some sign of the steep rise in the use of fertilizers (see figure 9). However according to *Mahowald et al.* [2008] only 14.3

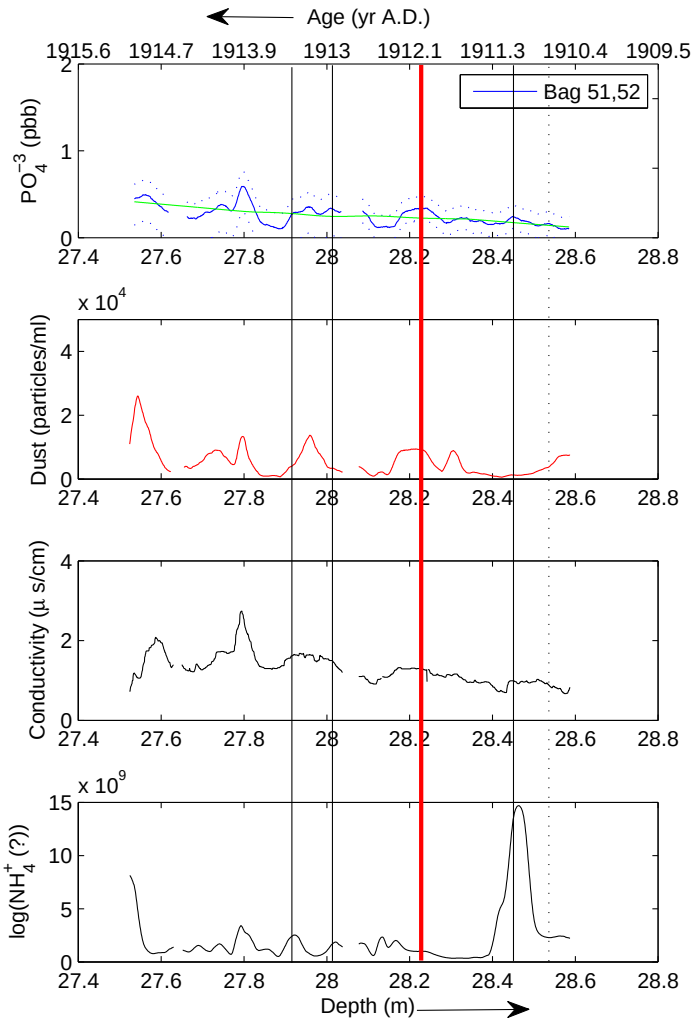

Figure 54: Measurements from bags 51 and 52. In the top graph solid blue represents phosphate and dotted blue is the amount of phosphate found using maximum and minimum baseline values. Green is smoothed phosphate. Second graph from top (red) is dust measurements and in the third from top solid black is conductivity. In the bottom graph ammonium measurements is shown, however something was wrong with the ammonium detection system and thus only the shape of the curve can be trusted not the absolute value. The horizontal axes are depth and age scale. Note that the age scale is not linear.
The vertical black dotted line marks a small bump in the phosphate, which does not show in the dust signal. The vertical black solid lines mark bumps in the phosphate, which do not show in the dust, but do to some extent show in the ammonium. The red fat vertical line marks were the volcanic eruption of Katmai in 1912, should be according to the dating, however it is more likely the high spike in the ammonium.

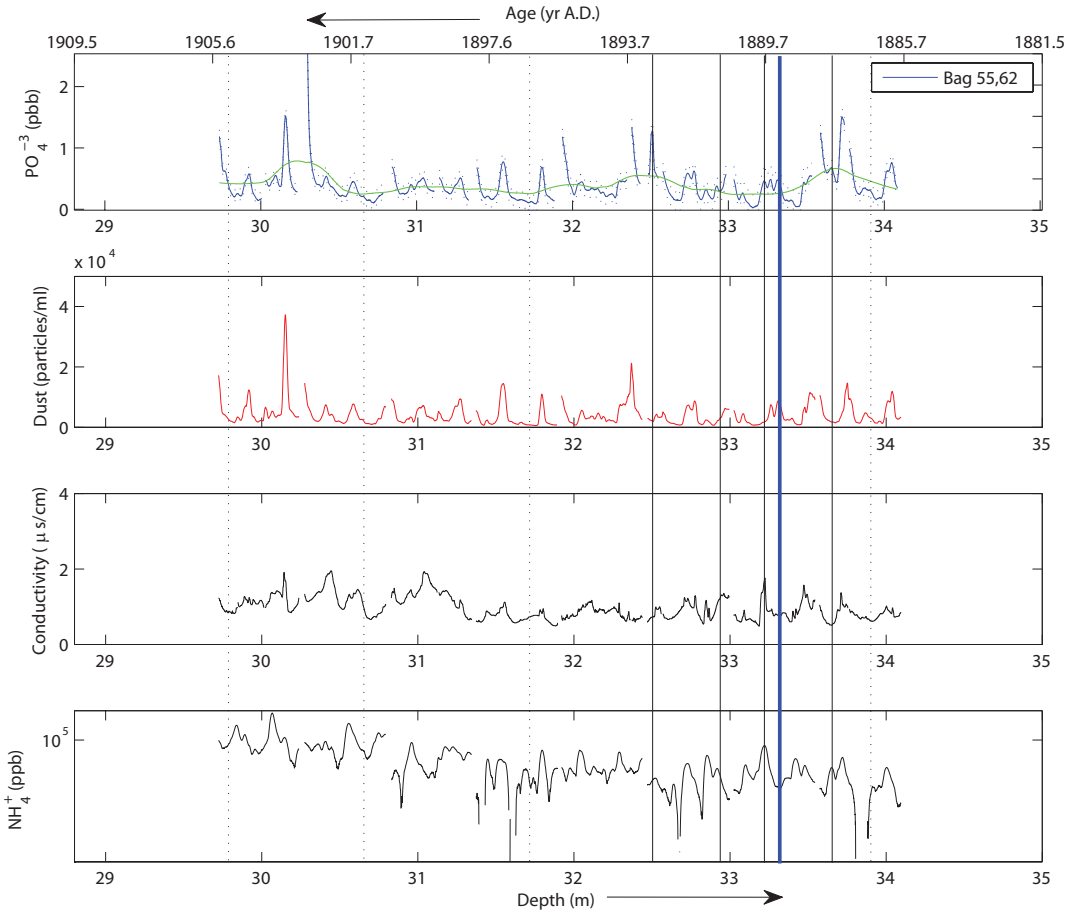

Figure 55: Measurements from bags 55 to 62. In the top graph solid blue represents phosphate and dotted blue is the amount of phosphate found using maximum and minimum baseline values. Green is smoothed phosphate. Second graph from top (red) is dust measurements and in the third from top solid black is conductivity. In the bottom graph ammonium measurements is shown, however something was wrong with the ammonium detection system and thus only the shape of the curve can be trusted not the absolute value. The down going trend with depth is most likely not a real effect. The horizontal axes are depth and age. Note that the age scale is not linear. The vertical black dotted line marks a small bump in the phosphate, which does not show in the dust signal. The vertical black solid lines mark bumps in the phosphate, which do not show in the dust, but do to some extent show in the ammonium. The vertical blue fat line represents a melt layer known to be present in 1889 in the NGRIP core.

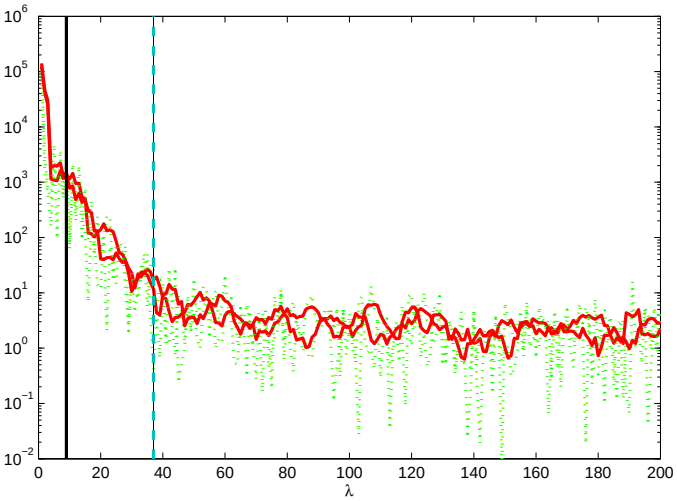

Figure 56: Spectral analysis of the NEEM S1 shallow core phosphate. Green; raw data. Red; a smoothed version of the raw data. λ denotes the number of sin curves used on the length used for the analysis (**1.10 m**), thus the wavelength corresponding to λ can be calculated by 1.10 meter·λ=wavelength. The vertical green line marks the position of the top representing a year (λ=7, year=0.157 meter) and blue line is the cut off signal length found as five times the noise (λ=37, year=0.029 meter). Analysis of two times 1.10 meter is shown.

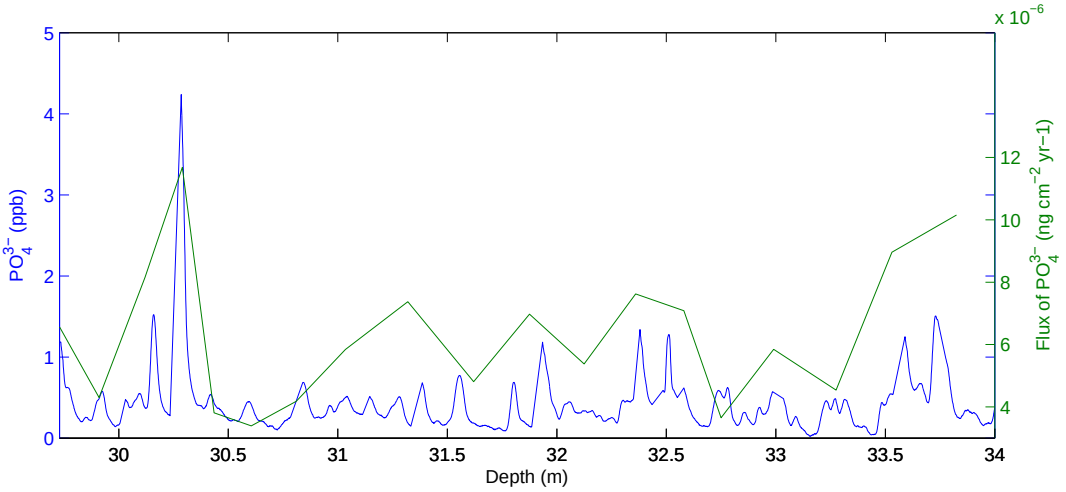

Figure 57: Phosphate flux (green) as calculated using equation 15, with interpolation where measurements are missing and the 2 cm smoothed phosphate concentration (blue). Data for bags 55 to 62.

% of today's phosphate signal is anthropogenic. The anthropogenic part of the phosphate signal expected is thus in mean values at most 0.05 ppb in the ice core and most likely it is much less since the increased use of fertilizer is only a part of the total anthropogenic effects. Any expected anthropogenic change is very hard to detect, within the limit of detection using the method. Further, fertilizers are used very close to the ground, and thus do not travel far, making transport to the ice sheet weak.

8.4.2 Dust

The phosphate signal shows a very high correlation with dust. The correlation corresponds to the approximately 50 % of phosphate that is suggested to arrive directly with mineral dust. If it further assumed that sea salt and fossil fuel are the only soluble parts of the sources seen in table 1 (a very rough assumption), then 92.5% of the signal seen in the ice could arrive with the dust detected by the Abakus.

Though the shape of the phosphate signal resembles that of dust, the dependence is not linear. This could either be due to the PO_4^{3-} arriving not only with dust and an underlying signal from another source enhancing the PO_4^{3-} sometimes or it could be explained if the dust contained various amounts of phosphate. In section 3.3 it is mentioned that dust contains 720 mg/kg (ppm) phosphorus with a variation of 30 %. The soluble fraction of the phosphorus and phosphate can cause even larger variations. Finally the correlation of dust and phosphate could be due to similar transport processes; during transport PO_4^{3-} will stick to the dust.

To get a rough theoretical estimation of the amount of phosphate, which does not come from dust, one could calculate:

$$PO_{4\text{Not dust}}^{3-}[mg] = PO_4^{3-}[mg] - C_{dust}[kg] \cdot 720[mg/kg] \cdot S \tag{16}$$

where PO_4^{3-} would be the detected phosphate, C_{dust} would be the amount of dust and S is the soluble fraction of phosphate. S however does vary for different kind of aerosols (see section 3.3). But probably the most correct to use is the soluble fraction found by *Hodson et al.* [2004], who found that the ratio of soluble phosphate over total phosphorus varied between 0.2 % and 3.4 %. I did not calculate the amount of phosphate arriving with dust using the NEEM S1 data, because the concentration of dust in kg were not measured. An estimate of the mean phosphate arriving with dust in the Holocene was calculated using the mean dust concentration in the Holocene 33 μg/kg ice [*Steffensen*, 1995] corresponding to a phosphorus amount of 0.024 μg/kg ice (ppb). Thus the theoretical amount of phosphate arriving with dust is lower than the value found experimentally. This could suggest that dust was not the source but rather the transport mechanism of other sources of PO_4^{3-} such as sea salt, biological decomposition, or forest fires.

It is also possible that there could be a dependence on the amount of phosphate arriving with dust in different **seasons**, due to the fact that different weather patterns are dominant, varying the source areas with possibly different phosphate content in the dust or complete different sources being dominant. This was investigated by testing the different seasons. The annual layer thickness's found by *Sauer* [2010] were used to divide the yearly layer into four seasons and calculating the mean PO_4^{3-} level for each season of each year, thus assuming equal amounts of precipitation in each season. This introduces some uncertainty since of course the precipitation of the seasons are not equal. In summer, *e.g.*, sublimation is known to occur from the ice sheet. Dust for the four seasons is plotted against PO_4^{3-} in figure 58.

A **yearly pattern** was found in the PO_4^{3-} signal. The highest mean concentration

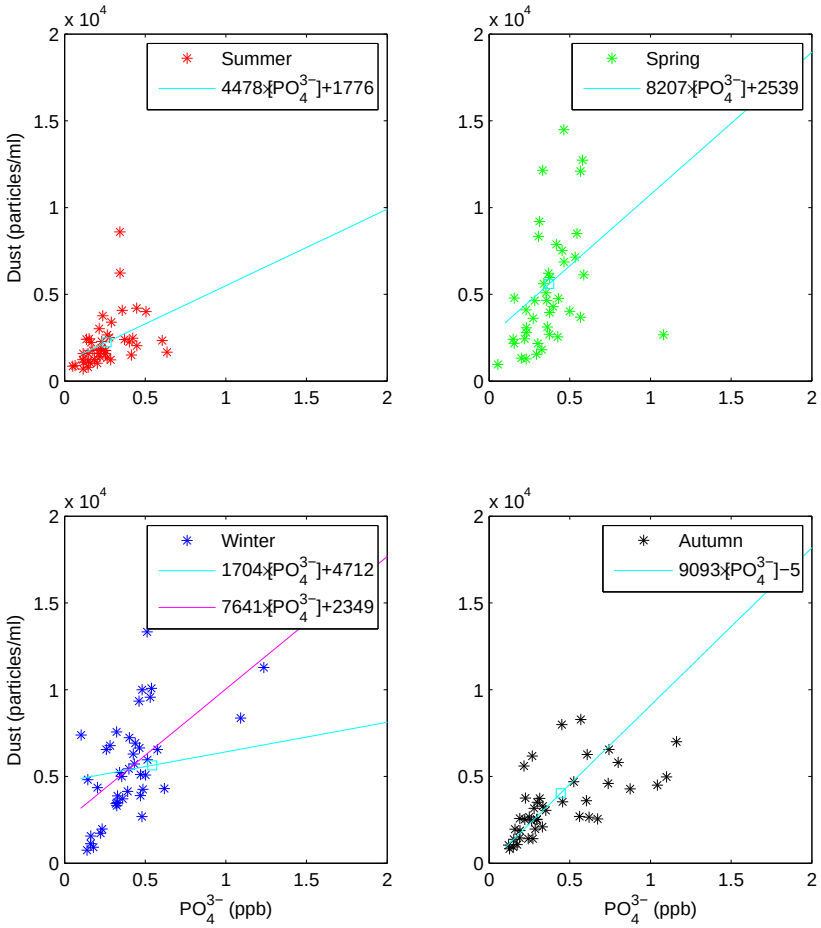

Figure 58: The phosphate to dust relationship for the different seasons is represented using a linear fit (light blue line) and by the seasonal mean (square). For winter a linear interpolation without two maximum phosphate values larger than 2.5 ppb is also presented (purple line). The fitted parameters are given in the figures.

occurs in winter with 0.54 ppb, autumn has a mean of 0.44 ppb, summer has the lowest amount 0.31 ppb and spring has 0.37 ppb PO_4^{3-}, but in trusting these values one should proceed with caution, since extreme values can have a very significant impact on the mean and because it is assumed that there is an equal amount of precipitation during the year. We should recall that the seas show double the amount of phosphorus in winter time as compared to summer [*Concright et al.*, 2000]. Thus the trend could be evidence of a sea salt signal. Aerosols had the maximum concentration of phosphorus in summer and fall (in mid-latitudes [*Mahowald et al.*, 2008]) and we clearly do not see a maximum summer concentration.

The mean dust data for winter, autumn, summer and spring are 5639 particles/mL, 4031, 2557 and 5599 particles/mL. The high values expected for spring are found, a summer low and a spring maximum is present.

It is evident from the linear approximation shown in figure 58, that if dust were the only PO_4^{3-} source, it had to come from a different place during summer to explain the variation between phosphate and dust in different seasons or come through different transportation processes, changing the amount of PO_4^{3-} arriving.

However the discrepancy between summer and the other seasons could also be explained by an extra PO_4^{3-} source in the summer, *e.g.*, some biological algae bloom or the removal of sea ice moving the sea source closer, increasing the phosphate to dust ratio [25]. In the autumn there is a lot of dust compared to phosphate. This could be explained by the PO_4^{3-} binding with Ca^{2+} from the dust. Then phosphate is not detected, because the method is not sensitive to phosphate-calcium bindings. As already mentioned transportation processes can influence, too. Phosphate could for example rain out in autumn and be affected by the acidity in the rain before deposition. Though the differences between the seasons are interesting, it is difficult to conclude on the linear relation, because the phosphate to dust relationship show large variations for all seasons.

The mean **Phosphate flux** was found to be 5.86 ng/cm^2/yr PO_4^{3-}. This number is lower by a factor of 10^4 than the amount in the Mediterrean which has been shown be 1.09-1.93 g/m2/yr P and is lower by a factor 100 than the South-Mediterranean 0.009 g/m^2/yr soluble inorganic phosphorus [*Bergametti et al.*, 1992; *Herut et al.*, 1999]. For the first numbers a factor of ten can be explained by the fact that the method used in the present study detects phosphate and soluble phosphorus and not all phosphorus. The rest of the difference can be explained by the high dust flow into the Mediterranean sea accounting for 3-12 g/m^2/yr in the western part and 20 -50 g/m^2/yr in the Eastern part. In comparison Greenland dust flux is 0.005 g/m^2/yr, [26] a factor of 600 to 10000 lower than the observations in the Mediterranean Sea.

The calculations of the flux could be done at an annual resolution only, because accumulation rates are available only at annual resolutions.

8.4.3 Ammonium

In general the correlation with **ammonium** was very low. However some of the PO_4^{3-} spikes not found in the dust signal were seen in the ammonium signal. Sources for both ammonium and phosphate could be biogenic sources. It has been suggested that ammonium could be a tracer for forest fires in North America and Canada [*Fuhrer et al.*, 1996]. Forest fires could also show signs of PO_4^{3-}. It was therefore investigated whether any major **forest fires** had been recorded, when phosphate and ammonium both have peeks. Peeks in phosphate and ammonium are clearly present in the years: *1886/1887*, 1890, 1891, *1894*, 1901, *1910/11*, 1912/13 and 1913. High PO_4^{3-} ($\geq$1ppb) occurs in the years 1887, 1888, 1893, *1894*, 1896, *1903/1904* and 1905[27].

It is difficult to find a complete forest fire record covering the period, but a list of some major fires in USA and Canada is presented in table 8. Though there are some correlation between some of the years of high PO_4^{3-} and of forest fires (1894 and 1903/1904), these also show high amounts of dust at the same time, so there is no reason to assume that these occurrences are related to forest fires. Three years are found in which there is significant size of ammonium and phosphate, but no dust spikes: *1886/1887, 1894* and *1910/11*. Although the list is incomplete and several fires could be missing and although special atmospheric conditions leading the plume over Greenland are needed for the signal to end in the ice cores, nevertheless it is possible that the correlation could be random, further the age scale is probably not accurate enough to make a year to year correlation. Even if it is actually a forest fire signature it is a difficult signal to see, since some of the bumps in the PO_4^{3-} record are very small. They would not be seen if not accompanied

[25] diminishing the linear interpolation coefficient.

[26] 33 μg [*Steffensen*, 1995] times the density of ice (917 kg/m^3) times the yearly layer thickness (0.166 m) equals 0.005 g/m^2/yr

[27] Italicization indicates that a year correlates with a known fire event in table 8.

Table 8: Years with large forest fires in the USA and Canada [wik, 2010f;e].

Year	**Place**	**Size (Ha)**
1886	Canada, Vancouver, Calgary	?
1889	USA, California	120000
1892	Canada, New Foundland	?
1894	USA, Minnesota	65000
1900	Canada, Quebeck	?
1903	USA, New York	188000
1904	Canada, Toronto	?
1910	USA, Idaho, Montana, Washington	1200000
1911	USA, Ontario	200000
1916	USA, Ontario	200000

by simultaneous records of ammonium and dust signals. Further using this method, the temporal resolution of PO_4^{3-} detection is not high, so the period back in time during which this method could be used for detection of forest fires is limited.

The PO_4^{3-} signal was also compared to other sources of fire history (*Furyakev et al.* [2001]; *Mouillot and Field* [2005]; *Girardin* [2007]; *McConnell et al.* [2007a]; *Girardin and Sauchyn* [2008]) but no correlation was found.

In **fertilizers** ammonium-phosphate is often used and this is a very soluble chemical connection. This means that the correlated signal in ammonium and phosphate could come from fertilizers. This could perhaps be checked by detecting sodium simultaneously, which is also used in fertilizers to see if spikes are present in this tracer too. Sodium does however have several other sources, so it would be a difficult signal to detect. If fertilizers are the source it does not explain why only some years have the spike, since fertilizers are used seasonally, but this could be due to transport variations between years.

Finally because of the high content of P not much biological material needs to be present in the ice to significantly change the PO_4^{3-} signal from the background level. Thus just a single **bird** flying over the ice sheet-can cause significant spikes in the PO_4^{3-} and this could be the explanation for some of them.

Lastly, the explanation for the small PO_4^{3-} spikes correlating with ammonium when no dust is present could be **contamination from human handling**. This could occur in places where the core was smaller than the melt head and some contamination might be detected in both phosphate and ammonium if this was the case. This however is not likely, since we were very careful when cutting and melting the pieces.

8.4.4 Special layers

The **melt layer in 1889** found in the North-GRIP core [*Svensson*, 2010] (170 km away from the NEEM S1 shallow core) is not clearly seen in the PO_4^{3-} or in any of the other parameters detected (see figure 55). Though both phosphate and dust have small peaks, it is not clear that these must be due to a melt layer. It could be that the reason they are not seen is due to the dating being wrong, but most likely this melt layer is not present in the NEEM S1 shallow ice core.

The volcanic layer from the **Katmai volcanic eruption in 1912**, also detected in the North-GRIP core is not very clear either, but phosphate and dust both have a peak,

which is broader than normal and this could be the volcanic layer (see figure 54). However the feature is not sufficiently pronounced to be seen in the PO_4^{3-} if its position was not all ready known and since there is not any significant spike in the conductivity the volcanic layer is most likely not present in the data at at all.

8.4.5 Spectral analysis

The **resolution** of PO_4^{3-} detection was found to be 1.3 to 2.9 cm (see figure 56), far below the annual layer thickness of 0.166 meters found by *Sauer* [2010], who used CFA measurements of Na^+, NH_4^+ and dust for 10.4 to 34 meters of depth to find seasonal signals and thus determine the years. A theoretical value for the expected resolution was calculated to be 0.6 cm to 1.0 cm in firn[28]. The reason for the worse resolution in the detected PO_4^{3-} is most likely that the theoretical resolution does not take noise into account as does the resolution found by spectral analysis. A reason for the poorer resolution in the measurements could be that the very low melt rate kept throughout the time of detection was not high enough to prevent the sucking of melt water into the ice due to capillary forces, thus smoothing the signal. It was speculated that a decreasing trend in the resolution could have occurred over time, due to the wear out of the tubing. No such trend was observed.

The **annual layer thickness** found in the spectral analysis is a bit lower (0.15 meter) than the annual layer thickness of 0.166 meter found by *Sauer* [2010]. The PO_4^{3-} detections are primarily from the deepest part of the section used by *Sauer* [2010] and the thickness in ice equivalent can be calculated as 0.15 meter times the density of snow (700 kg/m^3 at depth 30 meter) over the density of ice (917 kg/m^3), which ends up giving an ice equivalent of only 0.11 cm. Thus it is lower than the value found by *Sauer* [2010]. This could be explained by the spectral analysis being conducted on parts where the annual thickness was low. According to *Sauer* [2010] the yearly accumulation rate in ice equivalent was as low as 0.08 cm in some years. Thus the annual layer thickness found using the phosphate data is within the deviation.

But another possible explanation may be the fact that I only used 1.10 m at the time to find the annual layers. I could have made a check up on the data by checking how many years could be counted in the sections used using other proxies like ammonium and dust. This was not done, because the annual layer top found in the spectral analysis of the phosphate is not very distinct and thus can not be trusted. The lack of a significant yearly top is partly due to the significant smoothing of phosphate compared to the other proxies, but it is possible that the top would be more pronounced if a longer set of data was used. I do not suggest that phosphate is used to detect annual layers.

The optimized molybdenum method using a 2 meter LWCC proved successful in detecting PO_4^{3-} in the NEEM S1 shallow ice core. The detection of PO_4^{3-} covers parts of the last 120 yrs. A mean of 0.32 ppb was found. The mean flux was 5.86 ng/cm^2/yr. The distribution of PO_4^{3-} is probably lognormal. There is evidence of PO_4^{3-} being highly correlated with dust in the NEEM S1 shallow core suggesting a similar source or similar transport

[28]The melt rate was kept between 1.5 and 3 cm/min. I use 1.68 mL/min sample. So 0.9 mL/cm to 1.8 mL/cm is used for phosphate. Previously the response time was found to be 37 seconds (1.03 mL) to 43 seconds (1.20 mL) and thus a theoretical value for the resolution should be 1.20 mL/(0.90 mL/cm)=1.3 cm to 1.03 mL/(1.80 mL/cm)=0.57 cm firn ice.

processes. High amounts of PO_4^{3-} in the winter time correlating with high dust loads were found, while summer shows low PO_4^{3-} concentrations, but higher than expected if PO_4^{3-} only arrives as mineral dust, suggesting a second source. Sea concentrations of phosphate show the same yearly pattern as found in the NEEM S1 shallow ice core, suggesting sea salt as a source. The detected phosphate also show some spikes coinciding with ammonium, but not correlating with dust, that are possibly related to forest fires, however this could also be evidence of a fertilizer signal. No firm conclusion could be made on the matter. No trend was found over the period, nor was an anthropogenic signal detectable. In this section the optimized method for detection of phosphate in ice cores proved successful, in the next section it is used on the NEEM ice core, which covers a longer timespan including the last glacial.

9 Phosphate in glacial times

In the previous section the optimized method for detection of phosphate found in this study proved successful in detecting PO_4^{3-} in the NEEM S1 shallow ice core. In this section detections of PO_4^{3-} in the glacial part of the NEEM ice core using the optimized method with some modifications are presented and discussed.

The North Greenland Eemian Ice Drilling Project (NEEM) was initiated in 2007, with the purpose investigating the last interglacial; the Eemian (110.000-130.000 yr BP). In 2008 camp was built and drilling was started at the position 77.45°N 51.06°W, 2484 m above sea level. The bedrock was reached end of June 2010 at depth of 2537.36 meters. The detection of PO_4^{3-} covers part of the depth range 1607.65 to 1763.85 meter.

9.1 Detection at NEEM

The concentration of phosphate in the NEEM ice core was detected during June 2010 using the NEEM CFA system in combination with the method from this study. The CFA set-up used at NEEM is the Bern CFA system. At NEEM 110 cm cores were melted at one run corresponding to two bags. The melting took place on a melt head of size 36 mm×36 mm. The melt rate was approximately 3.3 cm/min dependent on the ice density. Melting took place in a cold trench. More on the CFA system used at NEEM can be found in section 5.1 and below.

9.1.1 Description of the set-up used at NEEM

The phosphate set-up had a waterline running with 0.9 mL/min from the CFA system. The reason for the low flow compared to the suggested set-up is that the NEEM set-up is used for detecting many species and in order to avoid low temporal resolution, flow for each component is limited. 0.08 mL/min molybdenum blue solution and the same rate of ascorbic acid was added to the sample flow. Air was introduced at a rate of 0.15 mL/min. All this took place in a heated box, the CFA-box. Transfer to another warm laboratory, the gas laboratory box, was through a 0.02" (0.5 mm) thick and 610 cm line, which to prevent freezing was heated over the 1.5 meter placed outside the boxes in the cold room.

During the time it took for the fluid to arrive at the gas laboratory box, where the rest of the system was positioned, some mixing had already taken place. However the liquid was further mixed in 100 cm tubing heated to 60 °C. Air was removed at a speed of 0.20 mL/min, leaving a total flow of 0.99 mL/min to enter the filter 2/3 filled with glass wool, which was inserted in order to avoid optical interference from dust in the 2 meter LWCC positioned after the filter. For detection a wavelength of 710 nm and a boxcar value of 2 was used. A picture of a part of the set-up residing in the gas laboratory box is shown in figure 59 and a diagram of the entire set-up is shown in figure 60.

Phosphate was detected 12 hours a day under surveillance and 12 hours not observed. When not observed disturbances such as small bubbles or dust filled filters caused failure in detection. For this reason there are breaks in bag records.

Standards were run after approximately every fourth core when under surveillance. However because of increased coating effects due to the low flow rate, of only 1 mL/min compared to 1.83 mL/min in the Copenhagen CFA set-up, and due to enhanced mixing caused by high dust loads, three standards took longer than 40 minutes to run, which was the time the rest of the CFA measurements needed to run their standards. Since phosphate detection was still at a test level, it was decided to finish PO_4^{3-} standards on

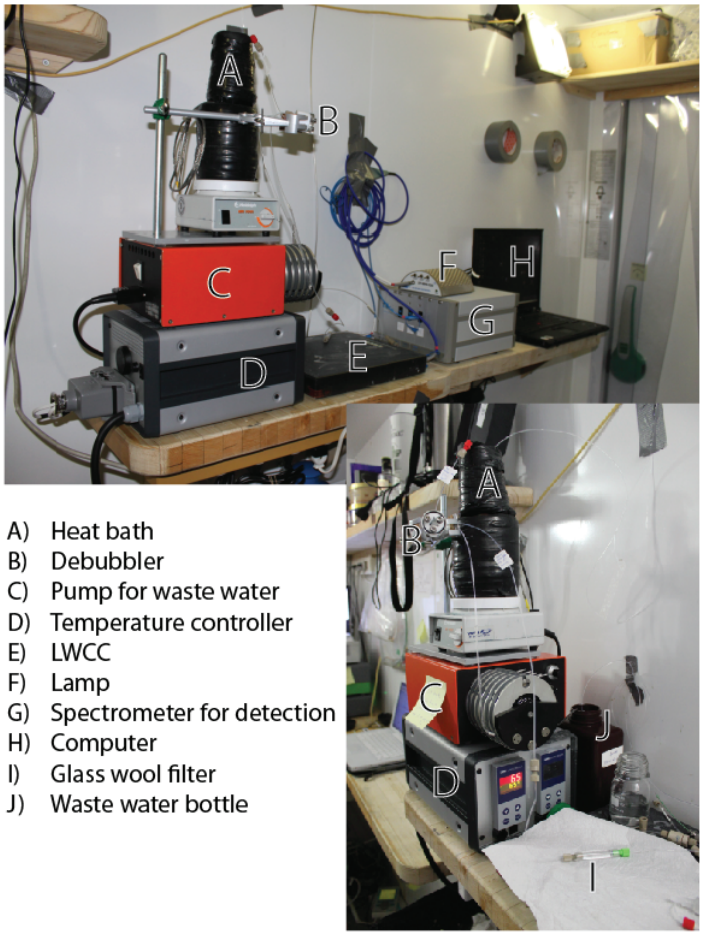

Figure 59: Part of the set-up positioned in the gas laboratory.

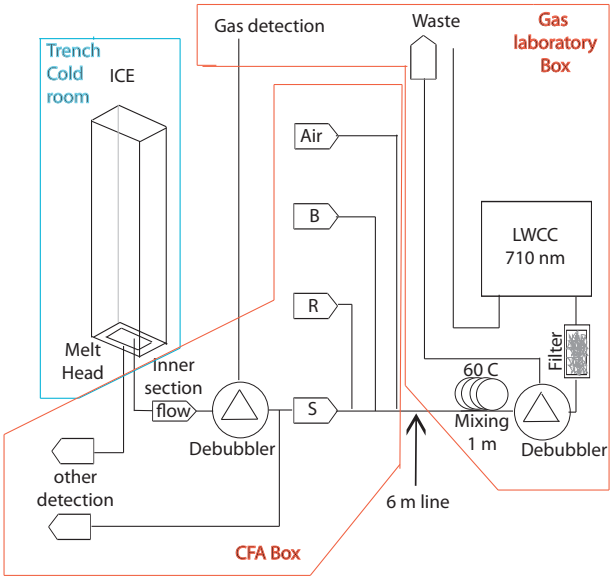

Figure 60: The NEEM CFA set-up. Ice is melted in the cold trench (-15 °C). The melt water is split between an inner and outer part. Inside in the CFA box the inner part is debubbled and the gas is led to the gas laboratory box where detection of gases takes place. The debubbled melt stream is split between different types of detection, of these only the phosphate line is shown. For phosphate the sample (S) is mixed with reagent (R), buffer(B) and air before being transported through a 6 meter line to the gas laboratory in where 1 meter of heated mixing takes place before a second debubbler removes the air dust is removed by a filter. Finally detection takes place in a 2 meter LWCC at 710 nm.

Figure 61: Example of the extreme coating observed during detection of phosphate at NEEM. Left the one meter mixing tubing and right the pump tubing going from the debubbler to waste. The latter was very significantly coated in the end which was in contact with the waste water. Note also that the highly acidic chemistry has corroded the nut.

the phosphate systems, while the other species kept on measuring bags. Bags are thus missing due to this decision, too.

Phosphate was measured in ice from the depth range 1607.65 meter (bag 2924) to 1764.95 (bag 3209).

9.1.2 Maintenance

The filter needed to be changed often; approximately after every 6th run when measuring the dust loaded cold glacial stadials (GS), which clogged the filter. But the filter could be used for 24 hours, corresponding to approximately 24 runs, when the dust load was low in the glacial inter stadials (GI).

Pump tubings were changed every week, *i.e.* three times during the phosphate detection period. The tubing for taking air and a little excess water out of the system turned to a dark blue color rather fast. An example of such blue coating can be seen in figure 61; this I believe is due to the slow pump rate allowing the reaction to proceed further combined with the high phosphate load. The blue coloring was more pronounced in the waste end of the tubing and could perhaps be explained by the contact with the waste water, which had time to reach full coloring.

9.2 Calibrating phosphate in glacial ice

The dust in the glacial ice caused detection problems not observed when measuring the NEEM S1 shallow core: There was a change in the baseline. Also a poorer temporal resolution was caused by the slower flow over the measurement period.

9.2.1 Baseline

The baseline was unstable and became lower and lower as more and more cores were run. This was probably due to dust residing at the end of the filter. The PO_4^{3-} in the water will tend to be deposited on the dust and will thus be removed from the aqueous solution and not be detected. The PO_4^{3-} concentration in the water will be lower until the dust is saturated with PO_4^{3-}, then concentrations will be up to normal again. When Milli-Q water without PO_4^{3-} is introduced again, it will take time to flush out the PO_4^{3-} stuck on the dust, and thus the baseline will tend to drift, explaining the long term change in baseline after each run. However the relative counts during core run should still be valid. An example of the very unstable baseline over time can be seen in figure 62.

Another reason for the lowering of the baseline may be that the system is slowly clogged letting less water through, this could enhance the time the reaction takes place and cause the baseline to drop. However this was not found to be the case.

The problem was solved by using as baseline a linear interpolation between the baseline value before running a core and the baseline value after. Choosing the baseline value 'after'

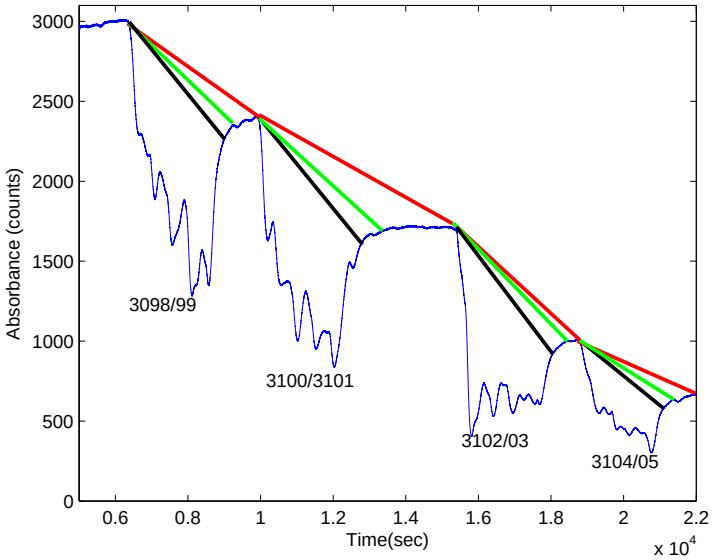

Figure 62: Blue: Measurements of ice cores. It is clear that the baseline does not return to the same value. In red, green and black are different approaches to correct using a linear interpolation between baseline before measurements and after. Red chooses the highest value before and after measurements. Green chooses highest baseline value before and the place where measurements turn to a somewhat stable baseline. Black is interpolating between highest value before and the place were measurements start to become linear again. All chosen by eye. Bag numbers are shown. The correlating depth can be calculated by dividing by 0.55 cm.

is not an easy task as illustrated in figure 62. The black line was chosen to be the most correct of the three, since the kink in the return from bag detection seemed to be present at all times, and it provided results in which no clear trend within a single bag was present.

When the baseline is high the difference between the highest (red) and lowest (black) base line causes an uncertainty of about 1.1 ppb, but a difference of up to 2.17 ppb is found when baseline is very low (500 counts).

Another way to deal with the baseline problem would be to integrate the amount of dust coming through over time and use this for interpolating the baseline from start of run to end of run. This however causes many additional computational difficulties, and it is not certain that all dust would cause the same shift of baseline. Hence using this approximation for the base line could thus introduce even more uncertainties, and I have decided to stick with a linear approximation.

Of cause the noise-15 counts (0.18 ppb) when baseline was 3000 counts has a larger relative uncertainty when baseline is low. The 15 counts cause an uncertainty of up to 1.1 ppb when the baseline is 500 counts.

Sometimes choosing the end value for a bag measurement is not an easy task. This is the case-(a) when a new bag run or standard run is started too quickly *e.g.* at the depth of 1691 to 1696 meter(GS-6)) or (b) if some air is introduced in the system. Air may be introduced in the system when the change from ice core to Milli-Q was not done fast enough, causing air in all parameters, or if PO_4^{3-} standards were not purged of air before running, causing air in only the phosphate. The latter could have been avoided by introducing another valve, for getting air out of the standards.

Some rinsing procedures for helping the return of baseline were tested by letting a rinsing solution run for 30 seconds in between runs. Rinsing was tested with methanol, a solution of 20 μL HCl acid in 20 mL Milli-Q water and a solution of 20 μL sodium hydroxide in 20 mL Milli-Q water. However none of these had a significant effect.

All in all, the maximum uncertainty on the detection caused by baseline fluctuations is about 2.2 ppb, but in most of the phosphate detection the uncertainty is lower.

Table 9: The linear relationship between phosphate concentration ($Conc$) and absorbance (Abs), by the equation $Abs = acdotConc + b$, where $Conc$ is the concentration in ppb. R^2 denotes the correlation between data and fit and the closer to unity the better the fit. All fits are reasonable.

Bag	**Depth** (meter from surface)	**Age** (kyr)	**a** (ppb^{-1})	**b**	$\mathbf{R^2}$
2924-2927	1607.65-1609.85	22.4-22.6	0.01172	0.10240	0.9951
2932-2939	1612.05-1616.45	22.9-23.4	0.01546	-0.07588	0.9910
2940-2947	1616.45-1620.85	23.4-23.9	0.01429	0.03410	0.9600
2948-2959	1620.85-1627.45	23.9-24.6	0.00993	0.08029	0.9728
2980-2983	1638.45-1640.65	25.6-25.8	0.01260	0.05479	0.9690
2984-2987	1640.65-1642.85	25.8-26.0	0.01294	0.08788	0.9858
2988-2991	1642.85-1645.05	26.0-26.2	0.01297	0.03360	0.9773
3004-3007	1651.65-1653.85	26.8-26.9	0.01663	-0.05202	0.9948
3008-3017	1653.83-1659.35	26.9-27.5	0.02367	0.07259	0.9987
3018-3029	1659.35-1665.95	27.5-28.2	0.02147	-0.04138	0.9994
3046-3049	1674.75-1676.85	29.1-29.3	0.02268	0.00072	0.9998
3050-3057	1676.85-1681.35	29.3-29.8	0.01957	-0.00053	0.9997
3058-3081	1681.35-1694.55	29.8-31.0	0.02543	-0.02138	0.9893
3082-3091	1694.55-1700.05	31.0-31.5	0.02573	-0.01989	0.9999
3092-3113	1700.05-1712.15	31.5-32.7	0.02232	-0.00002	0.9667
3124-3127	1717.65-1719.85	33.1-33.3	0.01625	0.00622	0.9950
3128-3143	1719.85-1728.65	33.3-34.1	0.01575	0.008405	0.9956
3152-3165	1733.05-1740.75	34.5-35.2	0.01200	0.007649	0.9986
3190-3209	1753.95-1764.95	35.9-36.8	0.02043	-0.01285	0.9721

9.2.2 Standards

Three standards were used to find the relation between phosphate counts and concentration in ppb. Standards were kept in polypropylene bottles and the concentrations were 49.20, 98.91 and 193.94 ppb for the first bags. At bag 2932 the standard concentration were reduced to 49.20, 24.67 and 9.88 ppb and at bag 3054 they were replaced by standards of concentration 9.88, 4.94 and 2.47 ppb. Standards were varied to better fit the concentration seen in the measurements of the ice.

A list of the measured bags and the corresponding calibration values is presented in table 9. Note that some of the calibrations are used for many bags due to the fact that measurements were done not under surveillance, and thus no calibration were done; this of cause increases the risk that the calibration does not fit the measurements. The most trust should be given to bags where the linear fit is best-that is the calibrations with highest R^2-value. Note in table 9 that the constant term b is very high for bags 2924 to 2927 probably because the highest standard is above the linear range. This can cause the level detected to be slighty too high for middle concentrations (100 ppb) and slightly too low for low concentrations ($\leq$10 ppb). Note also that the linear calibration coefficient a is lower than for the standards used for the NEEM S1 shallow ice core, due to the changed flow.

During the measurement campaign the temporal resolution or response time, again found as the time it takes for the response to a step function (a standard) to increase from 10% to 90% showed a significant trend towards longer response times (see figure 63). Measurement conditions were not changed during the period, except that on the 19th of June the heat bath was found to be empty of water, which can cause the calibration for

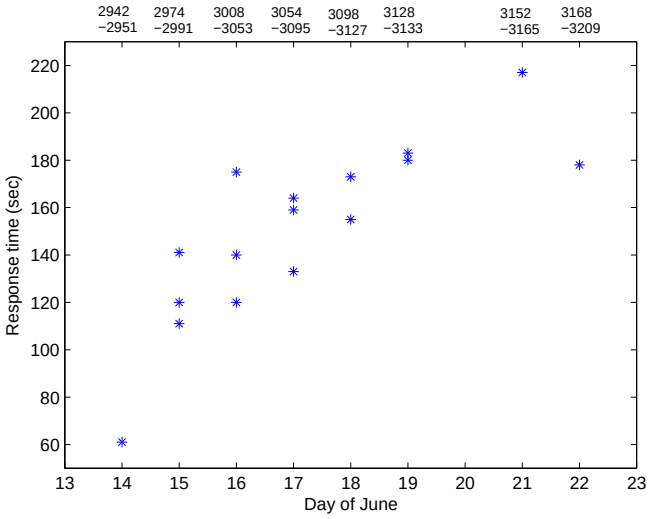

Figure 63: The response time, calculated by the time it takes for the response to a stepwise function (a PO_4^{3-} standard) to increase from 10 % to 90 % of full absorbance, as a function time during June, on the top axis the corresponding bag numbers are shown.

bag 3124 to 3127 (1718.2 to 1720.4 meters depth) to be wrong. The heat bath was refilled as soon as the problem was discovered and this seem to not have affected the response times. The change in response time also can not depend on filter effects, since the filter was changed once a day.

I suggest the reason for the increased response times is connected with coating effects of the tubing. If dust gets stuck somewhere in the very long line from where the reagent is introduced to the position before the filter, this could cause some interference with how fast a sample is seen, and there is a risk that the PO_4^{3-} will be deposited on the dust. There was evidence of particulate matter getting stuck in the debubbler over time, but the dust could also stick to the narrow tubing. If PO_4^{3-} is stuck on dust it does not react with the molybdenum in the water. As more standard comes through an equilibrium is reached between the amount of PO_4^{3-} stuck on the dust and the amount dissolved in the water and the molybdenum reacts with the PO_4^{3-} in the water. Over time more dust will be stuck in the tubings and thus it will taker longer time for equilibrium occurs between PO_4^{3-} stuck on dust and PO_4^{3-} in the water.

I do not expect that this will influence the equilibrium response to the standards. Equilibrium will be reached since PO_4^{3-} standards keeps coming through and there is only capacity for PO_4^{3-} adsorption on the dust.

Also the spikes were asymmetrical resembling a delayed signal, perhaps due to coating or to another memory effect. Examples of such spikes can be seen in figure 64. The spikes could perhaps be rectified by deconvolution, however this would have been a major task due to shift in response time over the period the filter function would not be the same for all measurements. The shape effect was seen not only in the phosphate but also in Ca^{2+}, acidity and conductivity detections, suggesting that the effect could be due to wear out of tubing used up stream of the phosphate detection system or some other effect originating up stream.

9.2.3 Calibration

The PO_4^{3-} concentration was derived from raw data using calibrations with standard solutions much as explained in section 8.2, with the major exception that a running baseline was introduced as explained in section 9.2.1 above. However the computer system for phosphate detection was not the same as in Copenhagen; at NEEM a computer separate

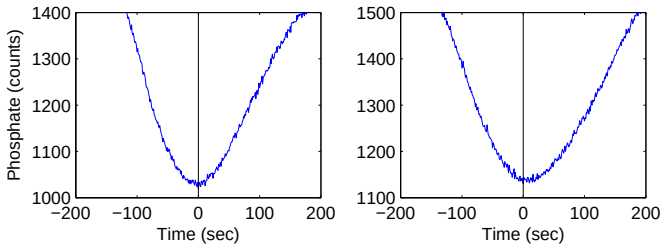

Figure 64: Examples of asymetric spikes in the raw phosphate data for which minimum counts corresponds to high phopshate level. Data is from the 12 and 15 th of June.

from the rest of the NEEM CFA system was used for phosphate detection.

This called for changes in the program used for calibrations. Log-files containing information such as the length of the two bags measured at one time, start time for the melting and end time as well as a break-file with information on break positions and the length of breaks was obtained from the main CFA system. Examples of log- and break-files are shown in appendix and A.5 and A.6. I could have obtained decoder information as well (melt speed) but due to the fact that the temporal resolution was very low, and considering the long additional time that would have been needed for implementing this in my program code. I decided not to use these data. Instead I used the mean melting speed calculated as the length of the bags over the time it took to melt them.

In the phosphate system the beginning and end of the bags were chosen by eye. This can cause some problems since milli-Q ice from the ends will sometimes cause a small spike before the real beginning of a bag, but since the concentration in the NEEM ice core was much larger than the contamination in the Milli-Q ice, it was not often seen.

By inspection I identified and removed data with spikes of low credibility due to their position close to breaks or at start and end of the bags. Such data were removed.

9.2.4 Dating

The dating were made using the depth scale GICC05modelext-NEEM-1 time scale. It is a time scale based on the NGRIP time scale GICC05 and converted to NEEM scale by *Rasmussen et al.* using interpolation points based mainly on ECM[29] data and on DEP[30] data.

9.3 Results from the NEEM ice core

As previously mentioned phosphate was detected for the depths between 1607.65 meter (22.4 kyr B.P.) and 1763.85 meter (36.8 kyr B.P.). Phosphate concentrations in the NEEM ice core can be seen in figure 65 where they are plotted together with δD, also from the NEEM ice core. The glacial interstadials (GI), the mild periods, are marked.

The mean level of PO_4^{3-} found over the entire period is 10.42 ppb. The standard deviation is 9.33 ppb. The maximum of detected PO_4^{3-} was 63.36 ppb at the depth 1619 meters.

In table 10 means and standard deviation can be found for the different climatic periods. There is a clear difference in the amount of phosphate between the glacial interstadials (GI) and the glacial stadials (GS). The glacial stadials show high levels of PO_4^{3-} with means between 6.48 ppb (GS-6) and 21.45 ppb (GS-3), with a standard variation between 9.64 ppb in GS-3 and 6.18 ppb in GS-8. The interstadials have very low levels

[29] electrical conductivity method
[30] DiElectric Profiling Method

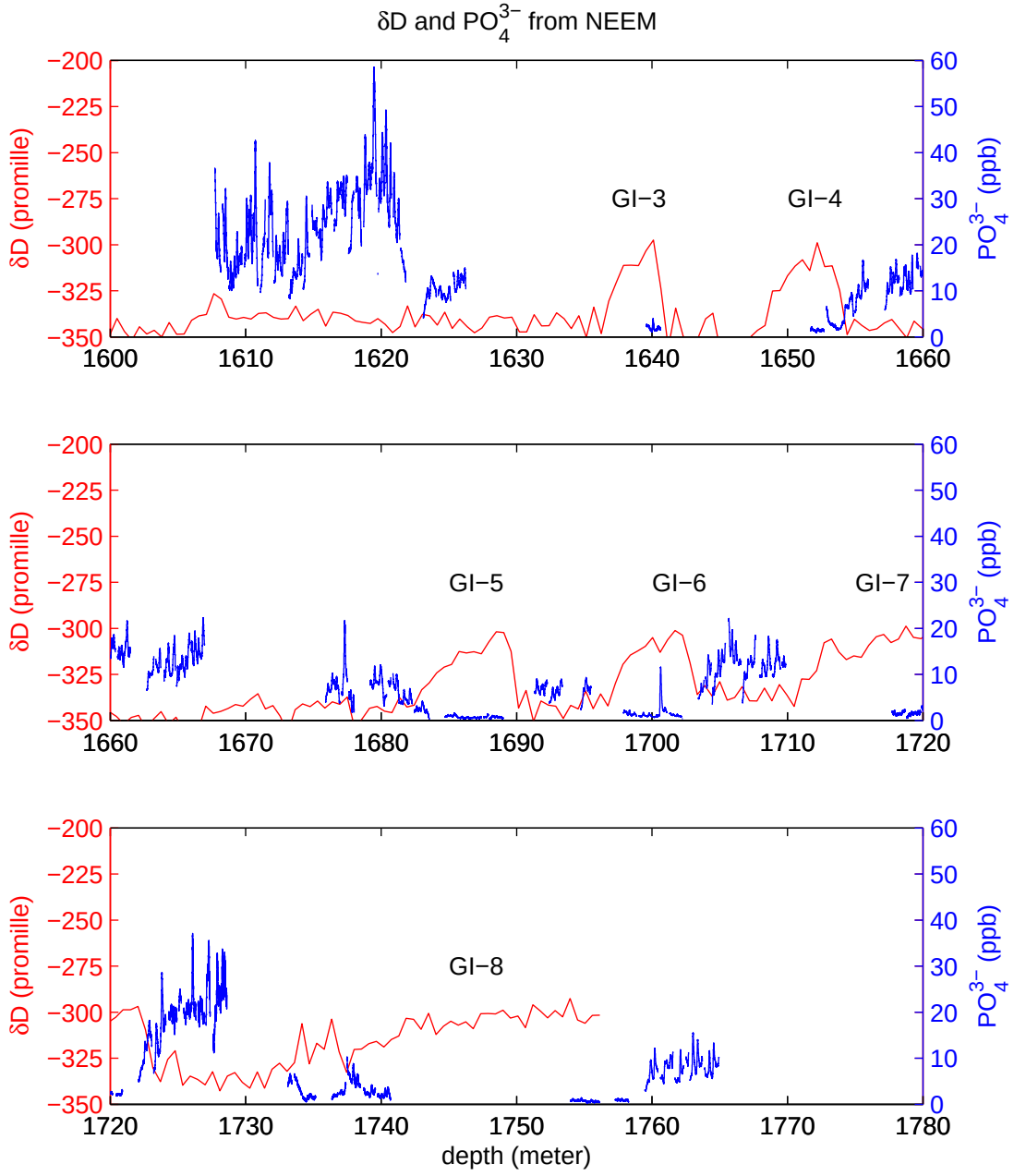

Figure 65: Phosphate (in the detected resolution) and δD (in bag means) from the NEEM ice core as a function of depth. Glacial Interstadials (GI-mild periods) are marked. δD has not yet been measured between 1757 meters depth and 1780 meters depth.

Table 10: The table show mean, variance (var) and standard deviation (STD) for phosphate for the glacial stadials (GS) and glacial interstsdials, and the depth which is used to define the periods.

Period	**Depth** (meter from surface)	Age (kyr B.P)	**Mean** (ppb)	**STD** (ppb)
GS-3	1607.7-1636.3	22.4-25.5	21.46	9.64
GI-3	1636.8-1640.6	25.5-25.8	1.97	0.56
GS-4	1641.8-1648.9	25.8-26.6	NaN	NaN
GI-4	1650.6-1654.2	26.7-26.9	2.12	1.03
GS-5	1654.9-1681.6	27.0-29.8	11.12	3.90
GI-5	1684.7-1690.2	30.1-30.5	0.75	0.24
GS-6	1690.2-1696.8	30.5-31.2	6.48	1.46
GI-6	1698.4-1702.2	31.4-31.7	1.55	1.57
GS-7	1703.9-1710.5	31.8-32.5	12.15	2.94
GI-7	1712.2-1721.2	32.7-33.4	1.71	0.50
GS-8	1723.7-1733.5	33.5-34.6	20.58	6.19
GI-8	1734.5-1758.3	34.7-36.2	2.13	1.77
GS-9	1759.6-1764.9	36.2-36.6	8.02	2.26

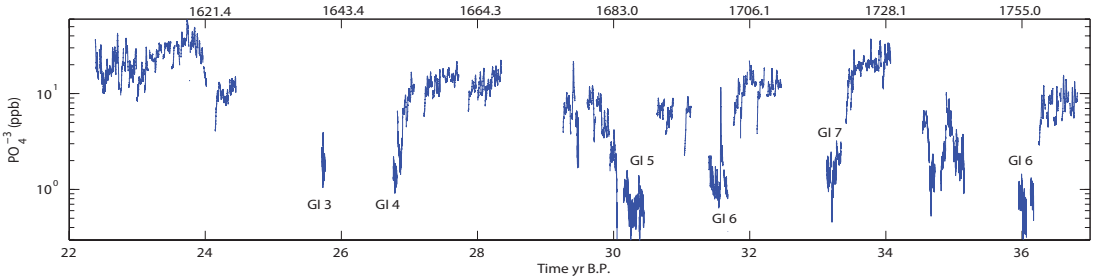

Figure 66: Log of phosphate as a function of the GICC05modelext-NEEM-1 time scale (bottom) and a depth (top). Glacial inter stadials (GI) are marked.

of PO_4^{3-} and show mean values between 0.75 ppb (GI-5) and 2.13 (GI-8), the standard deviation is below 1.77 ppb.

In figure 66 the phosphate concentration is plot on the GICC05modelext-NEEM-1 time scale. The maximum counting error is between 0.7 kyr at an age of 22.7 kyr B.P to 1.6 kyr at 38.3 kyr B.P [*Rasmussen et al.*].

In figure 67 the distribution of concentrations is shown for the glacial stadials (GS) and interstadials (GI).

In figure 68 phosphate is plotted together with δD from NEEM and dust, Ca^{2+}, NH_4^+ measured in the North-GRIP ice core using CFA as well as K^+ measured using IC in the North-GRIP core. North-GRIP depths are transformed to NEEM depths using a piece wise linear interpolation between fix points. The fix points are shown in table 11.

In figure 69 means of each run of phosphate (2 bags) are plotted against δD, dust, Ca^{2+}, NH_4^+ and K^+ for the same period. No linear correlation between dust, Ca^{2+} or NH_4^+ was observed. K^+ had the closest to linear response with phosphate. The high large deviations from linearity can be due to the transfer of North-GRIP to NEEM depths.

The correlation coefficient between the series of δD and PO_4^{3-} was found to be -0.60, reflecting that the cold periods (low δD) had high PO_4^{3-} concentration and that mild periods (high δD) had low PO_4^{3-} concentrations. Dust from North-GRIP and phosphate had a correlation of 0.84, while the correlation to Ca^{2+} was very similar at 0.87. Ammonium and phosphate had a correlation coefficient of 0.46 and finally that with K^+ was 0.71.

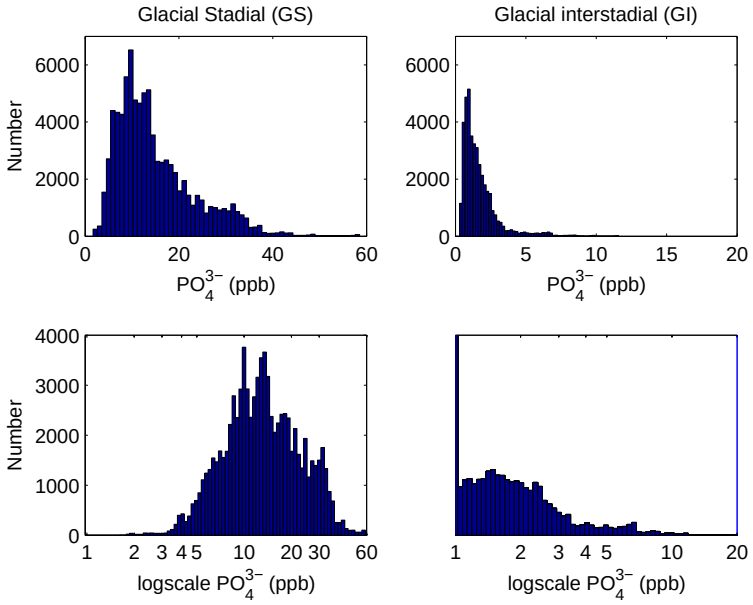

Figure 67: The distribution of concentrations of phosphate (mm resolution) detected in the NEEM ice core for glacial stadials (GS) and interstadials (GI). Shown on a linear scale (top) and on a log-normal scale (bottom).

Table 11: The depths fix point (meter from surface) used for interpolating the data from the North-GRIP core to the NEEM depths. The fix points are mainly chosen were clear transitions occur, *e.g.* from glacial stadial to glacial interstadial.

North-GRIP	**NEEM**
1604.64	1489.95
1793.20	1598.30
1869.42	1641.75
1891.57	1654.95
1951.66	1690.15
1974.56	1703.35
2009.45	1723.15
2032.25	1736.90
2053.15	1755.05
2070.03	1759.00
2094.40	1780.90

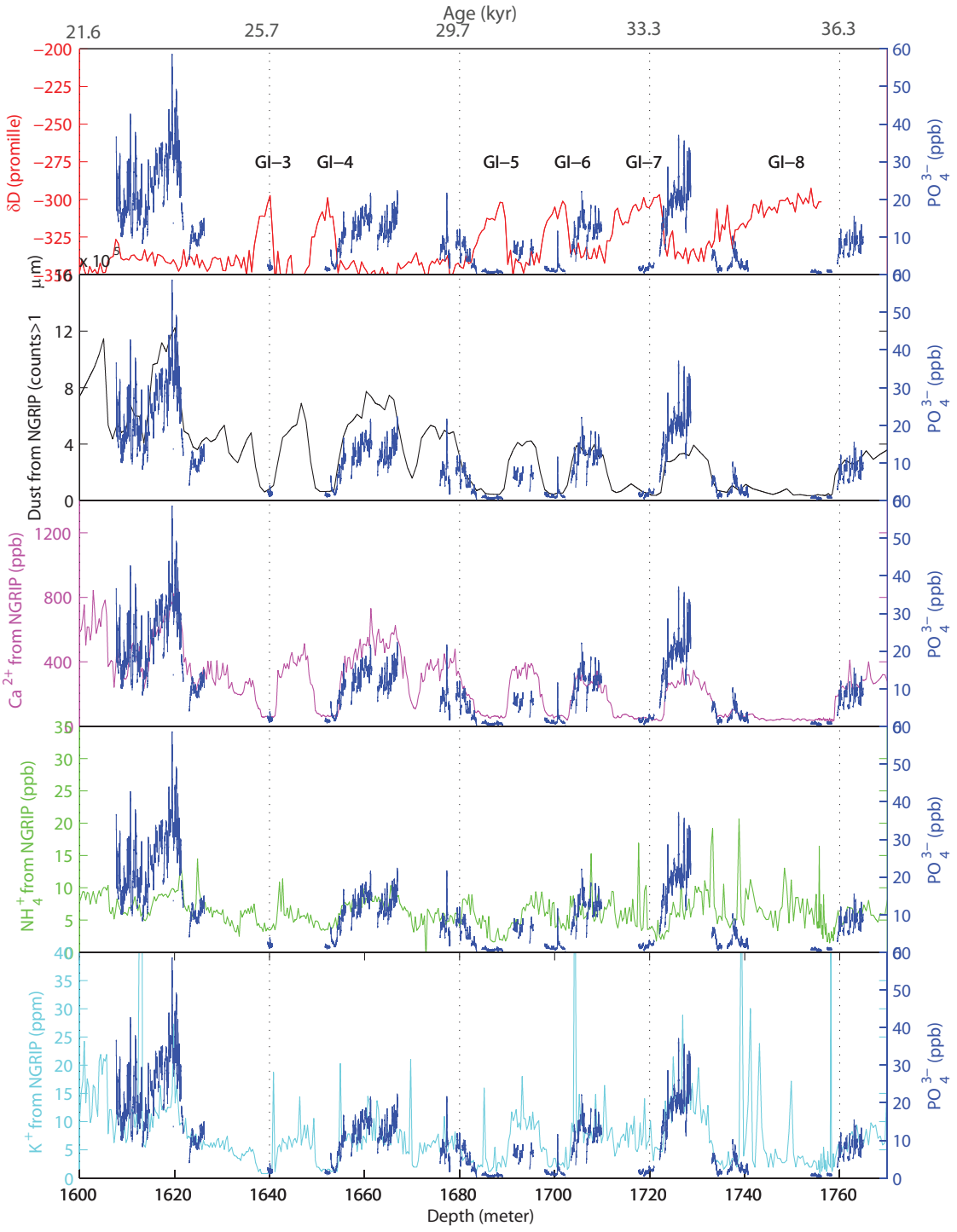

Figure 68: Phosphate from NEEM (blue) plottet on a depth scale with δD (red) from NEEM (top), dust (black) from North-GRIP, Ca^{2+} (pink) from North-GRIP, NH_4^+ (green) from North-GRIP and in the bottom with K^+ (light blue) from North-GRIP. Note that all plots have the same phosphate scale and depth scale but the different left hand scales. The North-GRIP data are from [*unpublished*, 2004; *Ruth et al.*, 2003].

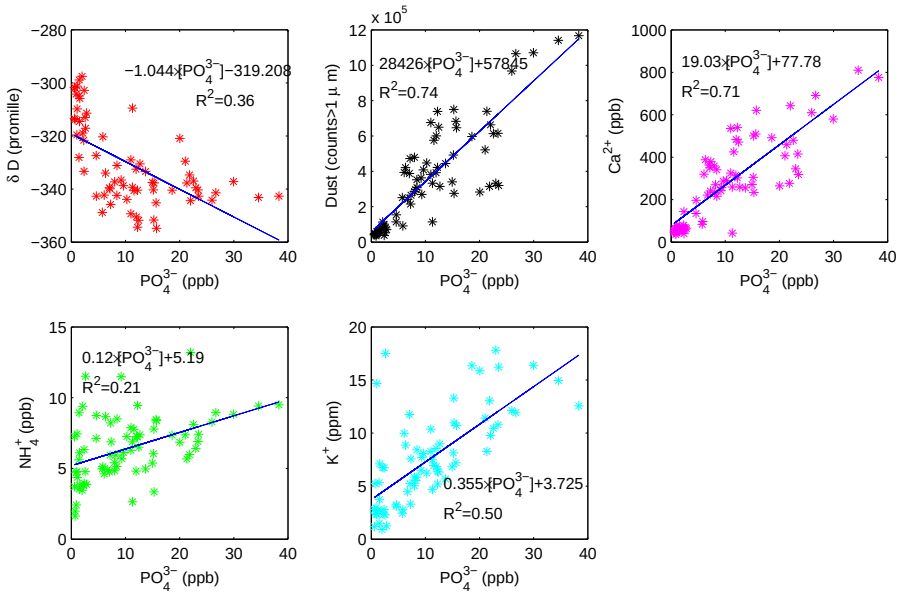

Figure 69: Phosphate from NEEM is plotted against δD (red) from NEEM , dust (black) from North-GRIP, Ca^{2+} (pink) from North-GRIP, NH_4^+ (green) from North-GRIP and K^+ (light blue) from North-GRIP. Means for each phosphate run (2 bags) were used. A linear regression and correlation coefficient was worked out as shown in the figures.

To investigate whether the relations ships between PO_4^{3-} and the other proxies was significantly different in the cold and mild periods the means over the glacial stadial (GS) and over the glacial interstadials (GI) were calculated. Phosphate is plotted against δD, dust, Ca^{2+}, NH_4^+ and K^+ for GI's and GS's in figure 70.

To further investigate long term climatic trends the ratio of PO_4^{3-} to δD, dust, Ca^{2+}, NH_4^+ and K^+ was calculated for the climatic periods (GI's and GS's) and is shown in figure 71.

A spectral analysis of the phosphate data is presented in figure 72. It was hard to determine a cut off value because the noise was showing a drifting signature. If using 5 times the noise, a cut off value of λ=1187 was found corresponding to a resolution of 0.010 meter. This is way below the resolution seen in the raw signal. A more reasonable cut off is λ=210, which gives a resolution of 0.057 meter.

Phosphate and sulfate (proxy for the acidity), magnesium (dust proxy) and sodium (sea salt proxy), and NO_3 (biological tracer) and Cl^- was also investigated, but no significant trend or information was derived from these investigations. The graphs are shown in appendix A.7.

9.4 Discussion of phosphate in the NEEM ice core

In the following I discuss the observations from the NEEM ice core presented above.

9.4.1 Level and trends

Significant changes in level between glacial stadial (GS) and interstadials (GI) are observed. GS's show a 6 times higher level of phosphate than GI's and high variation, while the warmer GI's show a mean level lower than 2.5 ppb and also less variability.

Comparing to the concentration found in the NEEM S1 shallow ice core, it is evident that the level in glacial times is higher. In Glacial stadials (GS) the mean level is up to a

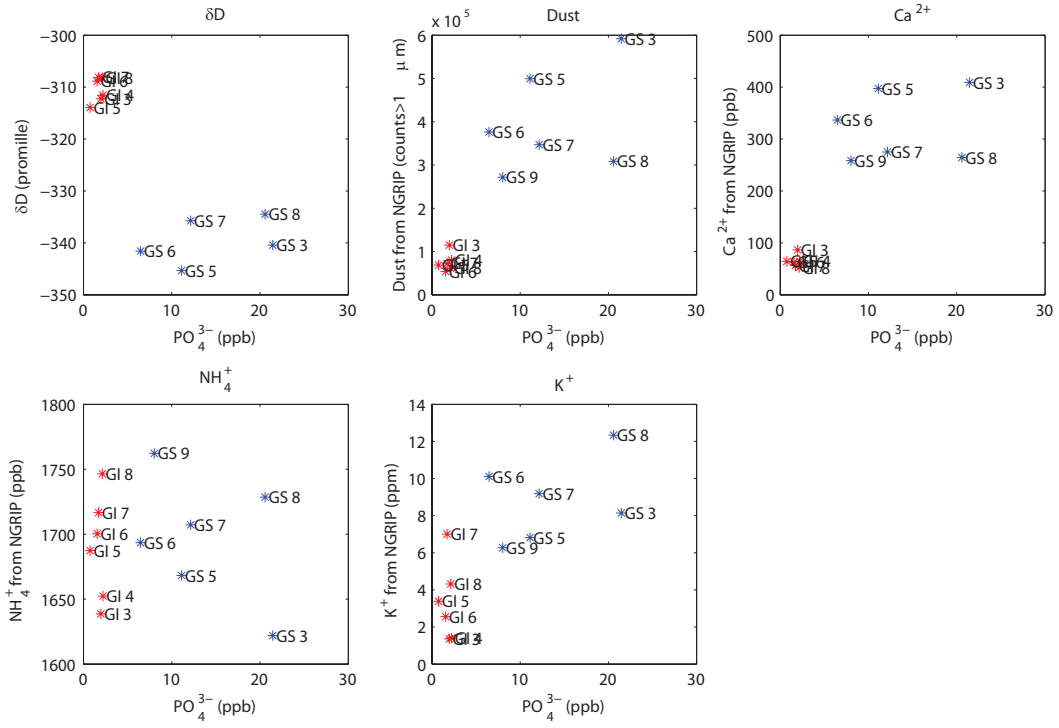

(a)

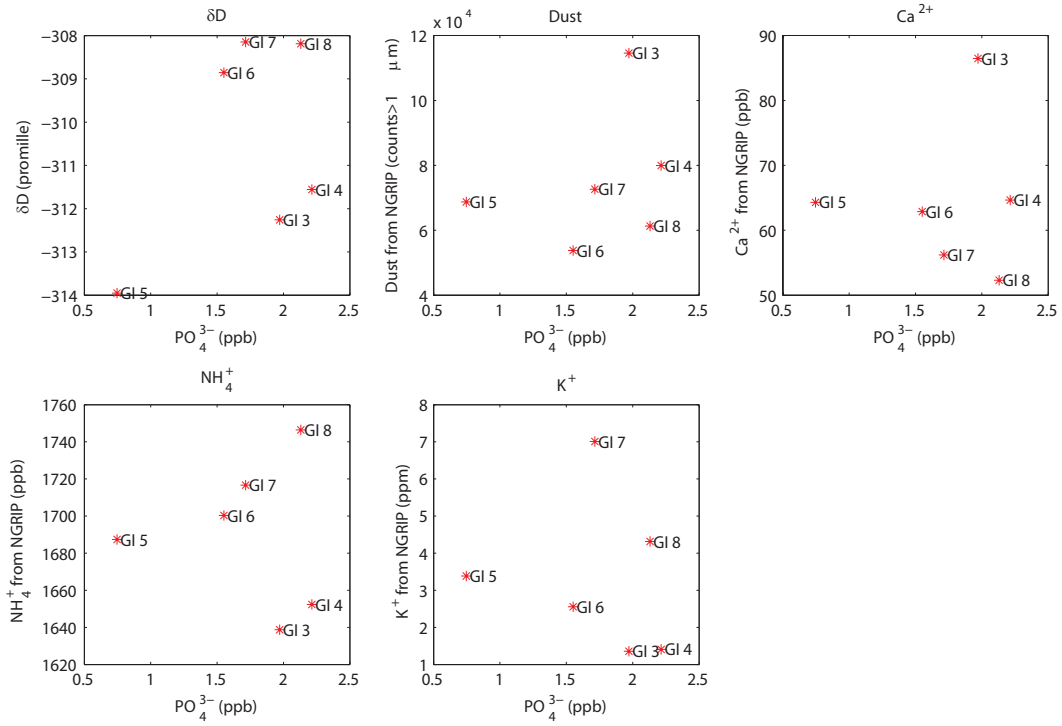

(b)

Figure 70: Phosphate from NEEM is plotted against δD (top left) from NEEM , dust (top middle) from North-GRIP, Ca^{2+} (top right) from North-GRIP, NH_4^+ (bottom left) from North-GRIP and K^+ (bottom right) from North-GRIP for the periods defined in table 10 (a) Glacial stadials (blue) and glacial interstadials (red). (b) A zoom on the glacial interstadials.

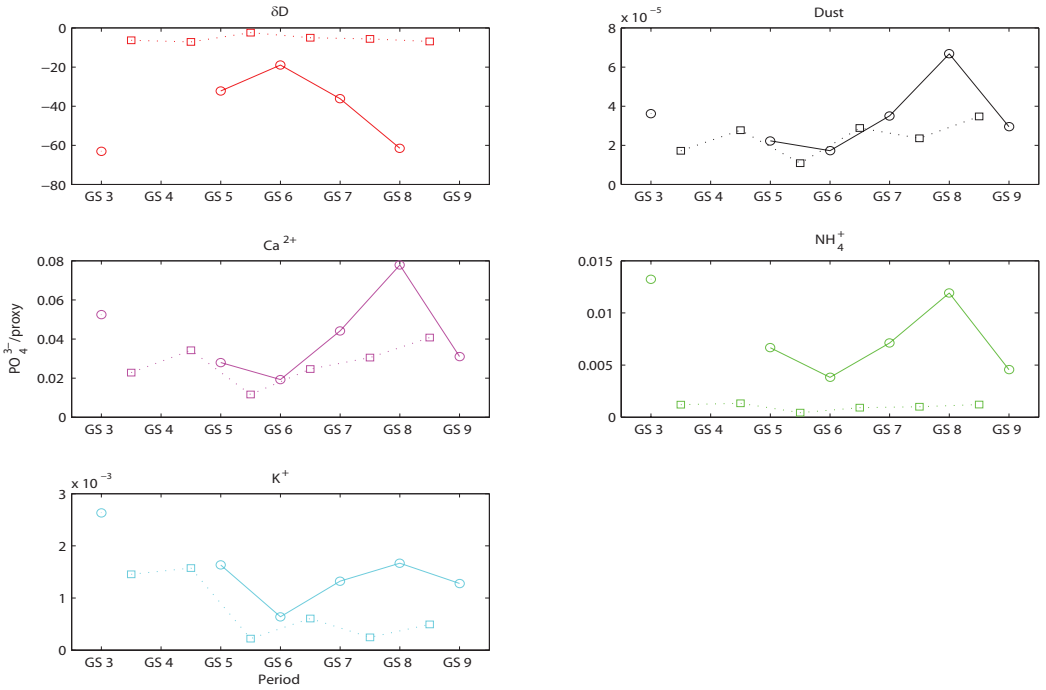

Figure 71: The ratio between phosphate from NEEM to δD (red) from NEEM , dust (black) from North-GRIP, Ca^{2+} (pink) from North-GRIP, NH_4^+ (green) from North-GRIP and K^+ (light blue) from North-GRIP. Interstadial periods are shown with squares and dotted lines, while glacial stadials are shown with circles and full lines.

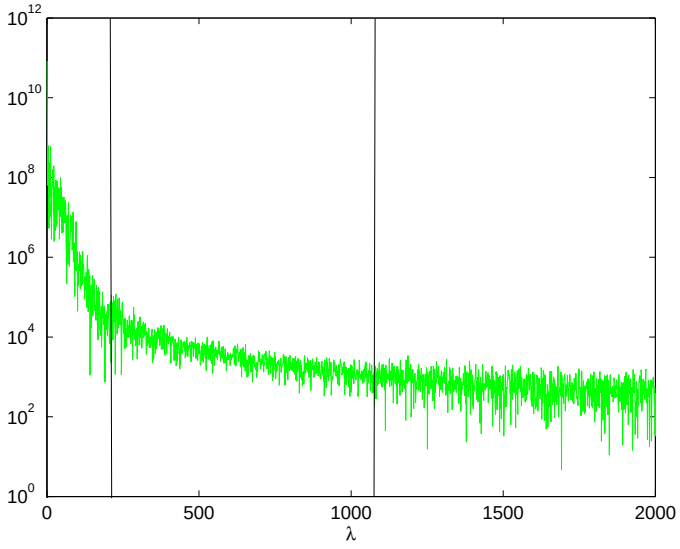

Figure 72: Spectral analysis of the NEEM ice core phosphate. λ denotes the number of sin curves employed on the length used for the analysis (11.998 m)-thus the wavelength corresponding to λ can be calculated by 11.998 meter$\cdot\lambda$=wavelength. The black lines are drawn to illustrate that it is very difficult to determine a cut off value. The one at the right is determined as five times the noise, while the one on the left is chosen by eye.

factor 200 higher, while the mild interglacials show values higher by a factor 16 than the Holocene.

The difference in concentration betweem the NEEM S1 shallow ice core and glacial time (NEEM) makes phosphate comparable to other dust proxies showing changes by a factor of approximate 100, and the factor 10 between glacial stadials and interstadials is convincing for categorising phosphate with dust as well.

The distribution of concentration is lognormal in the glacial inter stadials (GI's), while the distribution of all glacial stadials plotted together show evidence of more than one top, due to the high variability in the phosphate level among the periods.

The level found in the glacial is within the detected level of PO_4^{3-} in the melt stream from glaciers found by *Chillrud et al.* [1994]; *Tockner et al.* [2002]. I do not know the age of the glacier they used in the study, but it is likely that the glacier is younger than the part of the NEEM ice core used for detection of phosphate. The high level in the Argentinean glaciers could be explained their position closer to the sources.

The high levels of phosphate, found in the NEEM ice core, support the theory that more PO_4^{3-} could be transported to remote oceans as aerosols during the glacial and thus affect the primary production.

It was not possible to group any of the glacial stadials (GS's) or glacial inter stadials (GI's), though GS 3 and GS 8 show higher mean values ($\geq$20 ppb) of PO_4^{3-} than the other GS's. GS 6 shows the lowest mean value of PO_4^{3-}; however as all ready explained the low level in GS 6 might be too low because of baseline problems. The GI's show the same signal as Gs's. High level is found in GI 3, GI 4 and GI 8. The lowest mean value is in GI 5. This could suggest some longer trend for phosphate since relatively high levels are present in both GI and GS periods at the same time

A source for such a long level trend could be solar insulation. Some hypotheses on the influence on phosphate by solar insolation are presented below:

Hypothesis 1 Higher solar insulation would cause more energy in the oceans and thus lead to a larger biosphere. It should however be noted that the response of the biosphere is much more complicated than just higher temperatures giving a larger biosphere. However if the biosphere were enlarged it could cause the phosphate circle to be more active in the reuse of phosphate in the top ocean layers, increasing the amount of phosphate seen if the source in ice cores is from a marine origin.

Hypothesis 2 A higher sea surface biological activity could also mean that more phosphate was bound in biological material, which is made up of relative large particles, that when dying fall to the bottom and thus less phosphate is transported to the ice sheet from the surface waters.

Hypothesis 3 The influence of higher solar activity could also cause sea ice to melt and if the seas are the source of phosphate in ice cores the source would come closer and thus an increase in phosphate in ice cores would be expected.

From figure 73 it seems that phosphate shows maximum level, when solar insolation is lowest mainly supporting hypothesis 2. However due to the short period available it is not easy to reach any firm conclusion and most likely a direct effect is not present.

Another long term trend-sea level changes- is discussed in section section 9.4.3.

9.4.2 Deuterium

Deuterium is believed to behave with temperature much the same way as $\delta^{18}O$. An anti-correlation was found between deuterium and phosphate. It is clear that we have much

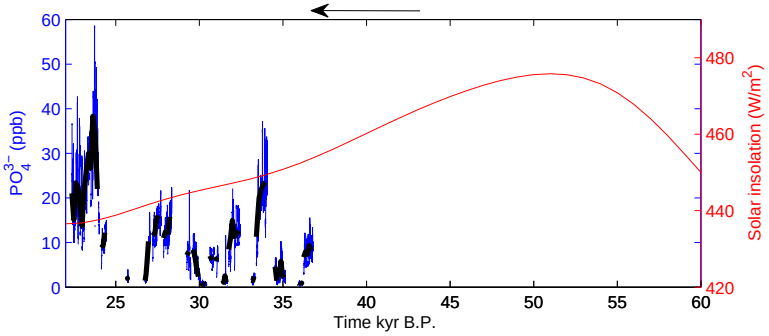

Figure 73: The summer solar insolation for 70N (red) [*Laskar et al.*, 2004] and phosphate using a 2 cm smoothing (blue) and using bag means (black) are shown on the GICC05modelext-NEEM-1 time scale. The arrow points in the direction of time.

larger concentration of phosphate in the cold periods. The effect seems to be strong. I would like to point to the depth 1730 to 1740 meters, where some short period spikes are seen in both phosphate and in δD. This could support a short response time for phosphate with temperature.

In figure 70, left column, it might seem that the periods GI 3 and GI 4 form a group and that GI 6, 7 and 8 form another group. However any such grouping occurs only in the amount of δD and not in the amount of phosphate so I would conclude that this observation is not significant.

9.4.3 Dust and Calcium

Dust shows high correlation with the detected phosphate (0.84). An even higher correlation would be expected from the results with the results from the NEEM S1 shallow core if dust had been measured in the NEEM ice core at higher resolution. Unfortunately these data are not yet available. The correlation coefficient relates more to large climate fluctuations visible in almost all proxies than to a direct relation between phosphate and dust and it is difficult to conclude on a more direct correspondence between the phosphate and other proxies, because of the low resolution available and because of the fact that the other proxies used for comparison are from another ice core. A high correlation is also found for Ca^{2+}, which is believed to have only dust as a significant source. However, as in the NEEM S1 shallow ice core, again I find that the dependence of phosphate to dust, is far from linear.

As mentioned in section 4.3.1 Ca^{2+} can affect the soluble fraction of phosphate. Assuming a linear response, I tried to investigate, if the effect of Ca^{2+} on the soluble fraction could explain the absence of linearity between dust and PO_4^{3-}; but either the effect is not linear (it could *e.g.* be necessary to include NH_4^+ and SO_4^{2-} into the relationship), or perhaps the effect of Ca^{2+} on the soluble fraction is not significant. No clear relation was discovered that would be capable of explaining the lack of linearity between PO_4^{3-} and dust.

Using equation 16 and the values for dust in different periods from *Steffensen* [1995] an approximation of the maximum amount of PO_4^{3-} arriving with dust was calculated assuming a soluble fraction of 100 %, and the minimum PO_4^{3-} arriving with dust assuming that the soluble fraction is only 0.2 % (see table 12). It is clear that the theoretical amount of PO_4^{3-} in dust is in the lower end of the concentrations detected in the NEEM ice core. Even assuming total solubility the theoretical levels are lower by a factor 7 than those levels found experimentally. The discrepancy could be explained if in general the dust transported to the ice has a very high PO_4^{3-} content, or if PO_4^{3-} has a second source besides dust.

A reason for the high phosphate levels could be if the Gobi desert has a high content

Table 12: The phosphate that would be expected from dust only, using dust values found in *Steffensen* [1995] and assuming soluble fractions of 100 % and 0.2 %.

Period		LGM	GI 3	GS 3 (1)	GS 3 (2)
Dust (μg/kg ice)		7600	191	3920	2290
$PO_{4\,dust}^{3-}$ (ppb)	S= 100%	5.47	0.14	2.82	1.61
$PO_{4\,dust}^{3-}$ (ppb)	S=0.2% (μg/kg ice)	0.011	0.003	0.006	0.003

of phosphate (lots of apatite), compared to the mean values of I have used for PO_4^{3-} in the crust. I have not succeeded in finding a value of the concentration of PO_4^{3-} in GOBI desert soil, but I found that Mongolia has 4-5 % of the global export of PO_4^{3-} [wik, 2010b], suggesting that the concentration could be higher than the global mean.

Another possible explanation is if phosphorus and phosphate are deposited on the shelf during periods of high sea level. During the cold periods, which are also the periods showing high PO_4^{3-} and dust, the shelf would be exposed because the water is retained as ice in the ice caps causing low sea levels. Dust coming from the shelves could contain relatively high amounts of PO_4^{3-} and this would explain why the concentration found in the NEEM ice core is higher than the value calculated from dust. However this theory is only valid assuming winds are strong enough to lift particles from the very low levels of the shelves and transport them all the way to the ice.

A way of checking this so called shelf-nutrient hypothesis is to investigate whether there is a long term trend in the PO_4^{3-} / dust ratio- a trend which corresponds to the sea level variations over time found by looking at marine cores and other proxies.

The ratios between phosphate and dust and between phosphate and Ca^{2+} (figure 71) show high amounts of phosphate relative to dust and Ca^{2+} in GS 3 (22-25 kyr BP) then a low in the amount of phosphate relative to dust and Ca^{2+} in GS 6 and GI 6 (30-31 kyr BP)[31] and then again an increase in the amount of phosphate in GS 8 (33-34 kyr BP) followed by a dip in GS 9 (36.000 BP).

The trend can be compared to sea level variations, but it is hard to make solid conclusions based on data of the available resolution. As shown in figure 74 *Sierro et al.* and *Sidall et al.* [2010] put sea level variations found in marine cores on a glacial time scale using North-GRIP data.

It seems that an effect of sea level could be present. In the period investigated in the present work a bump is present in almost all the sea level records, but the effect is not linear. The high concentrations of phosphate found early (35 kyr B.P.) could be explained by the sea level reaching a minimum, exposing more shelf with high PO_4^{3-} content. Then the sea level increases (33 kyr B.P.) and less PO_4^{3-} is transported to the ice sheet and finally (25 kyr B.P.) the sea level goes even lower than previously seen. However this does not lead to a very high phosphate content. This could be due to the sea level decreasing to a level lower than the shelf, -and thus not exposing a larger area of the shelf than the previous low and if the amount of PO_4^{3-} on the shelf depends on the time the shelf has been under water, and the shelf had already newly been exposed, this could explain the phosphate record. However care must be exercised with these interpretation, recalling that they are based on the available resolution of sea level, that the records show dips at different times and that phosphate has been detected over a very short period of time only.

Finally we should not forget that the correlation between phosphate and dust can be solely due to the phosphate being transported on the dust: More dust in the cold periods

[31] Remember that this period should not be trusted too much.

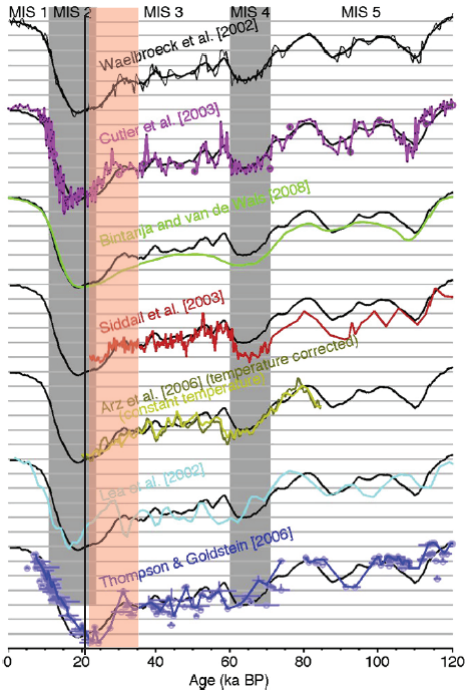

Figure 74: The figure show sea level detected from marine records and transferred to a time scale using the North-GRIP ice core*Sidall et al.* [2010]. Red transparent show the area in which phosphate is detected.

could increase the amount of phosphate actually making it to the ice sheet, because PO_4^{3-} could bind to the particulate matter and further the glacial is believed to have been very dry and the amount of PO_4^{3-}, which has rained out during transportation is thus perhaps diminished.

It was not possible to group any of the climatic (GI and GS) periods according to dust (figure 70).

9.4.4 Ammonium

There is definitely no linear relationship between ammonium and phosphate: The correlationcoefficient is not high 0.46. Looking at the GI's in figure 70b, one could argue that GI 3 and 4 form a group and that GI 6 and 7 from another group. Due to the resolution of both phosphate and ammonium and the fact that the ammonium is detected in another ice core no evidence can be seen, as in the NEEM S1 shallow core, of correlation between single spikes of ammonium and phosphate. Thus no firm conclusion on the relationship between ammonium and phosphate can be based on the available data.

9.4.5 Potassium

Phosphate and potassium are very highly correlated. Looking at figure 68 it immediately becomes evident that potassium is the parameter that follows phosphate best- but unfortunately the resolution of K^+ is not high. The correlation coefficient is 0.71. I suspect that the correlation would be even higher if the high spikes in potassium were removed and phosphate and potassium were obtained from the same ice core and were compared at the same resolution.

The only period where the levels of the two does not follow each other in is GS 6 where the phosphate level seems low. As mentioned earlier this climatic period probably contains the least reliable phosphate detections. However I do not believe that the baseline issues are the only reason that phosphate does not reach the high mean level of 17 ppb necessary

Table 13: The ratio of phosphate over potassium for different sources. Note that the biogenic ratio is based on limited information [wik, 2010g; *Concright et al.*, 2000; *Basile et al.*, 2003; Pot, 2010].

Source	Sea salt	Dust	Biogenic	Ice (this study)
PO_4^{3-}/K^+	$0.03 - 4 \cdot 10^{-4}$	$0.17 - 5.60$	$0.09 - 5.5$	10^{-3}

to follow the potassium in GS 6.

It makes good sense that the potassium and phosphate will follow each other: They have almost the same global cycle. In order to investigate the source of PO_4^{3-} I have compared the ratio of phosphate over potassium in different sources (see table 13), in order to determine which source is more likely. Note however that information on the biogenic ratio is based on limited literature. It is clear from this very simple analysis that sea salt is the source best capable of explaining the relationship between potassium and phosphate.

The fraction of PO_4^{3-} arriving to the ice coming from sea salt, $PO_{4\,ss}^{3-}$, can be calculated using the ratio between PO_4^{3-} and Cl in sea salt; $5.68 \cdot 10^{-6}$ and assuming that sea salt is the only source of Cl. The mean level of Cl is 105 ppm and the maximum level is 235 ppm in the North-GRIP ice core within the time period investigated in this work [*unpublished*, 2004]. Thus the amount of $PO_{4\,ss}^{3-}$, which is on average 0.6 ppb and maximum 1.3 ppb, suggests that it is not possible that the only source of PO_4^{3-} is sea salt if the North-GRIP concentration of Chloride is comparable to the concentration in the NEEM ice core. However we should recall that PO_4^{3-} is more abundant in the Arctic ocean, so the fraction of PO_4^{3-}/Cl^- might be slightly larger. According to the shelf nutrient hypothesis the level of nutrients can have been higher in the oceans too. The concentration of Potassium expected from sea salt (K_{ss}^+) is 2 to 4.5 ppm: thus all K^+ can also not be sea salt.

9.4.6 Spectral analysis

From the spectral analysis shown in figure 72 it is clear that finding the cut off value is not easy. The spectrum shows a memory effect; no place is a stable noise signal reached. This could very well be the memory effect all ready described in the discussion of the temporal response; the signal does not show a gaussian distribution but rather it is a gaussian distribution shifted to the right due to coating. This makes it very difficult to determine the cut off value. It is however clear that the NEEM set-up does exhibit poorer temporal resolution than the set-up used in Copenhagen for the NEEM S1 shallow core. I would recommend others who would want to detect phosphate in ice cores to keep high flow in the phosphate line in order to keep the resolution high.

The detection of phosphate in the NEEM ice core covers part of the depth 1607.65 to 1763.85 meters corresponding to interglacial periods 2 to 8 (22.4-36.8 kyr B.P.). A flow lower than recommended was used, which caused some coating issues. There were some troubles regarding baseline, due to high dust load in the glacial period. These troubles were probably due to heavy coating, possibly caused by precipitation caused by the dust reacting with the tartaric acid. The problem with the baseline introduce an uncertainty of about 2 ppb.

In the mild inter glacial periods the level was between 0.3 and 12 ppb phosphate with mean values for the periods between 0.75 and 2.1 ppb. In the glacial stadials the level was higher; concentrations between 1.9 and 59 ppb were detected. The mean of the glacial stadials showed concentrations from 6.5 to

21.5 ppb. The phosphate change in the level from glacial to interglacial stadials as well as the change between the level found in the NEEM S1 shallow ice core, could relate phosphate with dust proxies. The ratio between potassium and phosphate does however best follow a sea salt signal. The level of phosphate detected is higher than both the expected amount of phosphate from dust of about 5.5 ppb PO_4^{3-} and the expected amount from sea salt approximately 1.3 ppb PO_4^{3-}. The expected amount of the two combined is in the order of the detected, but it is not impossible that a third source is present.

The detection of phosphate in glacial ice had some complications. The next section discusses optimizations which can be done to diminish the complications found as well as other ideas for optimizing and evaluating the method for detection of phosphate in ice cores further.

10 Evaluating the method. Further ideas for optimization and validation

This section presents ways to further optimization of the molybdenum blue method using a 2 meter LWCC for detection of phosphate in ice cores. Suggestions are included for making more valid standards, finding interferences and diminishing coating effects. Further optimizations for high concentration detections are suggested.

10.1 Standards and linearity

Even when using polypropylene bottles some variation of the standards occurred (see section 7.4.4). If the bottles were flushed with HCl or H_2SO_4 before preparing the standards, the effect might be reduced. I suspect that the PO_4^{3-} sticking to the side of the bottles could be what caused the limit of detection (LOD) to be twice as high as found by *Zhang and Chi* [2002]. This result could be false- if half the standard for the low concentration were stuck on the side of the glass. This could also explain part of the variation between the various calibrations found during the detections at NEEM. However the variation of the calibration could also be due to wear out of tubings, causing a different flow or to optical effects in the LWCC changing over time due to coating or due to micro bubbles.

I do however also observe a significant drift of the baseline (15 counts), even when it is the most "stable"- this could be due to micro bubbles in the Milli-Q water used- this could also be larger than in the experiments by *Zhang and Chi* [2002], causing a poorer LOD.

It is possible that the drift of the baseline could be due to the air introduced when preparing the packages of water of different sizes. Since no mixing takes place from adding reagent and buffer to adding air, there is a risk that some water packages contain more reagent than others, making the baseline drift, because as shown in experiments the amount of molybdenum to sample is important for the baseline. However since the path way used is much longer than each package of water large fluctuations should not be caused. If fluctuations are due to different amount of molybdenum blue and buffer in each package it could be avoided by including about 20 cm of mixing after the buffer is added, before air is introduced.

10.2 Interference

It should be considered whether interferences could be the cause for the high detected phosphate content-as compared to the calculated amount.

Silicates can be present in both sea salt and dust. Silicate has not been detected and thus it is difficult to know how much is actually present in ice cores. However the silicate part of sea salt can be calculated in the same way as the PO_4^{3-} fraction of sea salt using the mean Cl^- concentrations found at North-GRIP and the fraction ratio between silicate and Cl^- in sea salt. Then concentrations of silicate from sea salt are found to be around 13 ppb in mean value, with a maximum of 32 ppb silicate (0.4 μM).

The silicate level is high in dust- the global mean is 27.7 % by weight. This means that the level of silicate arriving in dust could be as high as 2100 ppb (20 μM) in glacial times, but the soluble fraction of silicate is certainly lower.

The interference from silicate was calculated using equation 12. The temperature T was 338 °K(65 °C), and a pH of 1 was used. The apparent phosphate arising from silicate levels of 20 μM is approximately 0.6 μM PO_4^{3-} (6 ppt). So although silicate interference does occur, it is probably not significant.

I would however suggest that an experiment be conducted to detect how the amount of silicate interferes with the method after the modifications I have done. First of all the silicate level in ice cores should be determined using *e.g.* ICP-MS. If the level is within the range for significant interferences according to equation 12, the response of standards with known silicate concentrations in the range expected in ice cores should be tested using the optimized method for phosphate detection in ice determined in this study. Further, the response to combined standards of phosphate and silicate should be tested.

In theory reducing the temperature below 30 °C would diminish the silicate interference. Unfortunately this would at the same time aggravate the coating effects, and thus I do not suggest this as a solution, since the coating already has significant impact on the measurements.

One could consider using a mixing length shorter that used at NEEM in order to diminish the reaction time, because the silicate requires longer reaction times. Three meters should be sufficient for most color to have developed.

Further it might be possible to find some sort of **column**, which can remove some of the silicate present in the waters [*Bigler*, 2010], such as column could *e.g.* be the one used by *Yaqoob et al.* [2004] for removing interfering cations in an online system; a iminodiacetate chelating column. The column could help minimize effects of iron and Mn, too.

Arsenate is probably not present in ice cores in amounts sufficient to cause interference(probably sub ppb). However adding thiosulfate should remove any interference from arsenate (see section 6.3.1). I suggest this be added as well, since it would not require any large change of the set-up.

It is worth mentioning again that the method using molybdenum blue detects all the **reactive soluble phosphorus** and not only the PO_4^{3-}. This is a problem because what is detected is the part reactive at high acidity, and this means that it can not be assumed that all phosphorus detected is available to the biosphere, complicating the interpretation of changes in the phosphate available to the biosphere over time.

I suggest that PO_4^{3-} and P should be analysed using ion chromatography in at least three different sections of an ice core to investigate how much of the phosphorus is detected with the molybdenum method used here and more generally to validate the method.

10.3 Memory effects

As is evident, from both the changes over time of the temporal resolution changes, the shape of concentration peaks, the slow return of baseline and the spectral representation of the detected level in the NEEM ice core, memory effects are significant and on many time scales.

These a partly due to physical effects such as precipitated material causing mixing and partly due to chemical effects such as the PO_4^{3-} sticking to the glass the filter is made of and to Ca^{2+} and other positive charged ions that are stuck in the filter.

To diminish the coating several things could be tested. **Flushing** with some chemicals[32] was all ready tested, and found of no use.

Adding Ethylenediaminetetraacetic acid (EDTA), should be tested. The EDTA has the ability to sequester metal ions. The ions remain in the solution after being bound, but is less reactive [wik, 2010a]. This could perhaps diminish the coating observed by removing the ions that the PO_4^{3-} sticks to such as Ca^{2+}.

[32]Methanol, a solution of 20 μl HCl acid in 20 mL Milli-Q water and a solution of 20 μl sodium hydroxide in 20 mL Milli-Q water.

The increased dispersion could occur due to the tubing wearing out over time; this especially happens when detecting glacial cold sections, due to the increased amount of dust, damaging the inside of the tubing, then getting stuck in the scratches ans so providing a permanent trap for the PO_4^{3-}. Several optimizations could be done to diminish this effect. One could be to remove the dust earlier in the system by **moving the filter to a position before the reagent**. This however would affects the amount of detected phosphate, because some of the PO_4^{3-} might be stuck to the dust particles themselves and thus they would not be detected. Further this position of the filter was found to require a sample completely air free since the presence of even very tiny bubbles will block the filter. Such samples are hard to obtain, because the change from Milli-Q to ice often causes some additional air to get into the detection system; sometimes more air than can be handled by the debubbler positioned before the sample is split between different detection systems. A way to get around this would be to include an accurel before the filter, but the pressure required to press water through the filter is higher than the pressure the accurel can hold.

It might be possible to find **tubing in a different material**, which has an even smoother surface diminishing the dispersion [*Bigler*, 2010].

Finally if the previous approaches do not offer any significant improvement, it might be necessary to **change all tubing** used after a week of continuous detection or after events of high dust load in order to preserve temporal resolution over time. This would however significantly increase the time consumption of the method.

Nuts and ferrules also wear out over time, and on several occasions they literally broke in two and had to be replaced. This was observed both at NEEM and during experiments conducted in Copenhagen. I suspect that the wear out of connections may influence the amount of particles stopped there and thus influence on the dispersion

10.3.1 Filter effects

The memory effects are probably highly correlated to the use of a filter. As mentioned in section 6.2.6, glass filters can remove up to 66% of an initial inorganic phosphorus concentration of 1.55 ppb, so there is a risk that the fraction removed could be significant. I do not believe that this influences the response to the standards, because they run for a long time, so that in the end the filter must be saturated. But during detection in ice there is a risk that especially small spikes really are higher than what is detected, especially in the beginning of a detection.

Chemical exchange of PO_4^{3-} to the glass wool filter as well as to particles trapped in the glass wool does occur. In order to diminish the effect, it would perhaps improve the temporal resolution if PTFE wool replaced the glass wool currently used. PTFE wool is available, but I did not have the time to test if it works for trapping dust. Other types of filter material should be investigated as well; *Li and Hansell* [2008] had good results using polycarbonate or cellulose ester filters.

If another filter type is not found I would recommend that a test is conducted to investigate the amount of PO_4^{3-} stuck on the glass wool. This could be done by flushing a filter already used for ice core phosphate detection with some chemical, which would release the PO_4^{3-} and thus after flushing the chemical could be analysed for PO_4^{3-} concentrations using IC- since the molybdenum method could be influenced by the difference in chemistry compared to the Milli-Q water normally used as baseline.

Further the glass column should be changed to a material to which the PO_4^{3-} does not stick. It might be possible to make a filter using tubing of two sizes, where the one fits inside the other. If the thicker tube was filled with glass wool the thinner could work as end connectors, giving the further advantage that the dead volume would be diminished, when

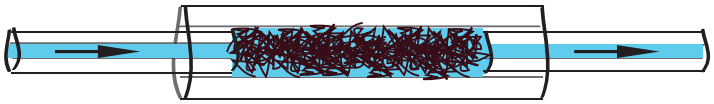

Figure 75: Illustration of an idea for another type of filter made using two different sizes of tubings and filling the thicker tube with glass or polypropylene wool. After filling the smaller tubing can be pressed together to minimize the dead volume. Arrows denote direction of flow.

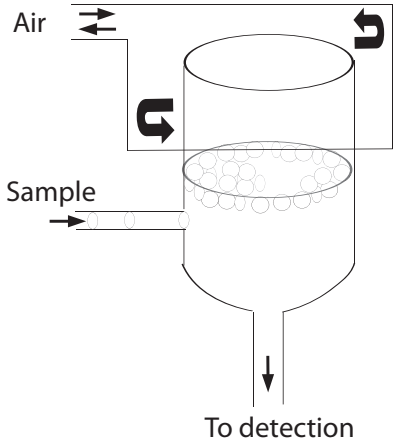

Figure 76: The idea behind a fourth type of debubbler. One of the advantages is that it does not have sharp edges in which the bubbles can get caught. Further air of known concentration is flowing through, removing the air bubbles and making the system sealed. Small circles illustrate bubbles.

pressing the two thin tubes into the bigger one. Figure 75 illustrates the idea. Finally the tubing type filter is probably easier to fill than the glass type, which requires at least 5 minutes to fill and another five minutes to introduce it into the system to avoid bubbles being trapped inside.

The ICP-MS system used at NEEM also used a filter. The system used two ICP-MS systems and shifted between them and when one system was not used with sample, the filter was back-flushed to get rid of particles. To implement such a **two way flush system** would increase the grade of complexity in the method used in this study, but would maybe help against the long term effect of dust being collected in the filter. Such a flushing could be done after each measurement. However it might require that a total double system containing two filters and two LWCC's be used, significantly increasing the cost of the system. After each measurement run one could change detection system and the one not in use could be flushed.

10.4 Debubbler

The debubbler used in the set-up accumulated black particles over time[33] increasing the mixing that took place. Further, due to the soap in the buffer, micro bubbles in the debubbler were extremely hard to get rid of and some times continued to the filter position creating a blockage of the entire system. **A better design of the debubbler** could perhaps solve the problem of micro bubbles. If the debubbler used today is used for further detection a spare one should be brought, so that the debubbler can be replaced when affected by soap foam or precipitations. In Bern they use a debubbler as shown in figure 76, which might work better because it does not have so many sharp edges that can trap the bubbles.

An **on line degassing system** produced by the company Alltech was used by *Zhang* [2006] in a method for detecting nitrite in a LWCC. The degassing system uses Teflon AF material (also used in the LWCC) of high gas permeability, and *Zhang* [2006] found that

[33]most likely dust and silicate, which is precipitated out by the tartaric acid

the baseline was significantly more stable using this sort of debubbler, due to fewer micro bubbles. For nitrite detection it improved the precision from 15% to 3% at a concentration of 20 nM nitrite. I suggest that this instrument is tested as a debubbler in the set-up for detecting phosphate.

10.5 High concentrations

Using the present method it was shown that the reactive phosphorus content in ice from the last glacial had concentrations up to 60 ppb. These high concentrations were not expected before conducting the measurements of the NEEM ice core. The high concentrations had not been investigated during the optimization procedures. It was found that the absorption depended linearly on concentration only up to approximate 40 ppb. I therefore suggest that linearity should be more thoroughly investigated, and means should be found for obtaining a better temporal resolution at higher concentrations.

I suggest that a **shorter LWCC** could be used to detect phosphate in the glacial stadials. *Adornato et al.* [2007] used a 50 cm LWCC and found a limit of detection of 0.97 ppb PO_4^{3-}. Using a shorter LWCC would increase the linear range and temporal resolution. Further a shorter LWCC would have less change of becoming clogged with bubbles and other stuff and the shorter length would would further diminish the back pressure. Therefore when using a shorter LWCC it might be necessary to check if micro bubbles develop. However as concentrations in the glacial inter stadials and the Holocene are close to the detection limit of the 2 meter LWCC (LOD=0.1 ppb) it is not advisable to use a shorter LWCC for detection in those periods.

A **shorter wavelength** should be considered as well, because the top of the wavelength spectra is shifted, when concentration is high (see section 7.7). A shift might extend the linear concentration range, but the precise effect should be investigated.

10.6 Suggestions for ice cores

To validate the method used in this study the level of PO_4^{3-} should be determined using both the method of this study and another method such as IC in the same ice core at equal depths.

For further validation of the method and to get a better idea of contamination sizes and risks it would be interesting to perform a double core analysis in both the following ways: (a) Taking two pieces from the same depth of the same core to check on the handling the core and (b) to make detections of two very close positioned cores, most ideally drilled by two different types of drill, using different drill liquid, to investigate the effects of post deposition changes occurring in the ice and of drilling method influence. However obtaining two pieces of ice for CFA in the same core at the same depth for double core validation is not an option, because the ice available is limited.

If phosphate is detected in a shallow ice core, detection of K^+ would also be interesting to determine whether the two really have the same source. This would be confirmed if the sub annual signals were of equal size and period.

Detecting phosphate in other ice cores from both Greenland and the Antarctica could help determine how global is the phosphate signal [34] and could also help in determining where the signals originate from. *E.g.*, measuring an ice core close to the sea (from the Hans Tausen or Renland sites) would show enhanced sea salt signal. However it is difficult to obtain an ice core close to the ocean, which is not closer to dust sources as well.

[34] Most likely it is not very global, because it arrives with dust events.

Though the method used in this study has proved successful, some optimization and testing remains to be done. It is suggested that the method be compared to a PO_4^{3-} analysis using for example IC detections on the same core. The reproducibility should be tested by detecting the same core twice. Silicate interference should be further investigated. New filters and new debubblers should be investigated to reduce coating effects and a new type of tubing should be tested too. The linearity should be investigated and by using e.g. a shorter flow cell the temporal resolution can be improved for detections in glacial ice, where concentrations of phosphate are large. A conclusion on the entire project can be found in the next section.

11 Conclusion

The main goal of this project was to find a method capable of detecting phosphate in ice cores using continuous flow analysis (CFA). To this end a literature study of the PO_4^{3-} cycle was performed in order investigate the effect of P and PO_4^{3-} on climate, and to find the concentrations to be expected in ice cores.

It was found that P is an important and sometimes limiting nutrient for primary production in the oceans. A large part of the phosphorus cycle is water transported, and only a fraction is transported as particulate matter in the atmosphere. The atmospheric transport of phosphate can however have significant impact on remote oceans. About 80 % of P and 50 % of PO_4^{3-} transported in the atmosphere is in the form of mineral dust. Because of deforestation and the use of phosphate as a fertilizer changes in the phosphate cycle have occurred over the last centuries. On longer time scales, sea level changes are thought as well to have caused changes in the phosphate cycle.

The amount of P found in the glaciers in previous studies are 0.25 ppb in Greenland using ICP-MS and up to 145 ppb is detected in melt streams from Argentinean glaciers [*Edwards et al.*, 2007; *Chillrud et al.*, 1994].

Ice cores can be used as a climate archive, because they keep layer upon yearly layer of accumulation, which after drilling can be analysed for various climate proxies, one way to analyse the ice is to do Continuous Flow Analysis (CFA). In continuous flow analysis the goal is to detect the specie with high resolution and a minimum of handling to minimize contamination. For this study the the Copenhagen CFA system, which detects only few species, but has a high resolution and the Bern CFA system, which detects several species, and thus has a lower temporal resolution was used.

Through the literature study, the method by [*Zhang and Chi*, 2002] was found to be the only method capable of detecting the low concentration expected in Greenland ice cores and at the same time capable of running using CFA. Therefore the method was found to be best for implementation for detection of phosphate in ice cores. The method is an absorption method using molybdenum blue as reagent and ascorbic acid as buffer. The method takes advantage of an increased path length enhancing detection limits using a 2 meter Long Waveguide Capillary Cell (LWCC) with special optical conditions.

Through optimization experiments it was realised that the optimum set-up had flow rates of 1.68 mL/min for sample, 0.15 mL/min for reagent and buffer each and introduced air at a flow rate of 0.20 mL/min to prevent dispersion. Reagent should be prepared by dissolving 0.37 g molybdenum blue in 25 mL 5N H_2SO_4 adding 5 mL tartaric acid and dissolving in 100 mL milli-Q water. Buffer should be prepared by dissolving 0.5 g L-ascorbic acid and 7 g sodium dodecyl sulfate in 100 mL milli-Q water. Standards should be prepared in polypropylene bottles to avoid that the PO_4^{3-} desorbs onto the container walls.

Mixing should occur over at least 300 cm of tubing of a diameter of 0.5 mm, in a heat bath at a temperature of about 65 °C. Air should be removed at a flow rate of 0.35 mL/min using a debubbler to avoid bubbles in the detection cell. A filter made of a 3 cm long glass capillary, with an internal volume of 0.2 mL should be at least 2/3 filled with compressed glass wool and positioned before the entrance of sample to the 2 m LWCC to prevent optical interference from dust.

Detection at 710 nm and a short wavelength integration range (Boxcar of 2), with an integration time of 300 ms is recommended.

Using this set-up, concentrations down to 0.1 ppb were detected and the noise was about 15 counts corresponding to about 0.18 ppb PO_4^{3-} when the baseline is 3000 counts.

Table 14: Mean concentrations of phosphate detected in the NEEM S1 shallow core and the NEEM ice core, glacial stadial (GS) and glacial interstadial (GI).

Ice core	NEEM S1	NEEM (GS)	NEEM (GI)
Concentration [ppb]	0.32	6.5-21.5	0.75-2.1

Linearity is good below 40 ppb.

The optimized method was used for detection of phosphate in two different ice cores: The NEEM S1 shallow core and the NEEM ice core.

In the NEEM S1 shallow core - representing sections of the last 120 yr - the mean level was 0.32 ppb PO_4^{3-}, with a large standard deviation in agreement with [*Edwards et al.*, 2007]. A small seasonal signal was detected with maximum in winter and minimum in summer suggesting sea salt as the source. High correlation with dust was found (0.72) supporting earlier observations in aerosols [*Mahowald et al.*, 2008]. It could not be determined whether this correlation is due to a common source or due to transport processes. Spikes in the phosphate record which did not correlate with dust, showed some correlation with ammonium. It was tested if a forest fires, a common source for phosphate and ammonium, correlated with the spikes. No clear conclusion could be made. No sign of any anthropogenic impact was found.

Phosphate was also detected in the NEEM ice core in depths from 1607.65 to 1763.85 meters corresponding to the inter glacial period 2 to 8 (∼22.4-36.8 kyr B.P.). The NEEM ice core showed a phosphate increase by about a factor 100 in the glacial as compared to the Holocene (NEEM S1). The glacial stadial to glacial interstadial transitions showed variations by about a factor of 10. These changes in level mean that phosphate transition rates are comparable to dust. The level in the glacial interstadials is approximately 2 ppb while the glacial stadials has a level between 6 and 21 ppb.

The distribution of concentrations is log normal. Comparison with potassium suggests similar sources for potassium and phosphate and the ratio between them support sea salt as the main source. The theoretical sea salt part of PO_4^{3-} - calculated using the amount of Chloride present in the NGRIP ice core - however suggest that sea salt can not be the only source. The combined theoretical amount of PO_4^{3-} arriving with sea salt and dust is 6.8 ppb and thus not far from the phosphate concentrations detected in the NEEM ice core.

Though the optimized molybdenum blue method using a 2 meter LWCC has proved successful for detecting phosphate in ice cores some issues remain to be solved. The increased amount of dust in glacial times reacts with the PO_4^{3-} when stuck somewhere in the long line or at the glass wool filter, cause a memory effect, which strongly reduces the temporal resolution and causes a drift in baseline between the start and end of each measurement. Rinsing with HCl and sodium hydroxide solutions as well as with methanol did not seem to solve the problem. It is possible that introducing EDTA in the flow or changing the filter to another type or remove it to a position earlier in the system would diminish the problems.

Silicate can react with molybdenum blue, causing a possible interference with the specificity of the method. Though the size of silicate in ice cores probably does not significantly interfere with the detection of phosphate, the interference remains to be investigated. If silicate interferes it could perhaps be removed by introducing an on line column.

Danish summary-Dansk resumé

Dette projekt havde til formål at finde en metode der kunne detektere fosfat kontinuert i iskerner. Fosfat er et vigtigt og til tider begrænsende næringsstof for liv. Specielt er det vigtigt for den primære produktion i havene. Størstedelen af fosforkredsløbet er vandbåret, kun en brøkdel transportereres som partikler i atmosfæren. I fjerne egne af oceanerne kan den atmosfæriske transport af fosfor imidlertid have stor betydning for den biologiske aktivitet. Omkring 80 % af den fosfor og 50 % af den fosfat der transporteres i atmosfæren er mineralsk støv. På grund af skovrydning og anvendelsen af fosfat som gødning har man set ændringer i fosforkredsløbet gennem de sidste par århundreder. Over tid kan ændringer i havniveauet have forårsaget ændringer i fosforkredsløbet. I tidligere studier har man fundet at koncentrationen af fosfor i den grønlandske indlandsis er 0.25 ppb, mens man i smeltevandet fra Argentinske gletschere har fundet helt op til 145 ppb fosfor [*Edwards et al.*, 2007; *Chillrud et al.*, 1994].
I iskerner er nedbør fra tidligere tider gemt. Ved at måle forskellige kemiske stoffer i iskernerne kan man blive klogere på fortidens klimaforandringer. Man kan ved at benytte "Continuous flow analysis"-metoden (CFA) opnå en meget høj tidsmæssig opløsning af målinger af ioner i iskernerne og samtidig har metoden den fordel, at man ikke får kontamineret isprøven. To CFA systemer er benyttet i dette studie. Det Københavnske som måler få klimaparametre med høj opløsning og et CFA system fra Bern, som måler mange forskellige parametre, med en lavere opløsning.
Mange metoder til måling af fosfat i vand blev undersøgt for at finde en der både kunne måle den forventede lave koncentration og samtidig kunne kombineres med CFA teknikken. En absorptionsmetode, der udnytter at fosfat reagerer med molybden blå, og derefter kan detekteres ved 710 nm, i kombination med en 2 meter lang detektions celle- en LWCC (liquid waveguide capillary cell) var den eneste der opfyldte begge krav. Metoden var tidligere benyttet af *Zhang and Chi* [2002] til måling af havvand. Diverse optimeringseksperimenter blev udført for at optimere metoden til detektion af lave fosfat koncentrationer. I den optimale metode var flowet 1,68 mL/min for prøve, 0,15 mL/min for reagens og for buffer. Derudover blev 0,20 mL/min luft indført for at minimere dispersion over den mindst 300 cm lange mixing der fulgte. Mixingen foregik ved 65 °C. Efter mixingen blev luften igen taget ud (0,35 mL/min) og blandingen fortsatte igennem et filter, før måling fandt sted ved 710 nm i den to meter lange LWCC. Reagensen blev lavet ved at opløse 0,37 g molybden blåt i 25 mL 5N H_2SO_4 og tilføje 5 mL vinsyre og 100 mL Milli-Q vand. 0,5 g L-ascorbinsyre og 7 g natriumdodecylsulfat opløst i 100 mL milli-Q vand udgjorde bufferen. Filteret som er sat i for at undgå at støv giver optiske forstyrrelser er lavet af et ca. 3 cm langt glasrør fyldt 2/3 dele med glasuld. Metoden gav en detektionsgrænse på under 0,1 ppb, dog med noget støj. Absorptionen er lineær som funktion af concentrationer under 40 ppb fosfat.
Metoden blev brugt til måling af fosfat i to forskellige iskerner: NEEM S1 iskernen og NEEM iskernen. I NEEM S1 iskernen blev fosfat detekteret i dele af de sidste 120 år. Middel koncentrationen var 0.32 ppb. En høj korelation med støv blev fundet og af de få toppe der ikke korrelerede med støv viste nogen korrelation med ammonium. Der blev ikke fundet nogen ændring over tid som følge af menneskeskabte ændringer. Målinger af fosfat i NEEM iskernen dækker perioden 22.4-36.8 tusind år før hvor tid. Niveauet er højt i kolde perioder og lavt i milde, henholdsvis 6 til 21 ppb og omkring 2 ppb. Under hele perioden var der ligesom i NEEM S1 iskernen en høj korrelation med støv, yderligere var niveauændringerne mellem milde og kolde peridoer i istiden sammenlignelige med støv. Fosfat blev også sammenlignet med kalium fra NGRIP iskernen og de havde samme skift

mellem milde og kolde perioder. Forholdet mellem kalium og fosfat tyder på havsalt er kilden. Den teoretiske værdi af fosfat fra havsalt og fosfat fra støv er samlet omkring 7 ppb.
Det er lykkedes med den valgte metode at måle niveauet af fosfat i iskerner. Metoden har dog stadig nogle problemer, som bør undersøges. I is fra sidste istid, findes der høje koncentrationer af støv som sætter sig i filteret og i den slange, hvori blandingen af reagens, buffer og prøve foregår. Det giver metoden en hukommelseseffekt, som i høj grad kan influere på den tidslige opløsning. En rutine hvori en rensende opløsning skyllede igennem den eksperimentelle opsætning mellem målinger blev testet, men hjalp ikke på hukommelses effekten. Der er en risiko for interferens fra silikat og arsenat, som bør undersøges og endelig er fosfat tilbøjelig til at sætte sig på glas og det bør derfor også undersøges, hvor meget af signalet der forsvinder pga. filteret.

References

(2009), World precision instruments, Manual for LWCC.

(2010), http://www.webelements.com/potassium/geology.html.

(2010a), http://en.wikipedia.org/wiki/Ethylenediaminetetraacetic_acid.

(2010b), http://www.miningmongolia.mn/en/index.php?option=com_content&task=view&id=135&Itemid=804-5.

(2010c), http://en.Wikipedia.org/wiki/Ion_Chromatography.

(2010d), http://en.Wikipedia.org/wiki/ICPMS.

(2010e), http://en.Wikipedia.org/wiki/List_of_fires_in_Canada.

(2010f), http://en.Wikipedia.org/wiki/List_of_wildfires#North_America.

(2010g), http://en.wikipedia.org/wiki/Sea_salt.

Adornato, L. R., E. K. Kaltenbacher, D. R. Greenhow, and R. H. Byrne (2007), High resolution in situ analysis of nitrate and phosphate in the oligotrophic ocean, *Environ. Sci. Technol.*, (41), 4045–4052.

Anagnostou, E., and R. M. Sherrell (2008), MAGIC method for subnanomolar ortophosphate determination in freshwater, *Limnol. Oceanogr.*, (Methods 6), 64–74.

Baker, A. R., T. D. Jickells, M. Witt, and K. D. Linge (2006), Trends in the solubility of iron, aluminium, manganese and phosphorus in aerosol collected over the atlantic ocean, *Marine Chemistry*, (98), pp. 43–58.

Basile, B., E. J. Reidel, S. A. Weinbaum, and T. M. DeJong (2003), Leaf potassium concentration, co2 exchange and light interception in almond trees (prunus dulcis (mill) d.a. webb), *Scientia Horticulturae*, *98*(2), 185 – 194.

Bergametti, G., E. Remoudaki, R. Losno, E. Steiner, and B. Chatenet (1992), Source, transport and deposition of atmospheric phosphorus over the northwestern mediterranean, *Journal of atmospheric chemistry*, *14*, 501–513.

Bigler, M. (2010), Personal communication.

Bolin, B., J. Crutzen, P. M. Vitousek, R. G. Woodmansee, E. D. Goldberg, and R. B. Cook (1981), Scope 21- the major biochemical cycles and their interactions-chap 1. interactions of biochemical cycles, *Workshop on the interactions of biogeochemical cycles*.

Cappelen, J., B. V. Jørgensen, E. V. Laursen, S. L.S., and R. S. Thomsen (2001), Technical report 00-18, the observed climate of greenland, 1958-99-with climatological standards normals, 1961-1990, *Danish Meterological Institute-ministry of transport*, pp. pp. 17–21.

Caraco, N., J. Cole, and G. E. Likens (1990), A comparison of phosphorus immobilization in sediments of freshwater and coastal marine systems, *Biogeochemistry*, *9*(3), pp. 277–290.

Carrillo, P., J. A. Delgado-Molina, J. M. Medina-Sánchez, F. J. Bullejos, and M. Villar-Argaiz (2008), Phosphorus inputs unmask negative effects of ultraviolet radiation on algae in a hight mountain lake, *Global change biology*, *14*, pp. 423–439.

Chen, H. Y., T.-H. Fang, M. Preston, and L. Saulwood (2006), Characterization of phosphorus in the aerosol of a coastal atmosphere: Using a sequential extraction method, *Atmospheric Environment*, *40*, pp. 279–289.

Chillrud, S. N., P. F. Temporetti, and H. F. Planas (1994), Chemical weathering of phosphate and germanium in glacial meltwater streams: Effects of subglacial pyrite oxidation, *Limnol. Oceanogr.*, *39*(5), pp. 1130–1140.

Concright, M. E., W. W. Gregg, and S. Levitus (2000), Seasonal cycle of phosphate in the open ocean, *Seep-Sea Ressearch I*, *47*, 159–175.

Dallas, T., and P. K. Dasgupta (2004), Light at the end of the tunnel: recent analytical applications of liquid-core waveguides, *Trends in analytical chemistry*, *23*(5), pp. 385–392.

Delaney, P. (2000), Nutrients in glacial balance, *Nature*, *405*, 288–291.

Diaz, R. J., and R. Rosenberg (2008), Spreading dead zones and consequences for marine ecosystems, *Science*, *321*(5891).

Drummond, L., and W. Maher (1995), Determination of phosphorus in aqueous solution via formation of the phosphoantimonylmolybdenum blue complex re-examination of optimum conditions for the anlysis of phosphate, *Analytica Chemica Acta*, *302*, 69–74.

Edwards, R. (2009), personal communication.

Edwards, R., J. R. McConnell, and J. R. Banta (2007), Atmospheric Deposition of Iron and Phosphorus to Greenland over the 20th- Century, *AGU Fall Meeting Abstracts*, pp. B1154+.

Elderfield, H., and R. E. M. Rickaby (2000), Oceanic Cd/P ratio and nutrient utilization in the glacial Southern Ocean, *Nature*, *405*, pp. 305–310.

Ellis, P. S., A. J. Lyddy-Meaney, P. J. Worsfold, and I. D. McKelvie (2003), Multi-reflection photometric flow cell for use in flow injection analysis of estuarine waters, *Analytica Chimica Acta*, *499*(1-2), 81 – 89.

Elser, J. J., C. E. Cleland, D. S. Gruner, W. S. Harpole, J. T. Ngai, E. W. Seabloom, J. B. Shurin, and J. E. Smith (2007), Global analysis of nitrogen and phosphorus limitation of primary producers in freshwater, marine and terrestrial ecosystems, *Ecology Letters*, *10*, 1135–1142.

Estela, J. M., and V. Cerdá (2005), Flow analysis tecniques for phosphorus: an overview, *Talanta*, *66*, pp. 307–331.

Evans, J., C. Ó Cofaigh, J. A. Dowdeswell, and P. Wadhams (2009), Marine geophysical evidence for former expansion and flow of the Greenland Ice Sheet across the north-east Greenland continental shelf, *Journal of quaternary science*, *24*, pp. 279–293.

Falkowski, P. G., R. T. Barber, and S. V. (1998), Biogeochemical controls and feedbacks on ocean primary production, *Science*, *281*, 200–205.

Filippelli, G. M. (2008), The global phosphorus cycle: Past, present, and future, *Elements*, *4*, 89–95.

Filippelli, G. M., C. Souch, B. Menounos, S. Slater-Atwater, A. J. Tomothy Jull, and O. Slaymaker (2006), Alpine lake sediment records of the impact of glaciation and climate change on the biogeochemical cycling of soil nutrients, *Quarternary ressearch*, *66*, pp. 158–166.

Floge, S. A., K. R. Hardy, E. Boss, and M. L. Wells (2009), Analytical intercomparison between type i and type ii long pathlength liquid core waveguides for the measurement of chromophoric dissolved matter, *Limnol. Oceanogr., Methods 7*, 260–268.

Fuhrer, K., A. Neftel, M. Anklin, T. Staffelbach, and M. Legrand (1996), High-resolution ammonium ice core record covering a complete glacial inter-glacial cycle-, *Journal of geophysical ressearch*, *101*(D2), pp. 4147–4164.

Furyakev, V. V., E. A. Vaganov, N. M. Tchebakova, and E. N. Valendik (2001), Effects of fire and climate on successions and structural changes in the siberian boreal forest, *Eurasian J. For. Res.*, *2*, pp. 1–15.

Gentle, B. S., P. S. Ellis, P. A. Faber, M. R. Grace, and I. D. McKelvie (2010), A compact portable flow analysis system for the rapid determination of total phosphorus in estuarine and marine waters, *Analytica Chimica Acta*, *674*, 117–122.

Gimbert, L. J., and P. J. Worsfold (2007), Environmental applications of liquid-waveguide-capillary cells coupled with spectroscopic detection, *Trends in Analytical Chemistry*, *26*(9), 914–930.

Gimbert, L. J., P. M. Haygarth, and P. J. Worsfold (2007), Determination of nanomolar concentrations of phosphate in natural waters using flow injection with a long path length liquid waveguide capillary cell and solid-state spectrophotometric detection, *Talanta*, *71*, 1624–1628.

Girardin, M. P. (2007), Interannual to decadal chnages in area burned in canada from 1781-1982 and the realtionship to nothern hemisphere land temperatures, *Global ecology and biogeography*, *16*, pp. 557–566.

Girardin, M. P., and D. Sauchyn (2008), Three centuries of annual area burned variability in northwestern north america inferred from tree rings, *The holocene*, *18*, 205.

Graham, W. F., and R. A. Duce (1982), The atmospheric transport of phosphorus to the western north atlantic, *atmospheric environment*, *16*(5), 1089–1097.

Hansson, M. E. (1994), The renland ice core. a northern hemisphere record of aerosol composition over 120.000 years, *Tellus*, (46B).

Herut, B., M. D. Krom, G. Pan, and R. Mortimer (1999), Atmospheric input of nitrogen and phosphorus to the southeast mediterranean: sources, fluxes and possible impact, *Limnology and Oceanography*, *44*(7).

Håkansson, L., J. Briner, H. Alexanderson, A. Aldahan, and G. Possnert (2007), 10be ages from central east greenland constrain the extent of the greenland ice sheet during the last glacial maximum, *Quaternary Science Reviews*, *26*(19), 2316–2321.

Hodson, A., P. Mumford, and D. Lister (2004), Suspended sediment and phosphorus in proglacial rivers: bioavailability and potential impacts upon the p status of ice-marginal receiving waters, *Hydrological processes*, *18*, pp. 2409–2422.

Hood, E., and D. Scott (2008), Riverine organic matter and nutrients in southeast alaska affected by glacial coverage, *Nature geoscience*, *1*, pp. 583–587.

Huang, X.-L., and J.-Z. Zhang (2006), Surfactant-sensitized malachite green method for trace determination of ortophosphate in aqueous solutions, *anbalytica Chimica Acta*, *580*, pp. 55–67.

Huang, X.-L., and J.-Z. Zhang (2008), Rate of phosphoantimonylmolybdenum blue complex formation in acidic persulfate digested sample matrix for total dissolved phosphorus determination: Importance of post-digestion ph adjustment, *Talanta*, *77*, pp. 340–345.

Kaufmann, P. R., U. Federer, M. A. Hutterli, M. Bigler, S. Schu¨pbach, U. Ruth, J. Schmitt, and T. F. Stocker (2008), An improved continuous flow analysis system for high-resolution field measurements on ice cores, *Environmental Science and Technology*, *42*(21), 8044–8050.

Kelly, M. A., and A. J. Long (2009), The dimensions of the greenland ice sheet since the last glacial maximum, *Pages NEWS*, *17*.

Kreutz, K. J. (2007), Glaciochemistry, *Elsevier B.V.*, *Ice core methods*.

Laskar, J., M. Gastineau, F. Joutel, P. Robutel, B. Levrard, and A. Correia (2004), A long term numerical solution for the insolation quantities of earth.

Levinson, R. (2001), *More modern chemical techniques*, 25-42 pp., Royal society of chemistry.

Levitus, S., M. E. Conkright, J. L. Reid, R. G. Naijar, and A. Mantyla (1993), Distribution of nitrate, phosphate and silicate in the world oceans, *Prog. Oceanog.*, *31*, 245–273.

Li, Q. P., and D. A. Hansell (2008), Intercomparison and coupling of magnesium-induced co-precipitation and long-path liquid-waveguide capillary cell techniques for trace analysis of phosphate in seawater, *Analytica Chimica Acta*, *611*(1).

Li, Q. P., D. A. Hansell, and J.-Z. Zhang (2008), Underway monitoring of nanomolar nitrate plus nitrite and phosphate in oligotrophic water, *Limnol. Oceanogr.*, (Methods 6).

Li, Z., M. Oshima, A. Sabarudin, and S. Motomizu (2005), Trace and ultratrace nalysis of purified water samples and hydrogen peroxide solutions for phosphorus by flow-injection method, *Analytical Sciences*, *21*.

Liang, Y., D. Yuan, Q. Li, and Q. Lin (2007), Flow injection analysis of nanomolar level ortophosphate in seawater with sold phase enrichment and colorimetric detection, *Marine chemistry*, *103*, 122–130.

Ma, J., D. Yuan, M. Zhang, and Y. Liang (2009), Reverse flow injection analysis of nanomolar soluble reactive phosphorus in seawater with a long path length liquid waveguide capillary cell and spectrophotometric detection, *Talanta*, *78*, 315–320.

Maher, B. A., J. M. prospero, D. Mackie, D. Gaiero, P. P. Hesse, and Y. Balkanski (2010), Global connections between aeolian dust, climate and ocean biogeochemistry at the present day and last glacial maximum, *Earth-science reviews*, *99*, pp. 61–97.

Mahowald, N., T. D. Jickells, A. R. Baker, P. Artaxo, C. R. Benietz-Nelson, G. Bergametti, T. C. Bond, Y. Ching, D. D. Cohen, B. Herut, N. Kubilay, R. Losno, C. Luo, W. Maenhaut, K. A. McGee, G. S. Okin, R. L. Siefert, and S. Tsukuda (2008), Global distribution of atmospheric phosphorus sources, concentration and deposition rates, and anthropogenic impact, *Global biochemical cycles*, *22*, GB4026.

McConnell, J. R., R. Edwards, G. L. Kok, M. G. Flanner, C. S. Zender, E. S. Saltzman, J. R. Banta, D. R. Pasteris, M. M. Carter, and J. D. W. Kahl (2007a), 20th-century industrial black carbon emissions altered arctic climate forcing, *Science*, *317*, 1381.

McConnell, J. R., R. Edwards, G. L. Kok, M. G. Flanner, C. S. Zender, E. S. Saltzman, J. R. Banta, D. R. Pasteris, M. M. Carter, and J. D. W. Kahl (2007b), Microparticle and trace element studies, *Elsevier*, pp. pp. 1207–1211.

Mills, M. M., C. Ridame, M. Davey, J. la Roche, and R. J. Geider (2004), Iron and phosphorus co-limit nitrogen fixation in the eastern tropical north atlantic, *Nature*, *429*, pp. 292–294.

Motomizu, S., J. P. Susanto, M. Oshima, H. Mikasa, and Y. Hori (1995), Ultra-trace determintaion of phosphate ion based on filtration-dissolution and flow-through spectrophotometric measurement, *Analytical Sciences*, *11*, pp. 155–160.

Mouillot, F., and C. B. Field (2005), Fire history and the global carbon budget: a 1° x 1° fire history reconstruction for the 20th century, *Global change biology*, *11*, pp. 398–420.

Murphy, J., and J. P. Riley (1958), a single-solution method for the determination of soluble phosphate in sea water, *J. mar. biol. Ass. U.K.*, *37*, 9–14.

Neves, M. S. A. C., M. R. S. Suoto, I. V. Tóth, S. M. A. Victal, M. C. drumond, and A. O. S. S. Rangel (2008), Spectrophotometric flow system using vanadomolybdophosphate detection chemistry and a liquid waveguide capillary cell for the determination of phosphate with improved sensitivity in surface and ground water samples, *Talanta*, *77*, 527–532.

Nielsen, M. E. (2009), Early holocene and eemian impurity profiles from the ngrip ice core, *Master thesis, Copenhagen University*.

Nixon, S. W., J. W. Ammerman, L. P. Atkinson, V. M. Berounsky, G. Billen, W. C. Boicourt, W. R. Boynton, T. M. Church, D. M. Ditoro, R. Elmgren, J. H. Garber, A. E. Giblin, R. A. Jahnke, N. J. P. Owens, M. E. Q. Pilson, and S. P. Seitzinger (1996), The fate of nitrogen and phosphorus at the land-sea margin of the north atlantic ocean, *Biogeochemistry*, *35*(1), pp. 141–180.

Nollet, L. M. L. (2007), *Handbook of Water Analysis-second edition*, 219-251 pp., CRC press.

Oelkers, E. H., and E. Valsami-Jones (2008), Phosphate minral reactivity and global sustainability, *Elements*, *4*, 83–87.

Papastefanou, C., and E. A. Bondietti (1991), Mean residence time in the boundary layer as determined from 210Bi/^{210}Pb activity ratios, *J. Aersol Sci.*, *22*(7), 927–931.

Paterson, W. S. B., and K. M. Cuffey (2010), *The physics of glaciers*, Elsevier, fourth edition.

Patey, M. D., M. J. A. Rijkenberg, P. J. Statham, M. C. Stinchcombe, E. P. Achterberg, and M. Mowlem (2008), Determination of nitrate and phosphate in seawater at nanomolar concentrations, *Trendes in Analytical Chemistry*, *27*(2), 169–182.

Paytan, A., and K. McLaughlin (2007), The oceanic phosphorus cycle, *Chem. Rev.*, *107*, 563–576.

Perez-Ruiz, T., C. Martínez-Lozano, T. V., and J. Martín (2005), High-performance liquid chromatographic assay of phosphate and organophosphorus pesticides using a post-column photochemical reaction and flourimetric detection, *analytica Chimica Acta*, *540*, 383–391.

Rasmussen, S., H. B. Clausen, A. Svensson, B. Vinther, and M. Winstrup (), Gicc05modelext-neem-1 time scale for the neem ice core constructed by stratigraphic transfer of the gicc05/gicc05modelext time scale from ngrip to neem.

Rasmussen, S. O., K. K. Andersen, S. J. Johnsen, M. Bigler, and T. McCormack (2005), Deconvolution-based resolution enhancement of chemical ice core records obtained by continuous flow, *Journal of geophysical ressearch*, *110*, D17,304.

Ridame, C., and C. Guieu (2002), Saharan input of phosphate to oligotrophic water of the open western mediterranean sea, *Limnol. Oceanogr.*, *47*(3), pp. 856–869.

Röthlisberger, R., M. Bigler, M. Hutterli, S. Sommer, B. Stauffer, H. G. Junghans, and D. Wagenbach (2000), Technique for continuous high-resolution analysis of trace substances in firn and ice cores, *Environmental Science and Technology*, *34*(2), 338–342.

Ruth, U. (2005), Mineral dust records from greenland ice cores, *PAGES news*, *13*(3), pp. 17–20.

Ruth, U., D. Wagenback, J. P. Steffensen, and M. Bigler (2003), Continuous record of microparticle concentration and size distribution in the central greenland ngrip ice core during the last glacial period, *Journal of geophysical research*, *108*(D3).

Ryther, J. H., and W. M. Dunstan (Mar. 12, 1971), Nitrogen, phosphorus, and eutrophication in the coastal marine environment, *Science*, *171*(3975), pp. 1008–1013.

Sañudo-Wilhelmly, S. A. (2006), A phosphate alternative, *nature*, *439*.

Sauer, S. (2010), Dating and analysis of a greenland shallow ice core, *Geoscientific project*.

Schindler, D. W. (1977), Evolution of phosphorus limitation in lakes, *Science*, *195*(4275), pp. 260–262.

Schlesinger, W. H. (1991), *Biochemistry, An analysis of global change*, Academic press.

Sidall, M., M. R. Kaplan, J. M. Schaefer, A. Putnam, and M. A. Kelly (2010), Changing influence of antarctic and greenlandic temperature records on sea-level over the last glacial cycle, *Quaternary science reviews*, *29*, pp. 410–423.

Sierro, F. J., N. Andersen, M. A. Bassetti, S. Berné, M. Canals, J. H. Curtis, B. Dennielou, J. A. Flores, J. Frigola, B. Gonzalez-Mora, J. O. Grimalt, d. A. Hodell, G. Jouet, M. Pérez-Folgado, and R. Schneider (), Phase relationship between sea level and abrupt climate change, *Quaternary Science Reviews*, (In press).

Sigg, A., K. Fuhrer, M. Anklin, T. Staffelbach, and D. Zurmuehle (1994), A continuous analysis technique for trace species in ice cores, *Environmental Science and Technology*, *28*(2), 204–209.

Steffensen, J. P. (1995), The size distribution of microparticles from selected segments of the greenland ice core project ice core representing different climatic periods, *Analyst*, *120*, pp. 187–191.

Survey, U. G. (2010), Phosphorus statistics. in: Kelly td, mantos gr (compilers) historic statistics for mineral and mineral commodities in the united states, *U.S. Geological Survey Data Series 140*.

Susanto, J. P., M. Oshima, and S. Motomizu (1995), determination of micro amounts of phosphorus with malachite green using a filtartion-dissolution preconcentration method and flow injection-spectrophotometric detection, *Analyst*, *120*, pp. 187–191.

Svensson, A. (2010), Personal communication.

Svensson, A., P. E. Biscaye, and F. E. Grousset (2000), characterization of late glacial continental dust in the greenland ice core project ice core, *Journal of geophysical ressearch*, *105*(D4), pp. 4673–4556.

Tamburini, F., and K. B. Föllmi (2009), Nutrients and organic matter in glacial river-foodplain system (val roseg, switzerland), *Biogeosciences*, *6*, pp. 501–513.

Tiessen, H. (1995), *Phosphorus in the global environment*, Springer.

Tockner, K., F. Malard, U. Uehlinger, and J. V. Ward (2002), Nutrients and organic matter in glacial river-foodplain system (val roseg, switzerland), *Limnol. Oceanogr.*, *47*(1), pp. 266–277.

Udisti, R., S. Becagli, E. Castellano, R. Mulvaney, J. Schwander, S. Torcini, and E. Wolff (2000), Holocene electrical and chemical measurements from the epica-dome c ice core, *Annals of glaciology*, *30*, pp. 20–26.

unpublished, N. (2004), Ngrip unpublished.

Wang, X., R. J. Mataer, and T. W. Trull (dec. 15, 2001), Modelling seasonal phosphate export and resupply in the subanctic and the polar frontal zones in the australian sector of the southern ocean, *Journal of geophysical ressearch*, *106*(C12).

Worsfold, P. J., P. Monbet, A. D. Tappin, M. F. Fitzsimons, D. A. stiles, and I. D. McKelvie (2008), Characterisation and quantification of organic phosphorus and organic nitrogen components in aquatic system: A review, *Analytica Chimica Acta*, *624*, pp. 37–58.

Yaqoob, M., A. Nabi, and P. J. Worsfold (2004), determination og nanomolar concentartions of phosphate in freshawaters using flow injection with chemiluminescence detection, *Analytica chimica acta*, *510*, pp. 213–218.

Zhang, J., and J. Chi (2002), Automated analysis of nanomolar concentrations of phosphate in natural waters with liquid waveguide, *Environmental scienc and technology*, *36*, 1048–1053.

Zhang, J.-Z. (2006), Enhanced sensitivity in flow injection analysis using a long pathlength liquid waveguide capillary flow cell for spectrophotometric detection, *Analytical science*, *22*, pp. 57–61.

Zhang, J. Z., C. J. Fischer, and P. B. Ortner (1999), Optimization of performance and minimization of silicate interference in continuous flow phosphate analysis, *Talanta*, *49*, 293–304.

List of Figures

List of Tables

A Appendix

A.1 Nomenclature

Boxcar: A measure of the wavelength integration range, the higher the number the more of the spectrum is used
B.P.: Before present
CFA: Continuous Flow Analysis
DEP: DiElectric Profiling Method
DOP: Hydrolysable dissolved organic phosphorus
ECM: Electrical conductivity method
GI: glacial interstadial
GS: glacial stadial
IC: Ion chromatography
ICP-MS: Inductively coupled plasma mass spectrometry
IP: Inorganic Phosphorus
L: liter
LOD: Limit of Detection
LWCC: Liquid Waveguide Capillary Cell
kyr: 1000 years
M: mol/L. This measure of concentration can be calculated using the molar weight of the species in question. For phosphorus it is 31 g/mol and the molecular weight of phosphate is 95 g/mol
MQ: Milli-Q water. Extremely clean water from which nearly all ions are removed
N: Normality-gram equivalent of a solute per liter of solution
NEEM: North Greenland Eemian Ice drilling project
NMR: Nuclear magnetic resonanse
PCTFE: Polychlorotrifluoroethylene
PEEK: Organic polymer thermoplastic
ppb: Parts per billion,μg/kg, $10^{-}9$
ppm: Parts per million, mg/kg, $10^{-}6$
ppt: Parts per trillion, ng/kg, $10^{-}12$
PTFE: Polytetrafluoroethylene
SMOW: Standard mean ocean water
SS: Sea salt
STD: Standard deviation
TRP: Total reactive phosphorus. The amount of phosphate and phosphorus that reacts in the molybdenum blue method
TP: Total phosphorus
ybp: years before present
yr: years

A.2 Deposition

This appendix contains a more theoretical approach to wet and dry deposition. The transport of any matter in the atmosphere can be formulated by the global amount of the matter in question in the atmosphere (M), the source strength (SS) and the sink during transport:

$$\frac{dM}{dt} = SS - S(M) \tag{17}$$

The sink is dependent on global average concentration (C) as well as on the deposition rate (V_d[m/day]). Thus the equation can be written:

$$\frac{dM}{dt} = SS - C \cdot V_d \tag{18}$$

The residence time (T) assuming steady state of any matter in the atmosphere is thus:

$$T = \frac{M}{S(M)} \tag{19}$$

The deposition rate is dependent on several processes, the most important being dry and wet deposition on land and water surfaces. Adsorption on surfaces also influences the amount of phosphate making it to the ice. Decomposition by atmospheric chemical and photochemical processes can also occur.

Dry deposition happens by sedimentation. The force of gravity acts on all particles and especially the ones larger than 5 μm will tend to settle fast. For gravitational settling Stokes law can be used:

$$v_d = \frac{g(a \cdot d)^2(\rho - \rho_a)}{18\mu} \tag{20}$$

where v_d is the settling velocity (cm/s), g is the gravitational acceleration (981 cm/s), a is a conversion factor (10^{-4}), d is the effective particle diameter (μm), ρ is the density of the particle in question ($2g/cm^3$), ρ_a is the density of air (0.001243 g/cm^3) and μ is the dynamic viscosity parameter ($1.77{\cdot}10^{-4}$ at 10 °C).

Further, electrostatic attraction between particle and surface as well as adsorption and chemical interaction can influence the dry deposition. However these are largest in and near by urban areas. The loading of particles in g/s can be calculated by:

$$L = v_d \cdot C \cdot A \cdot f \tag{21}$$

where C is the concentration of atmospheric particles, A is the receptor area (m^2) and f is the fraction by mass of the phosphorus or phosphate particle to the particulate matter.

Wet deposition is removal with precipitation and this includes both snow, rain and combinations thereof. The amount of phosphorus deposited by precipitation is both of particulate matter and dissolved phosphorus in rain droplets. The sodium-(Na_3PO_4), potassium- (K_3PO_4), rubidium- (Rb_3PO_4), caesium- (Cs_3PO_4) and ammonium- ($(NH_4)_3PO_4$)phosphates are all water soluble.

Wet deposition can either be from falling rain droplets containing a solution of phosphate or by droplets or snowflakes scavenging phosphate or phosphor particles on the way down. Wash out below the clouds, can be described by C_w, the concentration after rain, $C_{w,0}$, the concentration before the rain, t the duration of rain in seconds and λ the wash out coefficient.

$$\frac{dC_w}{dt} = -\lambda C_w \tag{22}$$

$$C_w = C_{w,0} \cdot e^{-\lambda t} \tag{23}$$

this makes the wet fall out per unit area:

$$D_w = (C_{w,0} - C_w)H = C_{w,0} \cdot (1 - e^{-\lambda t})H \tag{24}$$

where H is the height. The rainwater thus contain a concentration $C_{rain} = D_w/V_{rain}$, where V_{rain} is the volume of rain.

A.3 ICP-MS, FIC and CFA-Gas detection methods

Using **inductively coupled plasma mass spectrometry (ICP-MS)** elements such as Mg, Al, K, Mn, Rb, Sr, Zr, Ba, Nd and Pb can be measured down to the ppt range. The ICP-MS basically decomposes samples to elements and then measures them by their mass to charge ratios. First the sample is exposed to high velocity argon gas. This process reduces the aqueous sample into droplet form. Approximately 2% of the original sample is then led into an argon torch, which atomizes the sample and ionizes it. Further the sample is excited in the hot plasma, which is used for atomic spectroscopy measurements. The sample is then led into the mass discriminator, which can be of different types, most used is a quadrupole. The quadrupoles are set at different voltage making all but the wanted specie hit the rods and get stuck there, while only the element in question makes it to the detection unit, which amplifies the signal. Thus the element in question can be counted.

The ICP-MS system has the advantage that many elements can be measured at the same time, it has a relatively high sample throughput. However it is expensive both to buy and to run due to the argon gas required to run it.

The ICP-MS system is also not really continuous, but uses the CFA melt system mainly to avoid contamination. A two way valve can then be set up to allow one sample into the ICP-MS or the other, thus creating semi-discrete measurements. If two systems run simultaneously a very high time resolution can be accomplished [*Levinson*, 2001; wik, 2010d].

Ion Chromatography (IC) can be combined in the same way as the ICP-MS with a CFA system. The so called FIC (fast ion chromatography) can measure basically all ions, though not at the same time, since the spectra of some cover the spectra of others. The IC allows one measurement per minute and thus provides a high resolution. The detection limit is below 0.5 ppb for all species if preconcentration is used [*Udisti et al.*, 2000]. In an IC the analyte molecules are retained in a column based on ionic interactions. However the target analytes can be released from the stationary phase in the column by increasing a concentration of another ion to replace the target analytes. Hereafter the target analytes can be detected by using either conductivity measurements or UV/visible light absorbance [wik, 2010c].

CFA-gas systems use the gas which is debubbled from the CFA water part of the system. Measurements are conducted using a PICARRO, which is a refractive cell, making the path length very long. Measurements of species such as methane and oxygen are currently under development.

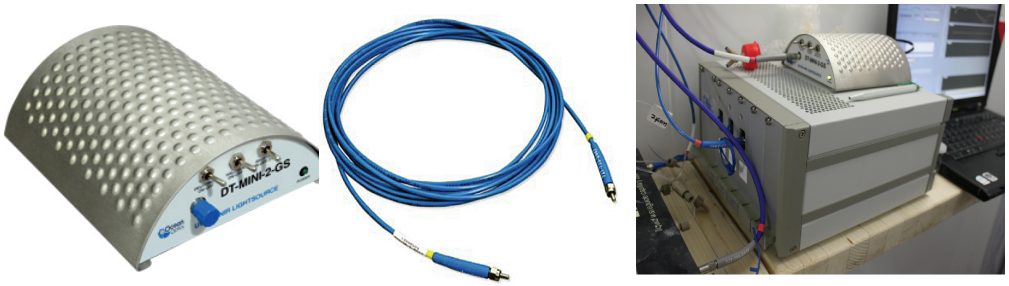

Figure 77: The lamp, optic fibres, and spectrometer used in the set-up.

Figure 78: The two types of pumps used for the measurements. Left, ISMATEC. Right, Ole Dich.

A.4 Instrumentation

Instrumentation included a lamp and ocean optics spectrometer used for detection, a 2 meter LWCC, Labview program, tubes, ferrules and a pump and pump tubes and a heat bath. Further, filter and debubblers were used, as described in sections 7.9 and 7.10.

The **Lamp** used in the set up was purchased from the company Ocean Optics and is the DT-MINI-2-GS lamp, which is a combined deuterium, halogen lamp with wavelength between 200 and 850 nm. It has the option of either being used as a halogen (1.2 Watts) or deuterium (3.8 Watts) lamp or both, which was what was used for the detection of phosphate. The lamp requires a 30 minutes warm up. The lamp is connected to the 2 meter LWCC (see section 6.2.5) with optic fibres of the type P400-2-UV/VIS also from the Ocean Optics company. The fibres are most efficient at 300-800 nm. Lamp and optical fibers are shown in figure 77.

The **Spectrometer** used for detection is also by Ocean optics. The spectrometer is a 2000S combined with and ADC100-USB converter. The spectrometer comes with a software (OOIBasse32), which provides the option of making an instant recording of spectrum. This was used for dust analysis. It also has a software built in for giving concentrations directly if provided with some known standards. This feature was not used.

Instead a **Labview** program, which was originally made Matthias Bigler, was used with some additional changes by Paul Vallelonga for controlling and saving data. The data saving provided the option Boxcar, which defines the spectrum integrated. **Integration time** was also adjustable. It was set between 200 ms and 300 ms. It was found that the higher the value the lower the limit of detection.

The **Tubing** was Polymer tubing (HPFA) and had an outer diameter of 1/8" and an inner diameter of either 0.02 or 0.03 inches. Flangeless fittings were used for connection between tubes. They had a tendency towards breaking after approximate 4 days use especially the one connecting

the buffer.

Two different types of **pumps** were used. they can be seen in figure 78. For initial testing and optimizing a pump produced by Ole Dich, Denmark, was used. It caused problems: From time to time flow rates could differ due to bending of the tubing in the pump.

For measurements of ice an ICP-pump purchased at ISMATEC was used. It did not bend tubing. However care was always needed and pump tubes should be reaplaced once a week, when measuring all the time or just when needed. The pump has the ability of running with flow between 0.002 and 44 ml/min depending on the size of the pump tubing and on the speed set on the pump. Pump tubing was the type Tygon LFL tubing and was also purchased from ISMATEC.

The **Heat bath** used is made from an old metal soda bottle, covered with insulating material, filled with water, which was heated using a temperature controller, of type JUMO dtron 308. The heat bath had a magnet inside for stirring water and in order to make sure that the temperature was everywhere constant. The stirrer was of the type MR1000 from the company Heidolph, with optional speed available. When the heat bath was used the mixing tubing was positioned inside the heat bath and an old lid from a soda bottle was used as lid, to prevent the water from vaporising. The heat bath can be seen in figure 59.

A.5 Example of a logfile

```
CFA-Bern; NEEM 2010; Simon Schüpbach, Daiana Leuenberger, Gideon Gfeller, Matthias Bigler

CFA Logfile

05/24/10 10:23 AM
/c/DATA/100524-002.neem

Depth top (m): 1282.60
Core length (cm): 93.2
MV on: 188
MV off: 1908
GC Start: NaN

CFA index Log code
161.000000 20000.000000
161.000000 20091.000000
174.000000 20090.000000
188.000000 10802.000000
188.000000 11000.000000
196.000000 11101.000000
196.000000 11101.000000
196.000000 11101.000000
210.000000 20001.000000
1160.000000 20091.000000
1161.000000 20090.000000
1161.000000 20091.000000
1162.000000 20090.000000
1162.000000 20091.000000
1163.000000 20090.000000
1163.000000 20091.000000
1164.000000 20090.000000
1164.000000 20091.000000
1165.000000 20090.000000
1165.000000 20091.000000
1165.000000 20090.000000
1166.000000 20091.000000
1166.000000 20090.000000
1167.000000 20091.000000
1167.000000 20090.000000
1269.000000 20091.000000
1269.000000 20090.000000
1270.000000 20091.000000
1271.000000 20090.000000
1272.000000 20091.000000
1275.000000 20090.000000
1276.000000 20091.000000
1276.000000 20090.000000
1582.000000 20091.000000
1583.000000 20090.000000
1584.000000 20091.000000
1584.000000 20090.000000
1585.000000 20091.000000
1586.000000 20090.000000
1586.000000 20091.000000
```

```
1592.000000 20090.000000
1592.000000 20091.000000
1596.000000 20090.000000
1596.000000 20091.000000
1597.000000 20090.000000
1597.000000 20091.000000
1597.000000 20090.000000
1597.000000 20091.000000
1599.000000 20090.000000
1599.000000 20091.000000
1600.000000 20090.000000
1606.000000 20091.000000
1606.000000 20090.000000
1821.000000 20091.000000
1824.000000 20090.000000
1825.000000 20091.000000
1825.000000 20090.000000
1825.000000 20091.000000
1840.000000 20090.000000
1875.000000 20091.000000
1882.000000 20002.000000
1908.000000 10800.000000
1908.000000 11001.000000
1911.000000 11102.000000


Abakus (Particlesize; Noise):
0.800000 0.900000 1.000000 1.100000 1.200000 1.300000 1.400000 1.500000 1.600000
1.700000 1.800000 1.900000 2.000000 2.100000 2.200000 2.300000 2.400000 2.600000
2.800000 3.000000 3.300000 3.600000 4.000000 4.500000 5.100000 5.800000 6.600000
7.500000 8.500000 9.500000 10.000000 0.000000
58.000000
```

A.6 Example of a break file

```
CFA-Bern; NEEM 2010; Simon Schüpbach, Daiana Leuenberger, Gideon Gfeller, Matthias Bigler

05/24/10 10:23 AM
/c/DATA/100524-002.neem

Break Pos. (cm) Cut Length (cm)
0.0 0.1
41.2 1.3
53.4 0.2
81.6 15.2
93.2 0.0
```

A.7 Proxies plotted with phosphate

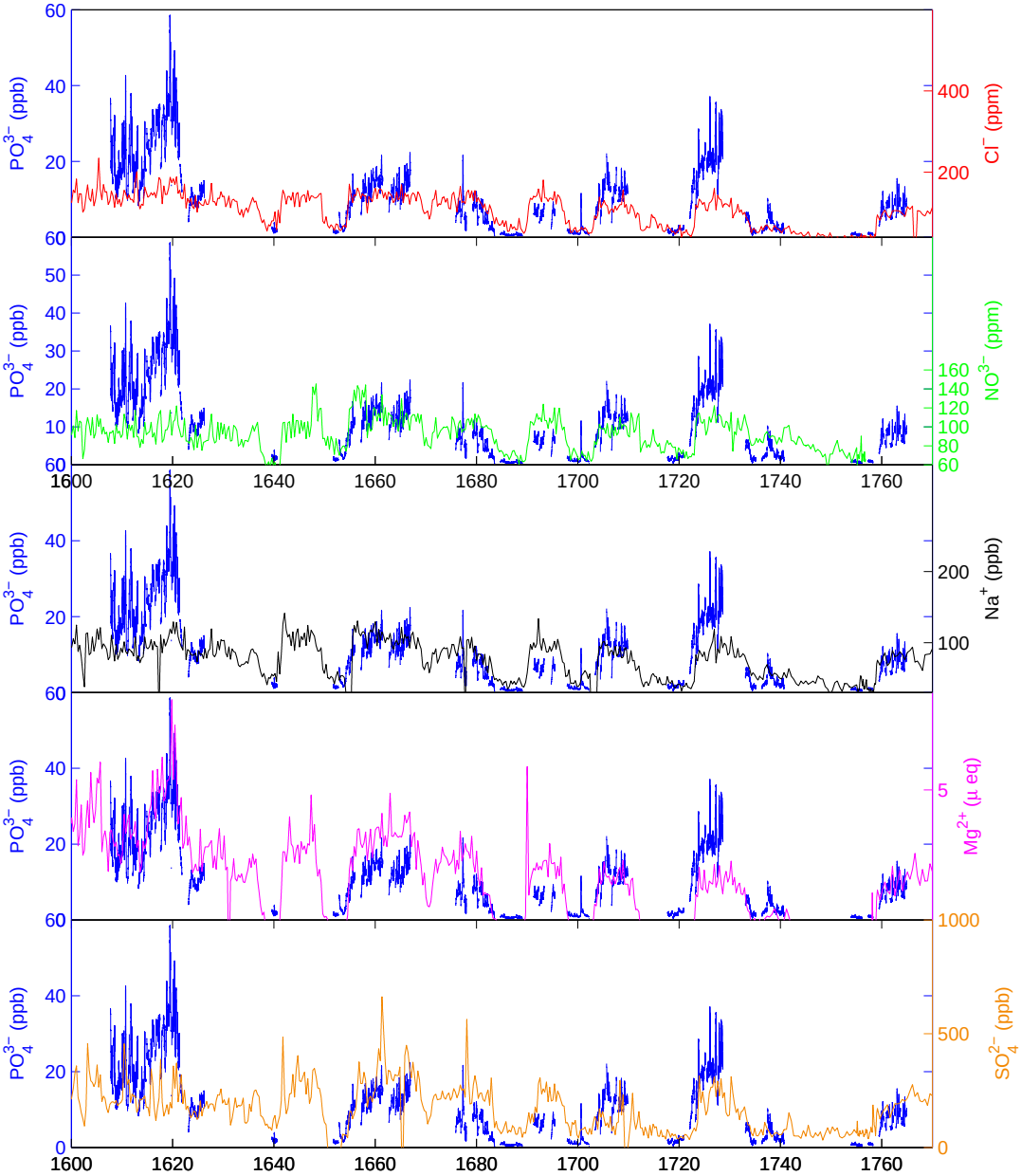

Figure 79: (A.7)Proxies from NGRIP plotted with Phosphate

More proxies from NGRIP compared to phosphate (blue). Mg^{2+}, Cl^- and NO_3^- is detected using IC and SO_4^{2-} and Na^+ using CFA.